

Response to 2nd round reviews for the paper “Secondary Organic Aerosol (SOA) yields from NO₃ radical + isoprene based on nighttime aircraft power plant plume transects” by J.L. Fry et al.

We thank the reviewers for their careful reading of and thoughtful comments on our paper. To guide the review process we have copied the reviewer comments in black text. Our responses are in regular blue font. We have responded to all the referee comments and made alterations to our paper (in bold text).

Responses to 2nd round reviews:

Anonymous Referee #1

I am overall satisfied by the author’s responses and changes to the manuscript. Together, the revisions make for a substantially improved manuscript, and do not change the conclusions. To my knowledge, there is no other study like this, and I appreciate the depth to which the authors have addressed the limitations of their study. In particular, new Fig. S9 clearly demonstrates the importance of NO₃ in the consumption of isoprene in the plume at night, and the error bars in Fig. 5 indicate clearly the variability in the derived yields. This change should be regarded not as skepticism of the yields, but rather a clear statement of the limitations of their measurement, which is not grounds for manuscript rejection.

While, in hindsight, there are some improvements to the experiments I’m sure the authors would like to have made to ensure the organic nitrates being detected in the plume were from isoprene+NO₃ (described below), this study represents a first approach and should be regarded as foundation for similar studies in the future. One such improvement to the experiment the authors might consider in the future is to use chemical ionization mass spectrometry (CIMS), or another complementary tool to the AMS, for qualitative or quantitative detection of isoprene+NO₃ oxidation products. Recent studies by Slade et al. (2017) and Lee et al. (2016) highlight this capability for monoterpene- and isoprene-derived organic nitrates.

My only criticism of the current manuscript is that the reported yields need hard uncertainty numbers. Given the error bars shown in Fig. 5, instead of using the standard deviation of the slope coefficient as the uncertainty, the authors should show how the slope varies accounting for the error in Δ isoprene and Δ pRONO₂. If you consider the max Δ pRONO₂~100 ppt at Δ isoprene ~400 ppt, the upper limit to the yield is ~25%. In contrast, it appears the lower limit of the yield (Δ pRONO₂~20 ppt at Δ isoprene~700 ppt) is ~3%. Therefore, a more accurate organic nitrate yield with uncertainty might be 9(+14/-6)%.

References

Lee, B. H., Mohr, C., Lopez-Hilfiker, F. D., Lutz, A., Hallquist, M., Lee, L., Romer, P., Cohen, R. C., Lyer, S., Kurten, T., Hu, W., Day, D. A., Campuzano-Jost, P., Jimenez, J. L., Xu, L., Ng, N. L., Guo, H., Weber, R. J., Wilde, R. J., Brown, S. S., Koss, A., de Gouw, J., Olson, K., Goldstein, A. H., Seco, R., Kim, S., McAvey, K. M., Shepson, P. B., Starn, T. K., Baumann, K., Edgerton, E. S., Liu, J., Shilling, J. E., Miller, D. O., Brune, W., Schobesberger, S., D’Ambro, E. L., and Thornton, J. A.: Highly functionalized organic nitrates in the southeast United States: contribution to secondary organic aerosol and reactive nitrogen budgets, Proc. Nat. Acad. Sci., 113, 1516-1521, 10.1073/pnas.1508108113, 2016.

Slade, J. H., de Perre, C., Lee, L., and Shepson, P. B.: Nitrate radical oxidation of γ -terpinene: hydroxy nitrate, total organic nitrate, and secondary organic aerosol yields, *Atmos. Chem. Phys.*, 10.5194/acp-2017-249, 2017.

Thank you for your comments. We have added a line referring to the CIMS methods you suggest in the last paragraph, at line 977:

“Future similar field studies would benefit from the co-deployment of the complementary tool of a Chemical Ionization Mass Spectrometer (CIMS) to detect NO_3 + isoprene products such as organic nitrates (Lee et al., 2016, Slade et al., 2017).”

Following your suggestion, we have added to Figure 5 lines showing the “outside” maximum uncertainty based on combined instrumental uncertainties, and have added text to the caption explaining these lines:

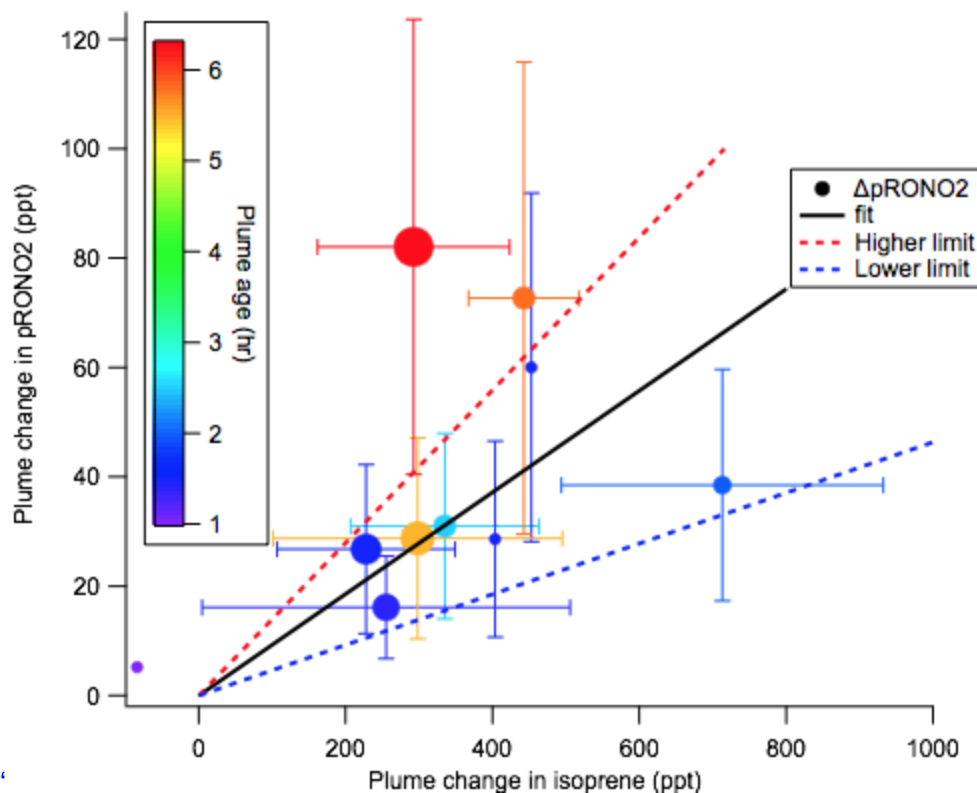


Figure 5. SOA molar yield can be determined as the slope of $\Delta p\text{RONO}_2$ vs. Δ isoprene, both in mixing ratio units. The linear fit is weighted by square root of number of points used to determine each in-plume pRONO₂, with intercept held at zero. The slope coefficient \pm one standard deviation is 0.0930 ± 0.0011 . **Larger “outside” high and low limits of the slope (shown as dashed red and blue lines) are obtained by adding and subtracting from this slope the combined instrumental uncertainties, based on adding in quadrature the**

PTR-MS uncertainty of 5% and the AMS uncertainty of 50%. This gives an overall uncertainty of 50.2%, resulting in upper and lower limit slopes of 0.140 and 0.046, respectively. Points are colored by plume age, and size scaled by square root of number of points (the point weight used in linear fit). This plot and fit includes the nine plumes listed in Tables 1 and 2, as well as the 03:14 “unreacted” plume (at Δ isoprene = -84 ppt). Error bars on isoprene are the propagated standard deviations of the (in plume - out plume) differences, for plumes in which multi-point averages were possible. Error bars on $p\text{RONO}_2$ are the same as in Figure 4. The points without error bars are single-point plumes.”

And we have updated the text discussion and yields reported in the abstract to show these ranges: at line 706: **“This slope error gives a rather narrow uncertainty range for the slope (0.0930 +/- 0.0011); to obtain an upper limit in the uncertainty of this molar yield we apply the combined instrumental uncertainties, based on adding in quadrature the PTR-MS uncertainty of 5% and the AMS uncertainty of 50%. This gives an overall uncertainty of 50.2%, resulting in upper and lower limit slopes of 0.140 and 0.046, respectively; we use this maximum uncertainty estimate to report the average molar yield as 9% (+/- 5%).”**

“for which the average over 9 plumes is 9% (+/- 5%). Corresponding mass yields depend on the assumed molecular formula for isoprene- NO_3 -SOA, but the average over 9 plumes is 27% (+/- 14%), **on average** larger than those previously measured in chamber studies (12 – 14% **mass yield as $\Delta\text{OA}/\Delta\text{VOC}$** after oxidation of both double bonds). ”

Anonymous Referee #2

Minor comments:

Regarding the answers marked R1.2. L: 651:

Schwantes et al., 2015, show that autoxidation is not very important in HO₂ regimes.

Rollins et al., 2009 likely operated in the RO₂ regime and autoxidation could have contributed to that yield already. The observation time here was several hours, thus NO₃ exposure was comparable to that in the plumes. So reaction time alone, cannot be an issue.

Thank you. We agree that reaction time alone will not determine whether initially formed RO₂ undergo autoxidation or bimolecular reactions, and that instead the peroxy radical lifetime, driven by e.g. the concentration of HO₂, will determine RO₂ fate. We hope that future studies with more speciated measurements are able to better elucidate RO₂ fate. We note however also that Rollins (2009) had NO₂ concentration of up to 40 ppb, O₃ up to 60 ppb, and two isoprene injections of 10 ppb each, meaning that radical concentrations are likely significantly higher, which would suppress autoxidation by competition of faster bimolecular rates.

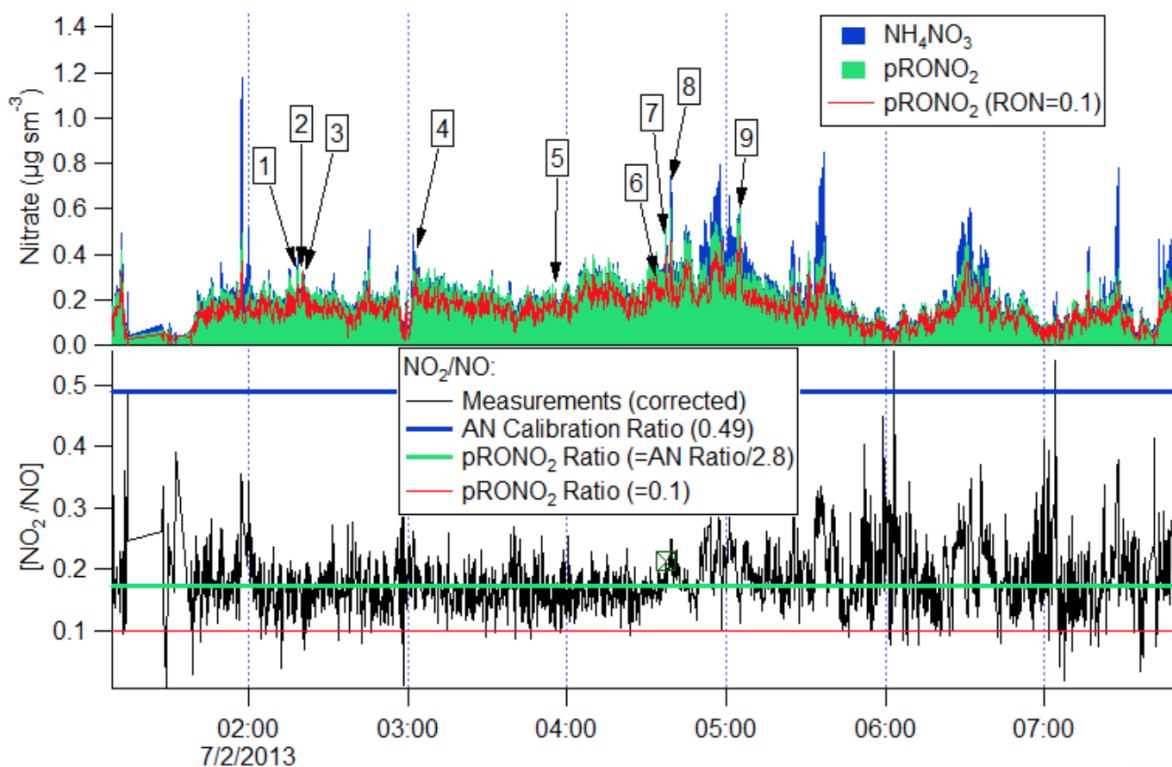
Anonymous Referee #3

Review for revised manuscript „Secondary Organic Aerosol (SOA) yields from NO₃ radical + isoprene based nighttime aircraft power plant plume transects” by J. L. Fry et al.

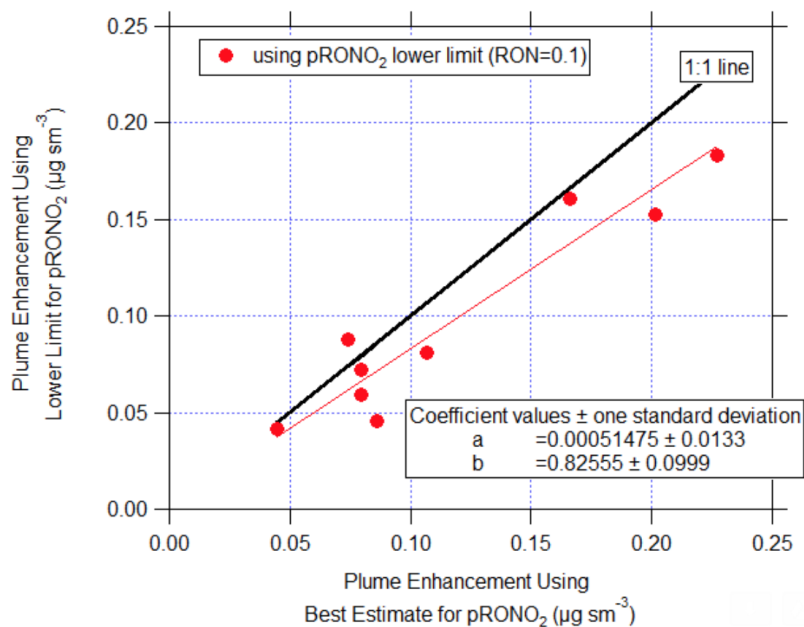
Fry et al. considerably improved the manuscript in their revised version. Yet there remains one major point, which needs modification before the manuscript can be published.

This reviewer requested, to show the uncertainty induced by not knowing the ratio R of $\text{NO}_2^+/\text{NO}^+$ from the organic nitrates present in the aerosol. One such approach – as suggested in the review – would be a discussion on the impact of lower R on derived SOA yield. As shown in figure 3 a significant fraction of data points (eyeballing > 30%) shows R values below 0.175. As mentioned in the review, applying an R value of 0.1 (the lower envelope of the data), would reduce SOA yields to 13%, values comparable to the literature cited by the authors. The authors do not explain why they consider this comparably large number of data points as invalid, or within errors the same as $R = 0.175$.

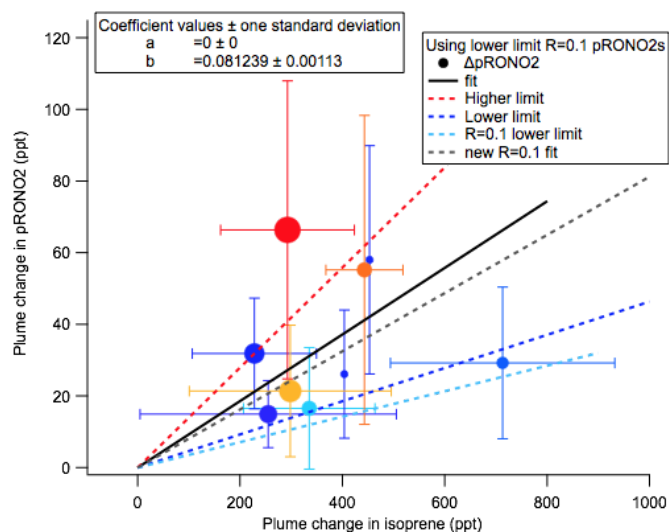
To fully investigate the possibility of a lower value for R (0.1), we propagated it for this data all the way to the yield calculations below. Looking at Fig. 3, the fraction that get apportioned to pRONO₂ is roughly the relative proportion that the NO_x ratio data lie between the pRONO₂ and NH₄NO₃ ratio lines. So, as an example, for data that the NO_x ratio is on the current green line of 0.175, moving the green line down to 0.1 would decrease the amount of pRONO₂ from ~100% to ~80% of the total nitrate (so ~20% decrease). Any data with NO_x ratios already below the green line would change less:



However, in order to be absolutely certain, we have re-calculated the pRONO₂ enhancements for each plume using $R=0.1$ to determine how these would affect the yields. Here is a correlation plot of the $R=0.1$ “Lower limit” pRONO₂ plume enhancement values against those calculated with our best estimate for R (ratio-of-ratios=2.8, resulting in $\text{RON}=0.175$). Linear fit is using $\text{ODR}=2$:



It is already clear that this will not affect the yields by a factor of two as suggested by this reviewer's comment. Nevertheless, we use these new "lower limit" pRONO₂ plume enhancement numbers to determine a new molar yield estimate:



This lower limit would shift the average molar yield from 9.3% to 8.1%, and the average mass yield from 27% to 24%. As described above, however, we now report a wider error range based shown in the plot above, to be even more conservative in our conclusions.

In sum, we still think that applying a ratio-of-ratios based on literature averages and using the stated accuracy is the most robust and unbiased method for computing pRONO₂ concentrations. In the SI, we already stated the uncertainty in pRONO₂ from uncertainty of the ratio-of-ratios as +/-20% (and overall pRONO₂ concentration uncertainty as +/-50%).

The response of the authors implies that they assume an average of literature R values to be relevant to the conditions they encounter in a regime where SOA is formed from the nighttime reaction of

isoprene with NO₃. This is not understandable, when only one reference (Rollins et al., 2009) explored organic nitrates formed from controlled chamber studies exploring isoprene + NO₃ reactions. That reference indicates an R value of 0.1. Why would other systems, with organic nitrates formed from e.g. aromatics (Sato et al.) or selected according to availability (Farmer et al.), be considered of the same relevance in this case?

We are not aware of any compelling evidence that the organic nitrate NO_x ratios have a composition dependence, nor reason that one would expect there to be. Regarding the Rollins 2009 study, they reported NO₂⁺/NO⁺ ratios were 0.156 for pRONO₂ and 0.35 for ammonium nitrate. Thus, it is not clear why the referee states that study supports a pRONO₂ ratio of 0.1. Moreover, in our methods, we use the ratio-of-ratio method, as stated in the manuscript, rather than a fixed ratio for pRONO₂ based on studies conducted on different instruments as others have done. For the Rollins 2009 study, the ratio-of-ratio would be 0.35/0.156 = 2.24. If that value was used instead here (rather than the 2.8 from averaging multiple studies), pRONO₂ concentrations (and overall SOA yields) calculated in this study would be higher (not lower as this referee seems to be arguing for). I.e. the green line in Fig. 3 would move up and a larger portion of the NO_x ratio data would fall below that line.

The major finding in the study, namely a larger SOA yield in the plumes than in previous chamber studies, directly depends on the R value used to calculate organic nitrate mass. Therefore a discussion of the uncertainty imposed by applying an unknown R value is mandatory to inform the reader on the certainty with which organic nitrate mass concentrations can be derived from AMS data sets. One such way is the application of an R-value as low as justifiable by the data, as this implies the analysis of data with respect to lower limits of organic nitrate mass and SOA yields.

We don't believe that including the lower limit R-value shown above in our manuscript is appropriate, because it introduces a bias in one direction. It also assumes that the choice of R is the largest uncertainty in this analysis, and we know that there are several other sources of uncertainty, so we don't wish to place sole emphasis on the choice of R. However, we think this reviewer may also be uncomfortable with the lack of uncertainty or range reported on the yield numbers reported in the abstract, which using R = 0.1 as an alternate value would provide. We have added to Figure 5 upper- and lower-limit yield slopes based on the outer bounds of the fully error-propagated x and y error bars, which provides a larger range of potential yields. The new, larger molar yield range of 9% (+/-5%) and corresponding mass yield range of 27% (+/-14%) does not unequivocally exclude the Rollins 2009 SOA (delOA/delVOC) mass yield report of 12-14%, but it does suggest that yields may be larger. We report this range in the hope that this will spur further work.

1 Secondary Organic Aerosol (SOA) yields from NO₃ radical 2 + isoprene based on nighttime aircraft power plant plume 3 transects

4

5 Juliane L. Fry¹, Steven S. Brown^{2,5}, Ann M. Middlebrook², Peter M. Edwards^{2,3,4}, Pedro
6 Campuzano-Jost^{3,5}, Douglas A. Day^{3,5}, José L. Jimenez^{3,5}, Hannah M. Allen⁶, Thomas B.
7 Ryerson², Ilana Pollack^{2,3,a}, Martin Graus^{3,b}, Carsten Warneke^{2,3}, Joost A. deGouw^{3,5}, Charles A.
8 Brock², Jessica Gilman^{2,3}, Brian M. Lerner^{2,3,c}, William P. Dubé^{2,3}, Jin Liao^{2,3,d}, André Welti^{2,3,e}

9

10 ¹Chemistry Department, Reed College, Portland, OR, USA

11 ²Chemical Sciences Division, Earth System Research Laboratory, National Oceanic and Atmospheric
12 Administration, Boulder, CO, USA

13 ³Cooperative Institute for Research in Environmental Sciences, University of Colorado, Boulder, CO, USA

14 ⁴Wolfson Atmospheric Chemistry Laboratories, Department of Chemistry, University of York, York, UK

15 ⁵Department of Chemistry, University of Colorado, Boulder, CO, USA

16 ⁶Division of Chemistry and Chemical Engineering, California Institute of Technology, Pasadena, CA, USA

17 ^anow at Department of Atmospheric Science, Colorado State University, Fort Collins, CO, USA

18 ^bnow at [Department](#) of Atmospheric and Cryospheric Sciences, University of Innsbruck, Austria.

19 ^cnow at Aerodyne Research, Inc., Billerica, MA, USA

20 ^dnow at Universities Space Research Association, Columbia, MD, USA and NASA Goddard Space Flight
21 Center, Atmospheric Chemistry and Dynamic Laboratory, Greenbelt, MD, USA

22 ^enow at Leibniz Institute for Tropospheric Research, Department of Physics, Leipzig, Germany

23

24 Abstract

25 Nighttime reaction of nitrate radicals (NO₃) with biogenic volatile organic compounds (BVOC)
26 has been proposed as a potentially important but also highly uncertain source of secondary
27 organic aerosol (SOA). The southeast United States has both high BVOC and nitrogen oxide
28 (NO_x) emissions, resulting in a large model-predicted NO₃-BVOC source of SOA. Coal-fired
29 power plants in this region constitute substantial NO_x emissions point sources into a nighttime
30 atmosphere characterized by high regionally widespread concentrations of isoprene. In this
31 paper, we exploit nighttime aircraft observations of these power plant plumes, in which NO₃
32 radicals rapidly remove isoprene, to obtain field-based estimates of the secondary organic
33 aerosol yield from NO₃ + isoprene. Observed in-plume increases in nitrate aerosol are
34 consistent with organic nitrate aerosol production from NO₃ + isoprene, and these are used to
35 determine molar SOA yields, for which the average over 9 plumes is 9% (+/- 5%).
36 Corresponding mass yields depend on the assumed molecular formula for isoprene-NO₃-SOA,
37 but the average over 9 plumes is 27% (+/- 14%), on average larger than those previously
38 measured in chamber studies (12 – 14% mass yield as ΔOA/ΔVOC after oxidation of both
39 double bonds). Yields are larger for longer plume ages. This suggests that ambient aging
40 processes lead more effectively to condensable material than typical chamber conditions allow.
41 We discuss potential mechanistic explanations for this difference, including longer ambient
42 peroxy radical lifetimes and heterogeneous reactions of NO₃-isoprene gas phase products.

Juliane Fry 7/31/2018 9:44 AM

Deleted: Institute

44 | ~~More in-depth studies are needed to better understand the aerosol yield and oxidation~~
45 | ~~mechanism of NO₃ radical + isoprene, a coupled anthropogenic – biogenic source of SOA that~~
46 | ~~may be regionally significant.~~

47 | 1 Introduction

48 | Organic aerosol (OA) is increasingly recognized as a globally important component of the fine
49 | particulate matter that exerts a large but uncertain negative radiative forcing on Earth's climate
50 | (Myhre et al., 2013) and adversely affects human health around the world (Lelieveld et al.,
51 | 2015). This global importance is complicated by large regional differences in OA concentrations
52 | relative to other sources of aerosol such as black carbon, sulfate, nitrate and sea salt. OA
53 | comprises 20 – 50% of total fine aerosol mass at continental mid-latitudes, but more in urban
54 | environments and biomass burning plumes, and up to 90% over tropical forests (Kanakidou et
55 | al., 2005, Zhang et al., 2007). Outside of urban centers and fresh biomass burning plumes, the
56 | majority of this OA is secondary organic aerosol (SOA) (Jimenez et al., 2009), produced by
57 | oxidation of directly emitted volatile organic compounds followed by partitioning into the aerosol
58 | phase. Forests are strong biogenic VOC emitters, in the form of isoprene (C₅H₈), monoterpenes
59 | (C₁₀H₁₆), and sesquiterpenes (C₁₅H₂₄), all of which are readily oxidized by the three major
60 | atmospheric oxidants, OH, NO₃, and O₃. The total global source of biogenic SOA from such
61 | reactions remains highly uncertain, with a review estimating it at 90 +/- 90 Tg C yr⁻¹ (Hallquist et
62 | al., 2009), a large fraction of which may be anthropogenically controlled (Goldstein et al., 2009,
63 | Carlton et al., 2010, Hoyle et al., 2011, Spracklen et al., 2011). As most NO₃ arises from
64 | anthropogenic emissions, OA production from NO₃ + isoprene is one mechanism that could
65 | allow for the anthropogenic control of biogenic SOA mass loading.

66 |
67 | Isoprene constitutes nearly half of all global VOC emissions to the atmosphere, with a flux of
68 | ~600 Tg yr⁻¹ (Guenther et al., 2006). As a result, accurate global biogenic SOA budgets depend
69 | strongly on yields from isoprene oxidation. Recent global modeling efforts find that isoprene
70 | SOA is produced at rates from 14 (Henze and Seinfeld 2006, Hoyle et al., 2007) to 19 TgC yr⁻¹
71 | (Heald et al., 2008), which implies that it could constitute 27% (Hoyle et al., 2007) to 48%
72 | (Henze and Seinfeld 2006) to 78% (Heald et al., 2008) of total SOA (based also on varying
73 | estimates of total SOA burden in each study). More recent observational constraints on SOA
74 | yield from isoprene find complex temperature-dependent mechanisms that could affect vertical
75 | distributions (Worton et al., 2013) and suggest that isoprene SOA constitutes from 17% (Hu et
76 | al., 2015) to 40% (Kim et al., 2015) up to 48% (Marais et al., 2016) of total OA in the
77 | southeastern United States. This large significance comes despite isoprene's low SOA mass
78 | yields – two recent observational studies estimated the total isoprene SOA mass yield to be
79 | ~3% (Kim et al., 2015, Marais et al., 2016), and modeling studies typically estimate isoprene
80 | SOA yields to be 4 to 10%, depending on the oxidant, in contrast to monoterpenes' yields of 10
81 | to 20% and sesquiterpenes' yields of >40% (Pye et al., 2010). Furthermore, laboratory studies
82 | of SOA mass yields may have a tendency to underestimate these yields, if they cannot access
83 | the longer timescales of later-generation chemistry, or are otherwise run under conditions that
84 | limit oxidative aging of first-generation products (Carlton et al., 2009).

85

Juliane Fry 5/15/2018 6:29 PM

Deleted: Future

Juliane Fry 5/15/2018 6:30 PM

Deleted: of aerosol composition from NO₃ radical + isoprene

Juliane Fry 5/15/2018 6:31 PM

Deleted: chemistry

Juliane Fry 5/15/2018 6:32 PM

Deleted: producing

Juliane Fry 5/15/2018 6:32 PM

Deleted: this potentially important

92 Laboratory chamber studies of SOA mass yield at OA loadings of $\sim 10 \mu\text{g m}^{-3}$ from isoprene
93 have typically found low yields from O_3 (1% (Kleindienst et al., 2007)) and OH (2% at low NO_x to
94 5% at high NO_x (Kroll et al., 2006, Dommen et al., 2009); 1.3% at low NO_x and neutral seed
95 aerosol pH but rising to 29% in the presence of acidic sulfate seed aerosol due to reactive
96 uptake of epoxydiols of isoprene (IEPOX) (Surratt et al., 2010)). One recent chamber study on
97 OH-initiated isoprene SOA formation focused on the fate of second-generation RO_2 radical
98 found significantly higher yields, up to 15% at low NO_x (Liu et al., 2016), suggesting that omitting
99 later-generation oxidation chemistry could be an important limitation of early chamber
100 determinations of isoprene SOA yields. Another found an increase in SOA formed with
101 increasing HO_2 to RO_2 ratios, suggesting that RO_2 fate could also play a role in the variability of
102 | previously reported SOA yields (D'Ambro et al., 2017).

103

104 For NO_3 oxidation of isoprene, early chamber experiments already pointed to higher yields (e.g.,
105 12% (Ng et al., 2008)) than for OH oxidation. Ng et al. (Ng et al., 2008) also observed chemical
106 regime differences: SOA yields were approximately two times larger when chamber conditions
107 were tuned such that first-generation peroxy radical fate was RO_2+RO_2 dominated than when it
108 was RO_2+NO_3 dominated. In addition, Rollins et al. (Rollins et al., 2009) observed a significantly
109 higher SOA yield (14%) from second-generation NO_3 oxidation than that when only one double
110 bond was oxidized (0.7%). This points to the possibility that later-generation, RO_2+RO_2
111 dominated isoprene + NO_3 chemistry may be an even more substantial source of SOA than
112 what current chamber studies have captured. Schwantes et al. (Schwantes et al., 2015)
113 investigated the gas-phase products of NO_3 + isoprene in the RO_2+HO_2 dominated regime and
114 found the major product to be isoprene nitrooxy hydroperoxide (INP, 75-78% molar yield), which
115 can photochemically convert to isoprene nitrooxy hydroxyepoxide (INHE), a molecule that might
116 contribute to SOA formation via heterogeneous uptake similar to IEPOX. Here again, multiple
117 generations of chemistry are required to produce products that may contribute to SOA.

118

119 Because the SOA yield appears to be highest for NO_3 radical oxidation, and isoprene is such an
120 abundantly emitted BVOC, oxidation of isoprene by NO_3 may be an important source of OA in
121 areas with regional NO_x pollution. Since the SOA yield with neutral aerosol seed appears to be
122 an order of magnitude larger than that from other oxidants, even if only 10% of isoprene is
123 oxidized by NO_3 , it will produce comparable SOA to daytime photo-oxidation. For example,
124 Brown et al. (Brown et al., 2009) concluded that NO_3 contributed more SOA from isoprene than
125 OH over New England, where $> 20\%$ of isoprene emitted during the previous day was available
126 at sunset to undergo dark oxidation by either NO_3 or O_3 . The corresponding contribution to total
127 SOA mass loading was 1 – 17% based on laboratory yields (Ng et al., 2017). Rollins et al.
128 (Rollins et al., 2012) concluded that multi-generational NO_3 oxidation of biogenic precursors was
129 responsible for one-third of nighttime organic aerosol increases during the CalNex-2010
130 experiment in Bakersfield, CA. In an aircraft study near Houston, TX, Brown et al. (Brown et al.,
131 2013) observed elevated organic aerosol in the nighttime boundary layer, and correlated vertical
132 profiles of organic and nitrate aerosol in regions with rapid surface level NO_3 radical production
133 and BVOC emissions. From these observations, the authors estimated an SOA source from
134 NO_3 + BVOCs within the nocturnal boundary layer of $0.05 - 1 \mu\text{g m}^{-3} \text{h}^{-1}$. Carlton et al. (Carlton
135 et al., 2009) note the large scatter in chamber-measured SOA yields from isoprene

136 photooxidation and point throughout their review of SOA formation from isoprene to the likely
137 importance of poorly understood later generations of chemistry in explaining field observations.
138 We suggest that similar differences in multi-generational chemistry could explain the variation
139 among the (sparse) chamber and field observations of NO_3 + isoprene yields described in the
140 previous paragraph, and summarized in a recent review of NO_3 + BVOC oxidation mechanisms
141 and SOA formation (Ng et al., 2017).

142
143 The initial products of NO_3 + isoprene include organic nitrates, some of which will partially
144 partition to the aerosol phase. Organic nitrates in the particle phase (pRONO_2) are challenging
145 to quantify with online methods, due to both interferences and their often overall low
146 concentrations in ambient aerosol. Hence, field datasets to constrain modeled pRONO_2 are
147 sparse (Fisher et al., 2016, Ng et al., 2017). One of the most used methods in recent studies,
148 used also here, is quantification with the Aerodyne Aerosol Mass Spectrometer (AMS). Organic
149 nitrates thermally decompose in the AMS vaporizer and different approaches have been used to
150 apportion the organic fraction contributing to the total nitrate signal. Allan et al. (Allan et al.,
151 2004) first proposed the use of nitrate peaks at m/z 30 and 46 to distinguish various nitrate
152 species with the AMS. Marcolli et al. (Marcolli et al., 2006), in the first reported tentative
153 assignment of aerosol organic nitrate using AMS data, used cluster analysis to analyze data
154 from the 2002 New England Air Quality Study. In that study, cluster analysis identified two
155 categories with high m/z 30 contributions. One of these peaked in the morning when NO_x was
156 abundant and was more prevalent in plumes with lowest photochemical ages, potentially from
157 isoprene oxidation products. The second was observed throughout the diurnal cycle in both
158 fresh and aged plumes, and contained substantial m/z 44 contribution (highly oxidized OA). A
159 subsequent AMS laboratory and field study discussed and further developed methods for
160 separate quantification of organic nitrate (in contrast to inorganic nitrate) (Farmer et al., 2010). A
161 refined version of one of these separation methods, based on the differing $\text{NO}_2^+/\text{NO}^+$
162 fragmentation ratio for organic vs. inorganic nitrate, was later employed to quantify organic
163 nitrate aerosol at two forested rural field sites where strong biogenic VOC emissions and
164 relatively low NO_x combined to make substantial organic nitrate aerosol concentrations ((Fry et
165 al., 2013, Ayres et al., 2015)). Most recently, Kiendler-Scharr et al. (Kiendler-Scharr et al., 2016)
166 used a variant of this method to conclude that across Europe, organic nitrates comprise ~40%
167 of submicron organic aerosol. Modeling analysis concluded that a substantial fraction of this
168 organic nitrate aerosol is produced via NO_3 radical initiated chemistry. Chamber studies have
169 employed this fragmentation ratio method to quantify organic nitrates (Fry et al., 2009, Rollins et
170 al., 2009, Bruns et al., 2010, Fry et al., 2011, Boyd et al., 2015), providing the beginnings of a
171 database of typical organonitrate fragmentation ratios from various BVOC precursors.

172
173 Measurements conducted at the SOAS ground site in Centreville, Alabama in 2013 found
174 evidence of significant organonitrate contribution to SOA mass loading. Xu et al. (2015) reported
175 that organic nitrates constituted 5 to 12% of total organic aerosol mass from AMS data applying
176 a variant of the $\text{NO}_2^+/\text{NO}^+$ ratio method. They identify a nighttime-peaking "LO-OOA" AMS factor
177 which they attribute to mostly NO_3 oxidation of BVOC (in addition to O_3 + BVOC). They
178 estimated that the NO_3 radical oxidizes 17% of isoprene, 20% of α -pinene, and 38% of β -pinene
179 in the nocturnal boundary layer at this site. However, applying laboratory-based SOA yields to

Juliane Fry 7/31/2018 9:45 AM

Deleted: Xu et al.,

Juliane Fry 5/26/2018 6:00 PM

Deleted: Xu et al. (Xu et al., 2015)

182 model the predicted increase in OA, Xu et al. predict only $0.7 \mu\text{g m}^{-3}$ of SOA would be
183 produced, substantially lower than the measured nighttime LO-OOA production of $1.7 \mu\text{g m}^{-3}$.
184 The more recent analysis of Zhang et al. (Zhang et al., 2018) found a strong correlation of
185 monoterpene SOA with the fraction of monoterpene oxidation attributed to NO_3 , even for non-
186 nitrate containing aerosol, suggesting an influence of NO_3 even in pathways that ultimately
187 eliminate the nitrate functionality from the SOA, such as hydrolysis or NO_2 regeneration. Ayres
188 et al. (Ayres et al., 2015) used a correlation of overnight organonitrate aerosol buildup with
189 calculated net NO_3 + monoterpene and isoprene reactions to estimate an overall NO_3 +
190 monoterpene SOA mass yield of 40 – 80%. The factor of two range in this analysis was based
191 on two different measurements of aerosol-phase organic nitrates. These authors used similar
192 correlations to identify specific CIMS-derived molecular formulae that are likely to be NO_3 radical
193 chemistry products of isoprene and monoterpenes, and found minimal contribution of identified
194 first-generation NO_3 + isoprene products to the aerosol phase (as expected based on their
195 volatility). Lee et al. (Lee et al., 2016) detected abundant highly functionalized particle-phase
196 organic nitrates at the same site, with apparent origin both from isoprene and monoterpenes,
197 and both daytime and nighttime oxidation, and estimated their average contribution to
198 submicron organic aerosol mass to be between 3 – 8 %. For the same ground campaign,
199 Romer et al. (Romer et al., 2016) found evidence of rapid conversion from alkyl nitrates to
200 HNO_3 , with total alkyl nitrates having an average daytime lifetime of 1.7 hours.

201
202 Xie et al. (Xie et al., 2013) used a model constrained by observed alkyl nitrate correlations with
203 O_3 from the INTEX-NA/ICARTT 2004 field campaign to determine a range of isoprene nitrate
204 lifetimes between 4 and 6 hours, with 40-50% of isoprene nitrates formed by NO_3 + isoprene
205 reactions. Laboratory studies show that not all organic nitrates hydrolyze to HNO_3 equally
206 rapidly: primary and secondary organic nitrates were found to be less prone to aqueous
207 hydrolysis than tertiary organic nitrates (Darer et al., 2011, Hu et al., 2011, Boyd et al., 2015,
208 Fisher et al., 2016). This suggests that field-based estimates of the contribution of organic
209 nitrates to SOA formation could be a lower limit, if they are based on measurement of those
210 aerosol-phase nitrates. This is because if hydrolysis is rapid, releasing HNO_3 but leaving behind
211 the organic fraction in the aerosol phase, then that organic mass would not be accurately
212 accounted for as arising from nitrate chemistry. This was addressed in a recent modeling study
213 of SOAS (Pye et al., 2015) in which modeled hydrolysis products of particulate organic nitrates
214 of up to $0.8 \mu\text{g m}^{-3}$ additional aerosol mass loading in the southeast U.S. were included in the
215 estimate of change in OA due to changes in NO_x . Another recent GEOS-Chem modeling study
216 using of gas- and particle-phase organic nitrates observed during the SEAC⁴RS and SOAS
217 campaigns similarly finds RONO_2 to be a major sink of NO_x across the SEUS region (Fisher et
218 al., 2016, Lee et al., 2016).

219
220 Complementing these SOAS ground site measurements, the NOAA-led SENEX (Southeast
221 Nexus) aircraft campaign conducted 18 research flights focused in part on studying the
222 interactions between biogenic and anthropogenic emissions that form secondary pollutants
223 between 3 June and 10 July 2013 (Warneke et al., 2016). Flight instrumentation focused on
224 measurement of aerosol precursors and composition enable the present investigation of SOA
225 yields using this aircraft data set. Edwards et al. (Edwards et al., 2017) used data from the

Juliane Fry 5/15/2018 10:12 PM

Deleted: a factor of three

227 SENEX night flights to evaluate the nighttime oxidation of BVOC, observing high nighttime
228 isoprene mixing ratios in the residual layer that can undergo rapid NO_3 oxidation when sufficient
229 NO_x is present. These authors suggest that past NO_x reductions may have been uncoupled
230 from OA trends due to NO_x not having been the limiting chemical species for OA production, but
231 that future reductions in NO_x may decrease OA if NO_3 oxidation of BVOC is a substantial
232 regional SOA source. Because isoprene is ubiquitous in the nighttime residual layer over the
233 southeastern United States and the NO_3 + isoprene reaction is rapid, NO_3 reaction will be
234 dominant relative to O_3 in places with anthropogenic inputs of NO_x (Edwards et al. (Edwards et
235 al., 2017) concludes that when $\text{NO}_2/\text{BVOC} > 0.5$, NO_3 oxidation will be dominant). Hence, a
236 modest NO_3 + isoprene SOA yield may constitute a regionally important OA source.

237
238 Several modeling studies have investigated the effects of changing NO_x on global and SEUS
239 SOA. Hoyle et al. (Hoyle et al., 2007) found an increase in global SOA production from 35 Tg yr^{-1}
240 to 53 Tg yr^{-1} since preindustrial times, resulting in an increase in global annual mean SOA
241 mass loading of 51%, attributable in part to changing NO_x emissions. Zheng et al. (Zheng et al.,
242 2015) found only moderate SOA reductions from a 50% reduction in NO emissions: 0.9 – 5.6 %
243 for global NO_x or 6.4 – 12.0% for southeast US NO_x , which they attributed to buffering by
244 alternate chemical pathways and offsetting tendencies in the biogenic vs. anthropogenic SOA
245 components. In contrast, Pye et al. (Pye et al., 2015) find a 9% reduction in total organic aerosol
246 in Centreville, AL for only 25% reduction in NO_x emissions. A simple limiting-reagent analysis of
247 NO_3 + monoterpene SOA from power plant plumes across the United States found that between
248 2008 and 2011, based on EPA-reported NO_x emissions inventories, some American power
249 plants shifted to the NO_x -limited regime (from 3.5% to 11% of the power plants), and showed
250 that these newly NO_x -limited power plants were primarily in the southeastern United States (Fry
251 et al., 2015). The effect of changing NO_x on SOA burden is clearly still in need of further study.

252
253 Here, we present aircraft transects of spatially discrete NO_x plumes from electric generating
254 units (EGU), or power plants (PP), as a method to specifically isolate the influence of NO_3
255 oxidation. These plumes are concentrated and highly enriched in NO_x over a scale of only a
256 few km (Brown et al., 2012), and have nitrate radical production rates ($P(\text{NO}_3)$) 10 – 100 times
257 greater than those of background air. The rapid shift in $P(\text{NO}_3)$ allows direct comparison of air
258 masses with slow and rapid oxidation rates attributable to the nitrate radical, effectively isolating
259 the influence of this single chemical pathway in producing SOA and other oxidation products.
260 Changes in organic nitrate aerosol (pRONO_2) concentration and accompanying isoprene
261 titration enable a direct field determination of the SOA yield from NO_3 + isoprene.

262 **2 Field campaign and experimental and modeling methods**

263 The Southeast Nexus (SENEX: <http://esrl.noaa.gov/csd/projects/senex/>) campaign took place 3
264 June through 10 July 2013 as the NOAA WP-3D aircraft contribution to the larger Southeast
265 Atmospheric Study (SAS: http://www.eol.ucar.edu/field_projects/sas/), a large, coordinated
266 research effort focused on understanding natural and anthropogenic emissions, oxidation
267 chemistry and production of aerosol in the summertime atmosphere in the southeastern United
268 States. The NOAA WP-3D aircraft operated 18 research flights out of Smyrna, Tennessee,

269 carrying an instrument payload oriented towards elucidating emissions inventories and reactions
270 of atmospheric trace gases, and aerosol composition and optical properties (Warneke et al.,
271 2016). One of the major goals of the larger SAS study is to quantify the fraction of organic
272 aerosol that is anthropogenically controlled, with a particular focus on understanding how OA
273 may change in the future in response to changing anthropogenic emissions.
274

275 The subset of aircraft instrumentation employed for the present analysis of nighttime NO_3 +
276 isoprene initiated SOA production includes measurements used to determine NO_3 radical
277 production rate ($P(\text{NO}_3) = k_{\text{NO}_2+\text{O}_3}(\text{T}) [\text{NO}_2] [\text{O}_3]$), isoprene and monoterpene concentrations,
278 other trace gases for plume screening and identification, aerosol size distributions, and aerosol
279 composition. The details on the individual measurements and the overall aircraft deployment
280 goals and strategy are described in Warneke et al. (Warneke et al., 2016). Briefly, NO_2 was
281 measured by UV photolysis and gas-phase chemiluminescence (P-CL) and by cavity ringdown
282 spectroscopy, (CRDS), which agreed within 6%. O_3 was also measured by both gas-phase
283 chemiluminescence and CRDS and agreed within 8%, within the combined measurement
284 uncertainties of the instruments. Various volatile organic compounds were measured with
285 several techniques, including for the isoprene and monoterpenes of interest here, proton
286 reaction transfer mass spectrometry (PTR-MS) and canister whole air samples and post-flight
287 GC-MS analysis (iWAS/GCMS). A comparison of PTR-MS and iWAS/GCMS measurements of
288 isoprene during SENEX has high scatter due to imperfect time alignment and isoprene's high
289 variability in the boundary layer, but the slope of the intercomparison is 1.04 ((Warneke et al.,
290 2016); for more details on the VOC intercomparisons, see also Lerner et al., (Lerner et al.,
291 2017)). Acetonitrile from the PTRMS was used to screen for the influence of biomass burning.
292 Sulfur dioxide (SO_2) was used to identify emissions from coal-fired power plants. All gas-phase
293 instruments used dedicated inlets, described in detail in the supplemental information for
294 Warneke et al. (Warneke et al., 2016).
295

296 Aerosol particles were sampled downstream of a low turbulence inlet (Wilson et al., 2004), after
297 which they were dried by ram heating, size-selected by an impactor with 1 μm aerodynamic
298 diameter size cut-off, and measured by various aerosol instruments (Warneke et al., 2016). An
299 ultra-high-sensitivity aerosol sizing spectrometer (UHSAS, Particle Metrics, Inc., Boulder, CO
300 (Cai et al., 2008, Brock et al., 2011)) was used to measure the dry submicron aerosol size
301 distribution down to about 70 nm. Data for the UHSAS are reported at 1 Hz whereas AMS data
302 were recorded roughly every 10 seconds. The ambient (wet) surface areas were calculated
303 according to the procedures described in Brock et al., 2016 (Brock et al., 2016). A pressure-
304 controlled inlet (Bahreini et al., 2008) was employed to ensure that a constant mass flow rate
305 was sampled by a compact time-of-flight aerosol mass spectrometer (C-ToF-AMS) which
306 measured the non-refractory aerosol composition (Drewnick et al., 2005). The aerosol volume
307 transmitted into the AMS was calculated by applying the measured AMS lens transmission
308 curve (Bahreini et al., 2008) to the measured particle volume distributions from the UHSAS. For
309 the entire SENEX study, the mean, calculated fraction of aerosol volume behind the 1 micron
310 impactor that was transmitted through the lens into the AMS instrument was 97% (with $\pm 4\%$
311 standard deviation), indicating that most of the submicron aerosol volume measured by the
312 sizing instruments was sampled by the AMS.

313

314 After applying calibrations and the composition-dependent collection efficiency following
315 Middlebrook et al. (Middlebrook et al., 2012), the limits of detection for the flight analyzed here
316 were $0.05 \mu\text{g m}^{-3}$ for nitrate, $0.26 \mu\text{g m}^{-3}$ for organic mass, $0.21 \mu\text{g m}^{-3}$ for ammonium, and 0.05
317 $\mu\text{g m}^{-3}$ for sulfate, determined as three times the standard deviation of 10-second filtered air
318 measurements obtained for 10 minutes during preflight and 10 minutes during postflight (110
319 datapoints). Note that the relative ionization efficiency for ammonium was 3.91 and 3.87 for the
320 two bracketing calibrations and an average value of 3.9 was used for the flight analyzed here.
321 An orthogonal distance regression (ODR-2) of the volume from composition data (AMS mass
322 plus refractory black carbon) using a mass weighted density as described by Bahreini et al.
323 (Bahreini et al., 2009) versus the volume based on the sizing instruments (after correcting for
324 AMS lens transmission as above) had a slope of 1.06 for the entire SENEX study and 72% of
325 the data points were within the measurements' combined uncertainties of $\pm 45\%$ (Bahreini et al.,
326 2008). For the flight analyzed here, however, the same regression slope was 1.58, which is
327 slightly higher than the combined uncertainties. It is unclear why the two types of volume
328 measurements disagree more for this flight. This does not change the conclusions of this work
329 because this has been incorporated into the error in aerosol organic nitrate, which still show
330 positive enhancements in pRONO₂ for these plumes (see Figure 4 below). These complete
331 error estimates are also used in Figure 5 to clearly show the uncertainties in the yields. The
332 volume comparison is discussed further in the Supplemental Information and shown for the
333 plumes of interest in Fig. S1.

334

335 The C-ToF-AMS is a unit mass resolution (UMR) instrument and the mass spectral signals that
336 are characteristic of aerosol nitrate at m/z 30 and 46 (NO^+ and NO_2^+) often contain interferences
337 from organic species such as CH_2O^+ and CH_2O_2^+ , respectively. Here, the m/z 30 and 46 signals
338 have been corrected for these interferences by using correlated organic signals at m/z 29, 42,
339 43, and 45 that were derived from high-resolution AMS measurements during the NASA
340 SEAC⁴RS campaign that took place in the same regions of the SE US shortly after SENEX (see
341 Supplemental Information and Fig. S2). The corrections were applied to the individual flight
342 analyzed here from July 2. All of the corrections were well correlated with each other for the
343 SEAC⁴RS dataset and we used the organic peak at m/z 29 (from CHO^+) and the peak at m/z 45
344 (from CHO_2^+), respectively, since those corrections were from peaks closest (in m/z) to those
345 being corrected. Once corrected, the nitrate mass concentrations in the final data archive for
346 this flight were reduced by 0-0.24 $\mu\text{g sm}^{-3}$, an average reduction of $0.11 \mu\text{g sm}^{-3}$ or 32% from
347 the initial nitrate mass concentrations. The organic interferences removed from the m/z 30 and
348 m/z 46 signals are linearly correlated with the total organic mass concentrations, corresponding
349 to an average 1.3% increase in the total organic mass.

350

351 The ratio of the corrected $\text{NO}_2^+/\text{NO}^+$ signals was then used to calculate the fraction of aerosol
352 nitrate that was organic (pRONO₂) or inorganic (ammonium nitrate) based on the method
353 described first in (Fry et al., 2013). Here we used an organic $\text{NO}_2^+/\text{NO}^+$ ratio that was equal to
354 the ammonium nitrate $\text{NO}_2^+/\text{NO}^+$ ratio from our calibrations divided by 2.8. This factor was
355 determined from multiple datasets (see discussion in Supplemental Information). The
356 ammonium nitrate $\text{NO}_2^+/\text{NO}^+$ ratio was obtained from the two calibrations on 30 June and 7 July

Juliane Fry 5/31/2018 5:01 PM

Deleted: , since other flights during this field project compared better;

Juliane Fry 5/31/2018 5:01 PM

Deleted: t

Juliane Fry 5/31/2018 5:47 PM

Deleted: ,

Juliane Fry 5/31/2018 5:10 PM

Deleted: but

Juliane Fry 5/31/2018 5:10 PM

Deleted: comparisons are

Juliane Fry 5/26/2018 6:02 PM

Deleted: Fry et al. [27]

Juliane Fry 5/26/2018 10:18 PM

Deleted: compiled by Day et al (Day et al., 2017)

Juliane Fry 5/26/2018 10:19 PM

Deleted: , who discuss the uncertainties of this approach in detail

368 that bracketed the flight on 2 July, which is analyzed here. It was 0.514 and 0.488, respectively,
369 and for all of the data from both calibrations it averaged 0.490. Hence, the organic nitrate
370 $\text{NO}_2^*/\text{NO}^*$ ratio was estimated to be 0.175. This is the first time, to our knowledge, that UMR
371 measurements of aerosol nitrate have been corrected with HR correlations and used to
372 apportion the corrected nitrate into inorganic or organic nitrate species.

373

374 The time since emission of intercepted power plant plumes was estimated from the slope of a
375 plot of O_3 against NO_2 . For nighttime emitted NO_x plumes that consist primarily of NO (Peischl
376 et al., 2010), O_3 is negatively correlated with NO_2 due to the rapid reaction of NO with O_3 that
377 produces NO_2 in a 1:1 ratio:

378



380

381 Reaction R1 goes rapidly (NO pseudo first order loss rate coefficient of 0.03 s^{-1} at 60 ppb O_3) to
382 completion, so that all NO_x is present as NO_2 , as long as the plume NO does not exceed
383 background O_3 after initial mixing of the plume into background air. Subsequent oxidation of
384 NO_2 via reaction (R2) leads to an increasingly negative slope of O_3 vs NO_2 :

385



387

388 Equation (1) then gives plume age subsequent to the completion of (R1) in terms of the
389 observed slope, m , of O_3 vs NO_2 (Brown et al., 2006).

390

$$391 \quad t_{\text{plume}} = \frac{\ln[1-S(m+1)]}{sk_1\bar{O}_3} \quad (1)$$

392

393 Here S is a stoichiometric factor that is chosen for this analysis to be 1 based on agreement of
394 plume age with elapsed time in a box model run initialized with SENEX flight conditions (see
395 below); k_1 is the temperature dependent bimolecular rate constant for $\text{NO}_2 + \text{O}_3$ (R2) and \bar{O}_3 is
396 the average O_3 within the plume.

397

398 We calculate plume ages using both a stoichiometric factor of 1 (loss of NO_3 and N_2O_5
399 dominated by NO_3 reactions) and 2 (loss dominated by N_2O_5 reactions), although we note that
400 the chemical regime for $\text{NO}_3+\text{N}_2\text{O}_5$ loss may change over the lifetime of the plume, progressing
401 from 1 to 2 as the BVOC is consumed. We use $S=1$ values in the analysis that follows. Because
402 the more aged plumes are more likely to have S approach 2, this means that some of the older
403 plumes may have overestimated ages. Fig. S3 in the Supplemental Information shows the
404 plume age calculated by Eq. 1 using modeled NO_x , NO_y and O_3 concentrations for $S=1$ and
405 $S=2$, from nighttime simulations of plume evolution using an observationally constrained box
406 model. This confirms that for nighttime plumes, $S=1$ plume ages match modeled elapsed time
407 well. The model used for this calculation, and those used to assess peroxy radical lifetimes and
408 fates in Section 4.3, was the Dynamically Simple Model of Atmospheric Chemical Complexity
409 (DSMACC (Emmerson and Evans 2009)) containing the Master Chemical Mechanism v3.3.1
410 chemistry scheme (Jenkin et al., 2015). More details on the model approach are provided in the
411 SI.

Juliane Fry 5/15/2018 9:54 PM

Deleted: 2

Juliane Fry 6/1/2018 8:11 AM

Deleted: .

414 3 Nighttime flight selection

415 There were three nighttime flights (takeoffs on the evenings of 19 June, 2 July, and 3 July,
416 2013, local time) conducted during SENEX, of which one (2 July) surveyed regions surrounding
417 Birmingham, Alabama, including multiple urban and power plant plume transects. As described
418 in the introduction, these plume transects are the focus of the current analysis since they
419 correspond to injections of concentrated NO (and subsequently high $P(\text{NO}_3)$) into the regionally
420 widespread residual layer isoprene. The nighttime flight on 3 July, over Missouri, Tennessee
421 and Arkansas sampled air more heavily influenced by biomass burning than biogenic emissions.
422 The 19 June night flight sampled earlier in the evening, in the few hours immediately after
423 sunset, and sampled more diffuse urban plume transects that had less contrast with background
424 air. Therefore, this paper uses data exclusively from the 2 July flight, in which 9 transects of
425 well-defined NO_x plumes from power plants emitted during darkness can be analyzed to obtain
426 independent yields measurements.

427
428 A map of the 2 July flight track is shown in Fig. 1a. After takeoff at 8:08 pm local Central
429 Daylight Time on 2 July, 2013 (1:08 am UTC 3 July, 2016), the flight proceeded towards the
430 southwest until due west of Montgomery, AL, after which it conducted a series of east-west
431 running tracks while working successively north toward Birmingham, AL. Toward the east of
432 Birmingham, the aircraft executed overlapping north-south tracks at six elevations to sample the
433 E. C. Gaston power plant. During the course of the flight, concentrated NO_x plumes from the
434 Gaston, Gorgas, Miller and Greene City power plants were sampled. Around 1:30 and 2:30 AM
435 Central Daylight Time (5:30 and 6:30 am UTC), two transects of the Birmingham, AL urban
436 plume were measured prior to returning to the Smyrna, TN airport base.

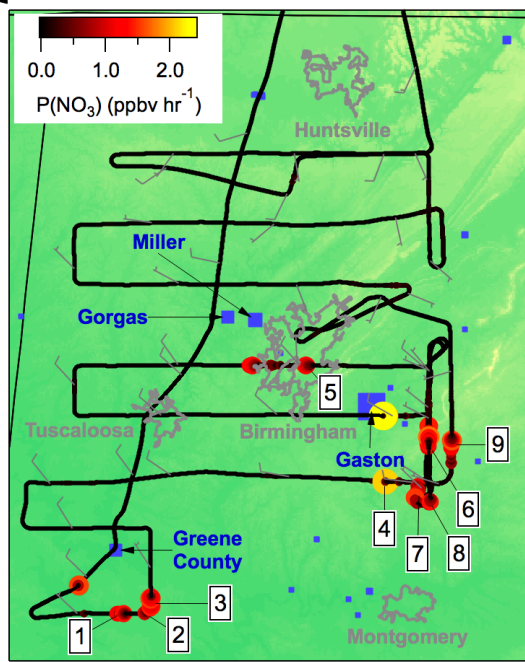
437
438 The flight track is shown colored by the nitrate radical production rate, $P(\text{NO}_3)$, to show the
439 points of urban and/or power plant plume influence:

$$440 \quad P(\text{NO}_3) = k_2(T) [\text{NO}_2][\text{O}_3] \quad (2)$$

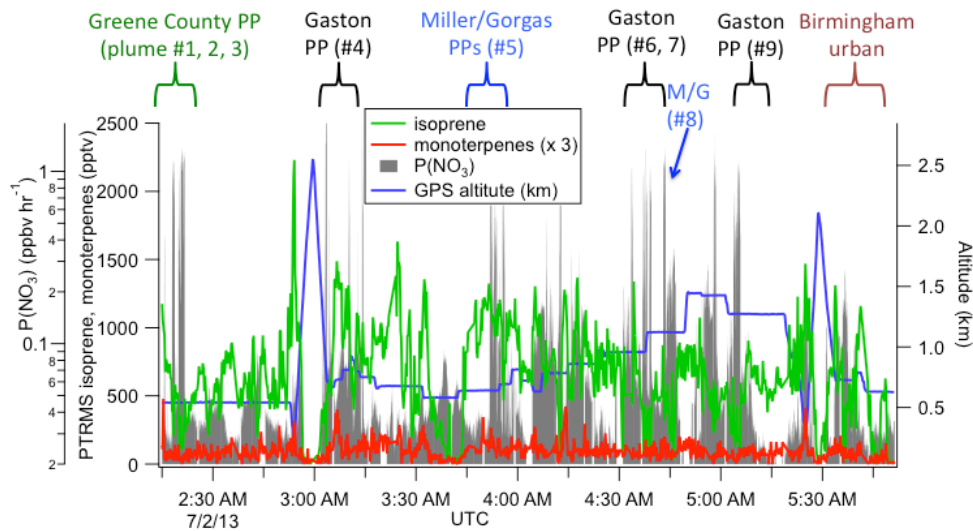
441
442 Here, k_2 is again the temperature-dependent rate coefficient for reaction of $\text{NO}_2 + \text{O}_3$ (Atkinson
443 et al., 2004), and the square brackets indicate **concentrations**. Fig. 1b further illustrates the
444 selection of power plants plumes: sharp peaks in $P(\text{NO}_3)$ are indicative of power plant plume
445 transects, during which isoprene mixing ratios also are observed to drop from the typical
446 regional residual layer background values of ~ 1 ppb, indicative of loss by NO_3 oxidation (an
447 individual transect is shown in more detail below in Fig. 2). Also shown in Fig. 1b are measured
448 concentrations of isoprene and monoterpenes throughout the flight, showing substantial residual
449 layer isoprene and supporting the assumption that effectively all NO_3 reactivity is via isoprene
450 (see calculation in next section). Residual layer concentrations of other VOCs that could
451 produce SOA (e.g., aromatics) are always below 100 pptv, and their reaction rates with NO_3 are
452 slow. Edwards *et al.* (Edwards et al., 2017) have shown that NO_3 and isoprene mixing ratios for
453 this and other SENEX night flights exhibit a strong and characteristic anticorrelation that is
454 consistent with nighttime residual layer oxidation chemistry.
455
456

Juliane Fry 5/15/2018 9:06 PM

Deleted: number densities



458 1a
459 1b



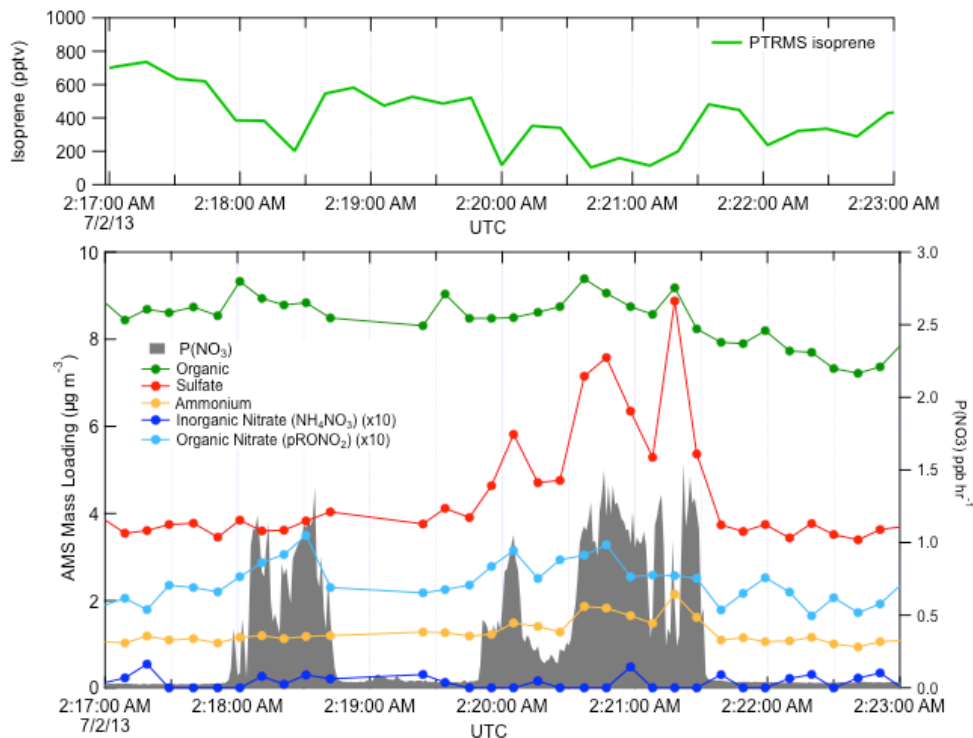
460
461 **Figure 1a.** Map of northern Alabama, showing the location of the flight track of the 2 July 2013
462 night flight used in the present analysis, with plume numbers labeled and wind direction shown.
463 Although the wind direction changed throughout the night, these measurements enable us to

464 attribute each plume to a power plant source (see labels in Figure 1b and Table 2). Color scale
465 shows $P(\text{NO}_3)$ based on aircraft-measured $[\text{NO}_2]$ and $[\text{O}_3]$, while power plants discussed in the
466 text are indicated in blue squares with marker size scaled to annual NO_x emissions for 2013
467 (scale not shown). Isoprene emissions are widespread in the region (Edwards et al., 2017).
468 **Figure 1b** shows time series data from the same flight, with plume origins and numbers labeled,
469 showing aircraft-measured isoprene and monoterpene concentrations, altitude, and $P(\text{NO}_3)$
470 determined according to Eq. 2 (log scale), showing that the isoprene was uniformly distributed
471 (mixing ratios often in excess of 1 ppbv), while the more reactive monoterpenes were present at
472 mixing ratios below 100 ppt except at the lowest few hundred meters above ground in the
473 vertical profiles (not used in the present analysis). Figure 1b also shows that sharp peaks in
474 nitrate radical production rate occur both at the lowest points of these vertical profiles, when the
475 aircraft approached the surface, but also frequently during periods of level flight in the residual
476 layer, which correspond to the power plant plume transects analyzed in this paper.

477 **4 Results**

478 **4.1 Selection of plumes**

479 Figure 2 shows a subset of the July 2 flight time series data, illustrating three NO_x plumes used
480 for analysis. The large NO_3 source and isoprene loss was accompanied by an increase in
481 organic nitrate aerosol mass, which we attribute to the $\text{NO}_3 + \text{isoprene}$ reaction based on prior
482 arguments. We observed each plume as a rapid and brief perturbation to background
483 conditions, of order 10 – 50 sec., or 1 – 5 km in spatial scale. Each plume's perturbed
484 conditions can correspond to different plume ages, depending on how far downwind of the
485 power plant the plume transect occurred.



487
 488 **Figure 2.** Three representative plume transect observations from the 2 July 2013 flight (plumes
 489 are identified by the peaks in $P(\text{NO}_3)$, listed in Table 1 at times 02:18, 02:20, and 02:21 UTC).
 490 Note the difference in sulfate enhancement in the three plumes, which is largest in the third
 491 plume, and is accompanied by increases in ammonium. In all three cases, the isoprene
 492 concentration drops in the plumes, accompanied by a clear increase in organic nitrate, no
 493 changes in the inorganic nitrate, and a modest changes in organic aerosol mass concentrations.
 494

495 Candidate plumes were initially identified by scanning the time series flight data for any period
 496 where the production rate of nitrate radical ($P(\text{NO}_3)$) rose above 0.5 ppbv hr^{-1} . This threshold
 497 was chosen to be above background noise and large enough to isolate only true plumes (see
 498 Fig. 1a). The value is thus subjectively chosen, but was consistently applied across the dataset.
 499 For each such period, a first screening removed any of these candidate plumes that occurred
 500 during missed approaches or other periods where radar altitude above ground level (AGL) was
 501 changing, because in the stratified nighttime boundary layer structure, variations in altitude may
 502 result in sampling different air-masses, rendering the adjacent out of plume background not
 503 necessarily comparable to in-plume conditions. A second criterion for rejection of a plume was
 504 missing isoprene or AMS data during brief plume intercepts. No selected plumes on July 2
 505 showed enhanced acetonitrile or refractory black carbon, indicating no significant biomass

506 burning influence. Finally, two plumes downwind of the Gaston power plant (at 03:10 and
507 03:14) were removed from the present analysis, because (03:10) the background isoprene was
508 changing rapidly, preventing a good baseline measurement, and (03:14) there was no observed
509 decrease in isoprene concentration in-plume (as well as no increase in nitrate aerosol). The
510 03:14 plume was apparently too recently emitted to have undergone significant nighttime
511 reaction; its O_3/NO_2 slope was unity to within the combined measurement error of O_3 and NO_2
512 (Eq. 1). After this filtering, there are 9 individual plume observations for determination of NO_3 +
513 isoprene SOA yields (see Table 1). The rapid increases in $P(NO_3)$ appeared simultaneously with
514 significant decreases in isoprene and increases in aerosol nitrate. The aerosol and isoprene
515 measurements (taken at data acquisition rates < 1 Hz) were not exactly coincident in time which
516 leads to some uncertainty in the yield analysis below.

517

518 Derivation of SOA yields from observed changes in isoprene and aerosol mass in plumes
519 depends on two conditions, and has several caveats that will be discussed in the text that
520 follows (see Table 3 below for a summary of these caveats). The two conditions are: (1) that the
521 majority of VOC mass consumed by NO_3 in plumes is isoprene (rather than monoterpenes or
522 other VOC), and then either or both (2a) that the change in aerosol organic mass concentration
523 during these plumes is due to NO_3 + isoprene reactions, and/or (2b) that the change in aerosol
524 nitrate mass concentration is due to NO_3 + isoprene reactions. There are separate
525 considerations for each of these conditions.

526

527 For the first condition, we note that the isoprene to monoterpenes ratio just outside each plume
528 transect was always high (a factor of 10 to 70, on average 26). With the 298 K NO_3 rate
529 constants of $\sim 5 \times 10^{-12} \text{ cm}^3 \text{ molec}^{-1} \text{ s}^{-1}$ for monoterpenes and $6.5 \times 10^{-13} \text{ cm}^3 \text{ molec}^{-1} \text{ s}^{-1}$ for
530 isoprene (Calvert et al., 2000), isoprene (~ 2 ppb) will always react faster with nitrate than
531 monoterpenes (~ 0.04 ppbv). At these relative concentrations, even if all of the monoterpene is
532 oxidized, the **production rate of oxidation products will** be much larger for isoprene. Contribution
533 to aerosol by N_2O_5 uptake is also not important in these plumes. Edwards et al. (Edwards et al.,
534 2017) calculated the sum of NO_3 and N_2O_5 loss throughout this flight and showed that it is
535 consistently NO_3 +BVOC dominated (Fig. S4 of that paper). As isoprene depletes, N_2O_5 uptake
536 will increasingly contribute to NO_3 loss, but as shown below, we are able to rule out a
537 substantial source of inorganic nitrate for most plumes. We also know that despite increased
538 OH production in-plume, the isoprene loss is still overwhelming dominated by NO_3 (Fig. S5 in
539 Edwards, et al. (Edwards et al., 2017)).

540

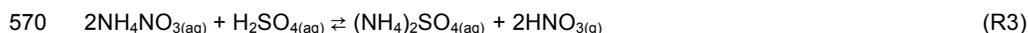
541 The second condition requires that we can find an aerosol signal that is attributable exclusively
542 to NO_3 + isoprene reaction products, whether it be organic aerosol (OA) or organic nitrate
543 aerosol ($pRONO_2$) mass loading, or both. We note that the ratio of in-plume aerosol organic
544 mass increase to $pRONO_2$ mass increase is noisy (see discussion below at Fig. 6), but indicates
545 an average in-plume ΔOA to $\Delta pRONO_2$ ratio of about 5. The large variability is primarily due to
546 the fact that the variability in organic aerosol mass between successive 10-second data points
547 for the entire flight is quite large (of order $0.75 \mu\text{g m}^{-3}$) and comparable to many of the individual
548 plume ΔOA increases, far exceeding the expected organonitrate driven increases in OA, which
549 are roughly twice the $pRONO_2$ mass increases. It is also possible that in these plumes, where

Juliane Fry 5/15/2018 9:56 PM

Deleted: mass of hydrocarbon conversion
will

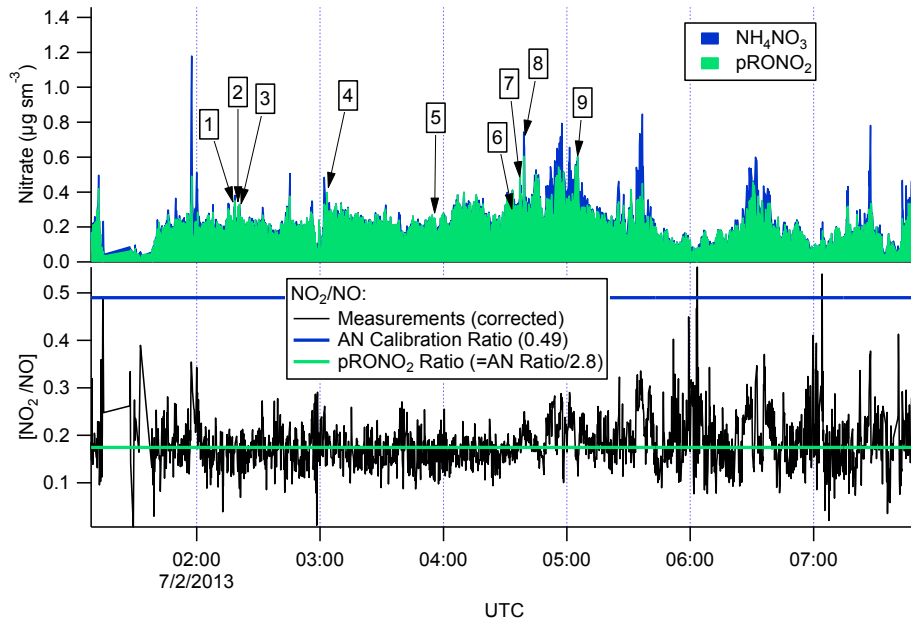
552 total aerosol mass is elevated, semivolatile organic compounds may re-partition to the aerosol
553 phase, contributing a non-pRONO₂ driven variability in ΔOA. For example, if some gas phase
554 IEPOX is present in the residual layer, it may be taken up into the highly acidic aerosol from the
555 power plants. Alternatively, very polar gas-phase compounds could partition further into the
556 higher liquid water associated with the sulfate in the plume. Therefore, in-plume organic aerosol
557 increases cannot be attributed clearly to NO₃ + isoprene SOA production, so we do not use
558 them in the SOA yield calculations.

559
560 This leaves consideration 2b, whether all increase in nitrate mass is due to NO₃ + isoprene
561 reactions. Here we must evaluate the possibility of inorganic nitrate aerosol production in these
562 high-NO_x plumes. Fine-mode aerosol inorganic nitrate can be formed by the (reversible)
563 dissolution of HNO_{3(g)} into aqueous aerosol. In dry aerosol samples, inorganic nitrate is typically
564 in the form of ammonium nitrate (NH₄NO₃), when excess ammonium is available after
565 neutralization of sulfate as (NH₄)₂SO₄ and NH₄(HSO₄). Because of the greater stability of
566 ammonium sulfate salt relative to ammonium nitrate, in high-sulfate plumes with limited
567 ammonium, inorganic nitrate aerosol will typically evaporate as HNO_{3(g)} (Guo et al., 2015)
568 (reaction R3):



571
572 Inorganic nitrate can also form when crustal dust (e.g. CaCO₃) or seasalt (NaCl) are available.
573 Uptake of HNO₃ is rendered favorable by the higher stability of nitrate mineral salts, evaporating
574 CO₂ or HCl. [Inorganic nitrate can also be produced by the heterogeneous uptake of N₂O₅ onto
575 aqueous aerosol; Edwards et al. \(2017\) demonstrated that this process is negligible relative to
576 NO₃ + BVOC for the July 2 SENEX night flight considered here.](#)

577
578 There are several lines of evidence that the observed nitrate aerosol is organic and not
579 inorganic. First, examination of the NO₂⁺/NO⁺ (interference-corrected *m/z* 46:*m/z* 30) ratio
580 measured by the aircraft AMS (Fig. 3) shows a ratio throughout the July 2 flight, including the
581 selected plumes, that is substantially lower than that from the bracketing ammonium nitrate
582 calibrations. This lower AMS measured NO₂⁺/NO⁺ ratio has been observed for organic nitrates
583 (Farmer et al., 2010), and some mineral nitrates (e.g. Ca(NO₃)₂ and NaNO₃, (Hayes et al.,
584 2013)), which are not important in this case because aerosol was dominantly submicron. As
585 described above, we can separate the observed AMS nitrate signal into pRONO₂ and inorganic
586 nitrate contributions. These mass loadings are also shown in Fig. 3, indicating dominance of
587 pRONO₂ throughout the flight.



589

590 **Figure 3.** For the flight under consideration, the estimated relative contributions of ammonium
 591 and organic nitrate to the total corrected nitrate signal (top panel) was calculated from the ratios
 592 of the corrected peaks at m/z 30 and 46 (lower panel). Each of the plumes is identified here by
 593 plume number. The ratios of $\text{NO}_2^+/\text{NO}^+$ (black data in the lower panel) from the corrected peaks
 594 at m/z 46 and 30, respectively, are compared to the ratios expected for ammonium nitrate (AN
 595 Calibration Ratio, blue horizontal line at 0.49) or organic nitrate (pRONO_2 Ratio, green
 596 horizontal line at 0.175 which is estimated from the AN calibration ratio using multiple data sets
 597 (see discussion in Supplemental Information). The measured ratio for most of the flight is more
 598 characteristic of organic nitrate than ammonium nitrate.
 599

600 We can also employ the comparison of other AMS-measured aerosol components during the
 601 individual plumes to assess the possibility of an inorganic nitrate contribution to total measured
 602 nitrate. Fig. S5a shows that the in-plume increases in sulfate are correlated with increases in
 603 ammonium with an R^2 of 0.4. The observed slope of 5.4 is characteristic of primarily $(\text{NH}_4)\text{HSO}_4$,
 604 which indicates that the sulfate mass is not fully neutralized by ammonium. We note, however,
 605 that if the largest observed aerosol nitrate increase is due solely to ammonium nitrate, the
 606 ammonium increase would be only $0.11 \mu\text{g m}^{-3}$, which would be difficult to discern from the NH_4
 607 variability of order $0.11 \mu\text{g m}^{-3}$. However, the slope is consistent with incomplete neutralization
 608 of the sulfate by ammonium, which would make $\text{HNO}_{3(\text{g})}$ the more thermodynamically favorable
 609 form of inorganic nitrate. The ion balance for the ammonium nitrate calibration particles and the
 610 plume enhancements are shown in Fig. S5b. Complete neutralization of the calibration aerosols
 611 is nearly always within the gray 10% uncertainty band for the relative ionization efficiency of

Juliane Fry 5/26/2018 9:56 PM
 Deleted: by Day et al. (Day et al., 2017)

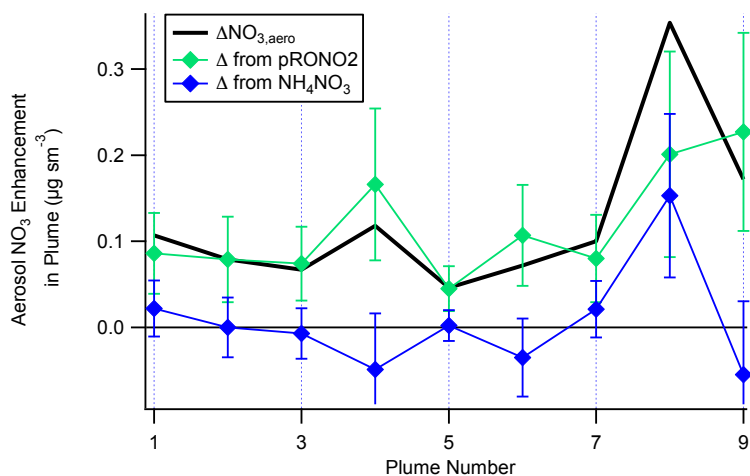
Juliane Fry 6/1/2018 8:39 AM
 Formatted: Normal

Juliane Fry 6/1/2018 8:39 AM
 Formatted: Font color: Auto

Juliane Fry 6/1/2018 8:39 AM
 Formatted: Font:Not Bold, Font color:
 Auto

613 ammonium (Bahreini et al., 2009). In contrast, many of the plume enhancements are near the
614 1:2 line (as primarily ammonium bisulfate) within the combined 10% ammonium and 15%
615 sulfate uncertainty error bars or without ammonium (sulfuric acid). Thus, NH_4NO_3 is unlikely to
616 be stable in the aerosol phase under the conditions of these plumes, consistent with the AMS
617 observations.

618
619 A plot of the calculated plume enhancements from the derived apportionment into organic
620 (pRONO_2) and inorganic (ammonium) nitrate is shown in Fig. 4. The increases in aerosol nitrate
621 for nearly all of the plumes appear to be mostly due to enhancements in pRONO_2 . Based on
622 these considerations, we conclude that in-plume pRONO_2 mass increases are a consequence
623 (and thus a robust measure) of organic nitrate aerosol produced from NO_3 + isoprene. Since
624 each isoprene molecule condensing will have one nitrate group, the ratio of these increases to
625 isoprene loss is a direct measure of the molar organic aerosol yield from NO_3 -isoprene
626 oxidation.



627

628

629 **Figure 4.** The contribution of each species to the nitrate enhancements in each of the plumes,
630 showing that the enhancements in most of the plumes are mainly due to enhancements in
631 organic nitrate, with the exception of Plume 8 which had enhancements in both organic and
632 ammonium nitrate. Error bars are estimated from the measurement variability, the UMR
633 corrections to the nitrate signals, apportionment between organic and inorganic nitrate, and the
634 total nitrate uncertainty (see Supplemental Information).

635

636 Table 1 shows the selected plumes to be used for yield analysis. Wherever possible, multiple
637 points have been averaged for in-plume and background isoprene and nitrate aerosol
638 concentrations; in each case the number of points used is indicated and the corresponding
639 standard deviations are reported. In two cases (2:20 and 3:03 plumes), the plumes were so
640 narrow that only a single point was measured in-plume at the 10 s time resolution of the PTR-

Juliane Fry 6/1/2018 8:39 AM

Formatted: Font:(Default) Times, 10 pt,
Font color: Auto

641 MS and AMS; for these “single-point” plumes it is not possible to calculate error bars. Error bars
642 were determined using the standard deviations calculated for in-plume and background
643 isoprene and nitrate aerosol concentrations, [accounting also for the additional uncertainty in the](#)
644 [AMS measurement described in the caption to Figure 4](#), and propagated through the yield
645 formula detailed in the following section.
646

647 **Table 1.** List of plumes used in this NO₃ + isoprene SOA yield analysis. For each plume, the
 648 delta-values listed indicate the difference between in-plume and outside-plume background in
 649 average observed concentration, and the standard deviations (SD) are the propagated error
 650 from this subtraction. (For ΔNO₃ from pRONO₂, the standard deviations also include error
 651 propagated as described in the caption for Figure 4) After each plume number, the numbers of
 652 points averaged for isoprene (10 s resolution) and AMS (10 s resolution), respectively, are
 653 listed. Because the isoprene data were reported at a lower frequency, these numbers are
 654 typically lower to cover the same period of time. Plume numbers annotated with * indicate brief
 655 plumes for which only single-point measurements of in-plume aerosol composition were
 656 possible. Additional AMS and auxiliary data from each plume is included in the Supplemental
 657 Information, Table S3.

plume number [#isop/#AMS]	7/2/13 plume time (UTC)	P(NO ₃) (ppbv hr ⁻¹)	ΔISOP (ppt) [± SD]	ΔNO _{3,aero} (μg m ⁻³) [± SD]	ΔNO ₃ from pRONO ₂ (μg m ⁻³) [± SD]	ΔNO ₃ from NH ₄ NO ₃ (μg m ⁻³) [± SD]
Typical variability (μg m ⁻³):				0.05	0.05	0.05
1 [2/3]	2:18	0.9	-335 [128]	0.107 [0.039]	0.086 [0.047]	0.022 [0.012]
2 [*]	2:20	0.8	-404	0.079	0.079 [0.049]	0
3 [4/5]	2:21	1.2	-228 [121]	0.067 [0.039]	0.074 [0.043]	-0.007 [0.027]
4 [*]	3:03	1.4	-453	0.118	0.166 [0.088]	-0.049
5** [3/4]	3:55	1.0	-255 [251]	0.046 [0.019]	0.045 [0.026]	0.002 [0.015]
6 [2/2]	4:34	0.6	-713 [219]	0.072 [0.031]	0.107 [0.059]	-0.035 [0.029]
7 [5/6]	4:37	0.8	-298 [197]	0.100 [0.082]	0.080 [0.051]	0.021 [0.034]
8*** [2/3]	4:39	0.9	-443 [75]	0.354 [0.058]	0.201 [0.120]	0.153 [0.057]
9 [7/8]	5:04	0.6	-293 [131]	0.172 [0.048]	0.227 [0.115]	-0.055 [0.042]

658 **Plume 5 has the smallest ΔNO_{3,aero} and may be affected by background pRONO₂ variability.

659 ***Plume 8 has a measurable increase in inorganic nitrate as well as organic.

660 4.2 SOA yield analysis

661 A molar SOA yield refers to the number of molecules of aerosol organic nitrate produced per
 662 molecule of isoprene consumed. In order to determine molar SOA yields from the data
 663 presented in Table 1, we convert the aerosol organic nitrate mass loading differences to mixing
 664 ratio differences (ppt) using the NO₃ molecular weight of 62 g mol⁻¹ (the AMS organic nitrate

Juliane Fry 6/1/2018 3:35 PM
Formatted: Subscript

Juliane Fry 6/1/2018 3:35 PM
Formatted: Subscript

Juliane Fry 5/26/2018 5:28 PM
Formatted: Table

Juliane Fry 5/26/2018 5:18 PM
Formatted: Superscript

Juliane Fry 5/26/2018 5:14 PM
Deleted: ΔISOP (ppt) ... [1]

Juliane Fry 5/26/2018 5:14 PM
Deleted: -335 ... [2]

Juliane Fry 6/1/2018 3:25 PM
Deleted: 33

Juliane Fry 5/26/2018 5:14 PM
Deleted: -404

Juliane Fry 5/26/2018 5:14 PM
Deleted: -228 ... [3]

Juliane Fry 6/1/2018 3:25 PM
Deleted: 8

Juliane Fry 5/26/2018 5:14 PM
Deleted: -453

Juliane Fry 5/26/2018 5:14 PM
Deleted: -255 ... [4]

Juliane Fry 5/26/2018 5:14 PM
Deleted: -713 ... [5]

Juliane Fry 6/1/2018 3:25 PM
Deleted: 34

Juliane Fry 5/26/2018 5:14 PM
Deleted: -298 ... [6]

Juliane Fry 6/1/2018 3:25 PM
Deleted: 077

Juliane Fry 5/26/2018 5:14 PM
Deleted: -443 ... [7]

Juliane Fry 6/1/2018 3:27 PM
Deleted: 12

Juliane Fry 5/26/2018 5:14 PM
Deleted: -293 ... [8]

Juliane Fry 6/1/2018 3:27 PM
Deleted: 056

689 | mass is the mass only of the $-\text{ONO}_2$ portion of the organonitrate aerosol). At standard
 690 conditions of 273 K and 1 atm (all aerosol data are reported with this STP definition), 1000 ppt
 691 $\text{NO}_3 = 2.77 \mu\text{g m}^{-3}$, so each $\Delta M_{\text{pRONO}_2}$ is multiplied by $361 \text{ ppt } (\mu\text{g m}^{-3})^{-1}$ to determine this molar
 692 yield:
 693

$$694 \quad Y_{\text{SOA,molar}} = \frac{(\text{pRONO}_2\text{plume} \pm \text{SD}_{\text{pRONO}_2\text{plume}}) - (\text{pRONO}_2\text{bkg} \pm \text{SD}_{\text{pRONO}_2\text{bkg}})}{-[(\text{isop}_{\text{plume}} \pm \text{SD}_{\text{isop}_{\text{plume}}}) - (\text{isop}_{\text{bkg}} \pm \text{SD}_{\text{isop}_{\text{bkg}}})]} \times \frac{361 \text{ ppt } \text{NO}_3}{\mu\text{g m}^{-3}} \quad (3)$$

695
 696 The SOA molar yields resulting from this calculation are shown in Table 2, spanning a range of
 697 5-28%, with uncertainties indicated based on the SDs in measured AMS and isoprene
 698 concentrations. In addition to this uncertainty based on measurement precision and ambient
 699 variability, there is an uncertainty of 50% in the AMS derived-organic nitrate mass loadings (see
 700 SI) and 25% in the PTR-MS isoprene concentrations (Warneke et al., 2016). The average molar
 701 pRONO_2 yield across all plumes, with each point weighed by the inverse of its standard
 702 deviation, is 9%. (As noted below, the yield appears to increase with plume age, so this average
 703 obscures that trend.) An alternate graphical analysis of molar SOA yield from all nine plumes
 704 plus one 'null' plume (03:14, in which no isoprene had yet reacted and thus not included in
 705 Tables 1 and 2) obtains the same average molar yield of 9% (Fig. 5). Here, the molar yield is
 706 the slope of a plot of plume change in pRONO_2 vs plume change in isoprene. The slope is
 707 determined by a linear fit with points weighted by the square root of the number of AMS data
 708 points used to determine in-plume pRONO_2 in each case. This slope error gives a rather narrow
 709 uncertainty range for the slope (0.0930 +/- 0.0011); to obtain an upper limit in the uncertainty of
 710 this molar yield we apply the combined instrumental uncertainties, based on adding in
 711 quadrature the PTR-MS uncertainty of 5% and the AMS uncertainty of 50%. This gives an
 712 overall uncertainty of 50.2%, resulting in upper and lower limit slopes of 0.140 and 0.046,
 713 respectively; we use this maximum uncertainty estimate to report the average molar yield as 9%
 714 (+/- 5%). We have not corrected the calculated yields for the possibility of NO_3 heterogeneous
 715 uptake, which could add a nitrate functionality to existing aerosol. Such a process could be rapid
 716 if the uptake coefficient for NO_3 were 0.1, a value characteristics of unsaturated substrates (Ng
 717 et al., 2017), but would not contribute measurably at more conventional NO_3 uptake coefficients
 718 of 0.001 (Brown and Stutz 2012).
 719
 720

Juliane Fry 5/26/2018 9:16 PM
 Formatted: Subscript

Juliane Fry 7/30/2018 11:14 PM
 Deleted: and assuming SD = 0.1 for single point plumes

Juliane Fry 6/1/2018 8:21 AM
 Formatted: Font:Not Bold, Font color: Auto

Juliane Fry 6/1/2018 8:21 AM
 Formatted: Font:11 pt, Not Bold, Font color: Auto

Juliane Fry 6/1/2018 8:21 AM
 Formatted: Font:Not Bold, Font color: Auto

Juliane Fry 6/1/2018 8:21 AM
 Formatted: Font:11 pt, Not Bold, Font color: Auto

Juliane Fry 6/1/2018 8:21 AM
 Formatted: Font:Not Bold, Font color: Auto

Juliane Fry 6/1/2018 8:21 AM
 Formatted: Font color: Auto

Juliane Fry 6/1/2018 8:21 AM
 Formatted: Font:Not Bold, Font color: Auto

Juliane Fry 6/1/2018 8:21 AM
 Formatted: Font:11 pt, Not Bold, Font color: Auto

Juliane Fry 6/1/2018 8:21 AM
 Formatted: Font:Not Bold, Font color: Auto

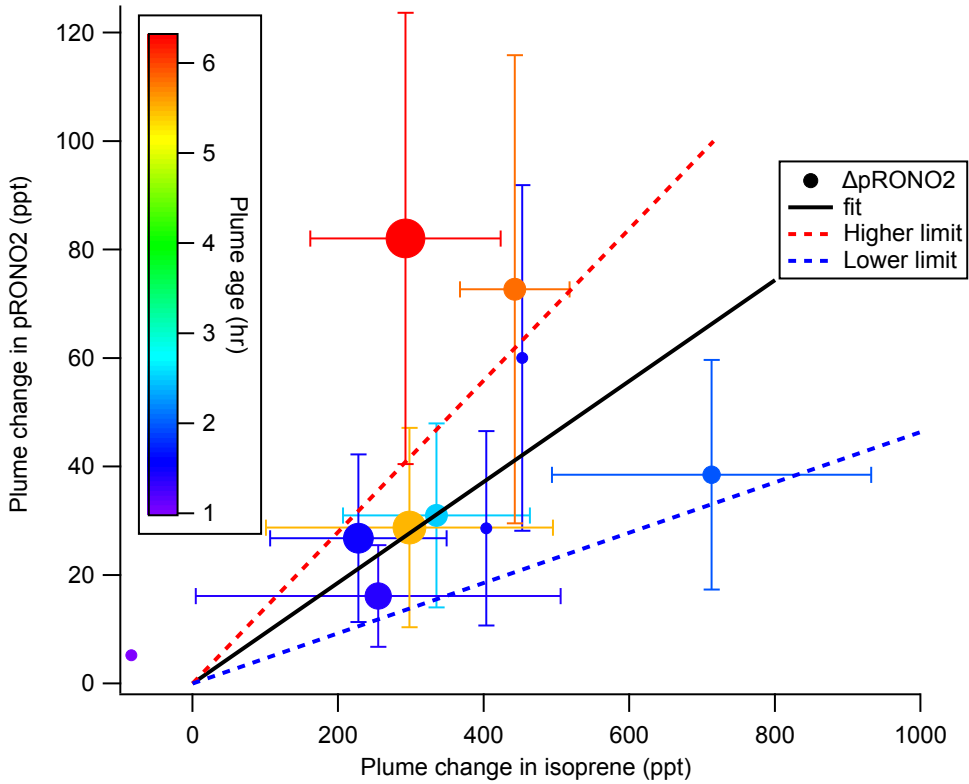
Juliane Fry 6/1/2018 8:21 AM
 Formatted: Font color: Auto

Juliane Fry 6/1/2018 8:21 AM
 Formatted: Font color: Auto

Juliane Fry 6/1/2018 8:21 AM
 Formatted: Font:Not Bold, Font color: Auto

Juliane Fry 6/1/2018 8:21 AM
 Formatted: Font:11 pt

723



724

725

726

727

728

729

730

731

732

733

734

735

736

737

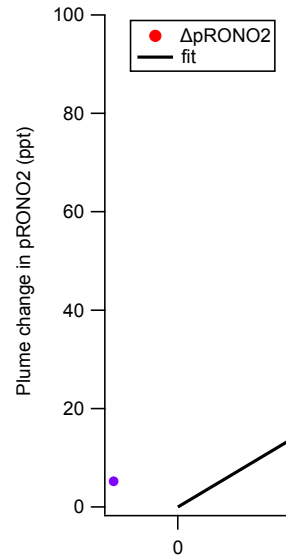
738

739

740

Figure 5. SOA molar yield can be determined as the slope of $\Delta p\text{RONO}_2$ vs. Δ isoprene, both in mixing ratio units. The linear fit is weighted by square root of number of points used to determine each in-plume $p\text{RONO}_2$, with intercept held at zero. The slope coefficient \pm one standard deviation is 0.0930 ± 0.0011 . Larger “outside” high and low limits of the slope (shown as dashed red and blue lines) are obtained by adding and subtracting from this slope the combined instrumental uncertainties, based on adding in quadrature the PTR-MS uncertainty of 5% and the AMS uncertainty of 50%. This gives an overall uncertainty of 50.2%, resulting in upper and lower limit slopes of 0.140 and 0.046, respectively. Points are colored by plume age, and size scaled by square root of number of points (the point weight used in linear fit). This plot and fit includes the nine plumes listed in Tables 1 and 2, as well as the 03:14 “unreacted” plume (at Δ isoprene = -84 ppt). Error bars on isoprene are the propagated standard deviations of the (in plume - out plume) differences, for plumes in which multi-point averages were possible. Error bars on $p\text{RONO}_2$ are the same as in Figure 4, converted to ppt. The points without error bars are single-point plumes.

Juliane Fry 5/26/2018 9:05 PM



Deleted:

Juliane Fry 5/26/2018 9:08 PM

Formatted: Normal

Juliane Fry 5/15/2018 7:09 PM

Deleted: 298

Juliane Fry 5/15/2018 7:09 PM

Deleted: 3.

Juliane Fry 6/3/2018 5:53 PM

Deleted: (red = longest)

Juliane Fry 5/26/2018 9:07 PM

Formatted: Font color: Auto

Juliane Fry 5/26/2018 5:28 PM

Deleted:

Juliane Fry 5/26/2018 9:07 PM

Formatted: Font color: Auto

Juliane Fry 5/26/2018 9:07 PM

Formatted: Font color: Auto

Juliane Fry 5/26/2018 9:07 PM

Formatted: Font color: Auto

Juliane Fry 5/26/2018 9:08 PM

Formatted: Font:(Default) Times, 10 pt, Font color: Auto

746 To estimate SOA **mass** yields, we need to make some assumption about the mass of the
 747 organic molecules containing the nitrate groups that lead to the observed nitrate aerosol mass
 748 increase. The observed changes in organic aerosol are too variable to be simply interpreted as
 749 the organic portion of the aerosol organic nitrate molecules. We conservatively assume the
 750 organic mass to be approximately double the nitrate mass (62 g mol^{-1}), based on an “average”
 751 molecular structure of an isoprene nitrate with 3 additional oxygens: e.g. a tri-hydroxynitrate
 752 (with organic portion of formula $\text{C}_5\text{H}_{11}\text{O}_3$, 119 g mol^{-1}), consistent with 2nd-generation oxidation
 753 product structures suggested in Schwantes, et al. (Schwantes et al., 2015). Based on this
 754 assumed organic to nitrate ratio, all plumes’ expected organic mass increases would be less
 755 than the typical variability in organic of $0.75 \mu\text{g m}^{-3}$. This assumed structure is consistent with
 756 oxidation of both double bonds, which appears to be necessary for substantial condensation of
 757 isoprene products, and which structures would have calculated vapor pressures sufficiently low
 758 to partition to the aerosol phase (Rollins et al., 2009). Another possible route to low vapor
 759 pressure products is intramolecular H rearrangement reactions, discussed below in Section 4.3,
 760 which would not require oxidant reactions at both double bonds. In the case of oxidant reactions
 761 at both double bonds, it is difficult to understand how the second double bond would be oxidized
 762 unless by another nitrate radical, which would halve these assumed organic to nitrate ratios
 763 (assuming the nitrate is retained in the molecules). On the other hand, any organic nitrate
 764 aerosol may lose NO_3 moieties, increasing the organic to nitrate ratio. Given these uncertainties
 765 in both directions, we use the assumed “average” structure above to guess an associated
 766 organic mass of double the nitrate mass. Thus, to estimate SOA mass yield, we multiply the
 767 increase in organic nitrate aerosol mass concentration by three (i.e., $2 \times \Delta M_{\text{pRONO}_2} + \Delta M_{\text{pRONO}_2}$),
 768 and divide by the observed decrease in isoprene, converted to $\mu\text{g m}^{-3}$ by multiplying by 329 ppt
 769 ($\mu\text{g m}^{-3}$)⁻¹, the conversion factor based on isoprene’s molecular weight of 68.12 g mol^{-1} .

$$771 Y_{\text{SOA, mass}} = \frac{(\text{pRONO}_2\text{plume} \pm \text{SD}_{\text{pRONO}_2\text{plume}}) - (\text{pRONO}_2\text{bkg} \pm \text{SD}_{\text{pRONO}_2\text{bkg}})}{-(\text{isopplume} \pm \text{SD}_{\text{isopplume}}) - (\text{isopbkg} \pm \text{SD}_{\text{isopbkg}})} \times 3 \times \frac{329 \text{ ppt}}{\mu\text{g m}^{-3}} \quad (4)$$

772
 773 Note that the SOA mass yield reported here is based on the (assumed) mass of organic aerosol
 774 plus the (organo)nitrate aerosol formed in each plume. If instead the yield were calculated using
 775 only the assumed increase in **organic** mass (i.e., $2 \times \Delta M_{\text{pRONO}_2}$ instead of $3 \times \Delta M_{\text{pRONO}_2}$), which
 776 would be consistent with the method used in Rollins, et al. (Rollins et al., 2009) and Brown et al.
 777 (Brown et al., 2009), the mass yields would be 2/3 the values reported here. However, since
 778 SOA mass yield is typically defined based on the total increase in aerosol mass, we use the
 779 definition with the sum of the organic and nitrate mass here. This results in an average SOA
 780 mass yield of 27%, with propagated instrumental errors (see caption to Fig. 5) giving a range of
 781 27% +/- 14%.

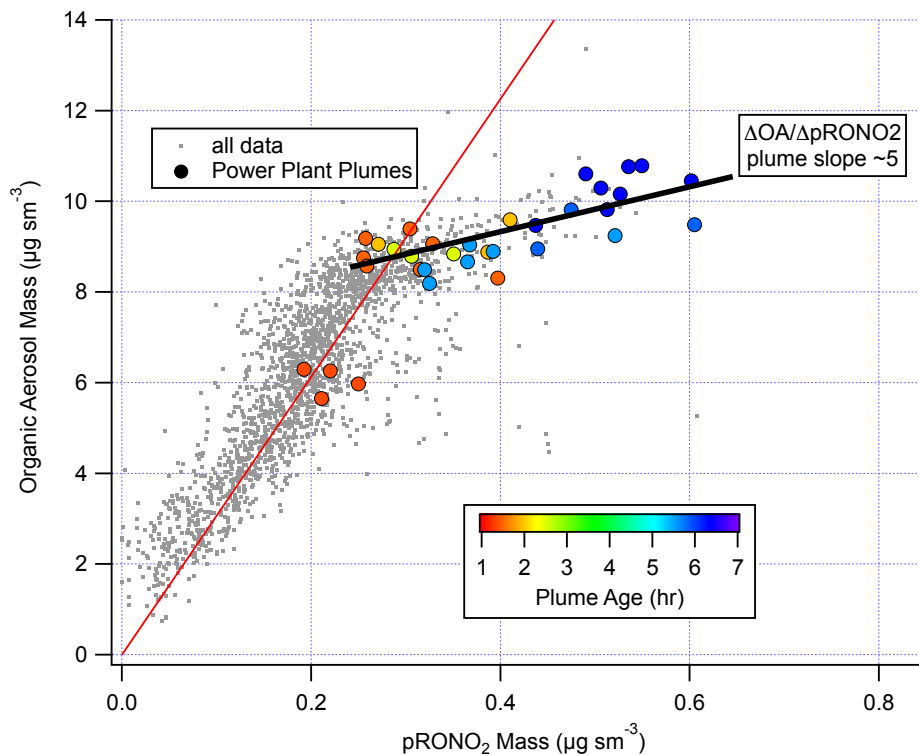
782
 783 We note also that correlation of in-plume increases in OA with pRONO₂ (Fig. 6) point to a
 784 substantially larger 5:1 organic-to-nitrate ratio; if this were interpreted as indicating that the
 785 average molecular formula of the condensing organic nitrate has 5 times the organic mass as
 786 nitrate, this would increase the SOA mass yields reported here. However, due to the
 787 aforementioned possibility of additional sources of co-condensing organic aerosol, which led us
 788 to avoid using ΔOA in determining SOA yields, we do not consider this to be a direct indication

Juliane Fry 5/15/2018 8:20 PM
 Deleted: However

Juliane Fry 5/15/2018 8:17 PM
 Deleted: the

Juliane Fry 5/15/2018 8:17 PM
 Deleted: y

792 of the molecular formula of the condensing organic nitrate. Including OA in the SOA yield
793 determination, based on this 5:1 slope rather than the assumed 2:1 OA:pRONO₂, would give
794 2.5 times larger SOA mass yields than reported here.
795



796
797 **Figure 6.** Correlation of organic aerosol mass concentration with pRONO₂ mass concentration
798 for the full 2 July flight (grey points and red fit line, fitted slope and thus average OA/pRONO₂
799 mass ratio of ~ 30) and for the points during the selected plumes (colored points, colored by
800 plume age, average OA/pRONO₂ mass ratio of ~ 5).

801
802

803 **Table 2.** SOA Yields for each plume observation, estimated plume age, and likely origin. See
 804 text for description of uncertainty estimates. For the mass yields, the calculated SOA mass
 805 increase includes both the organic and (organo)nitrate aerosol mass; the measurements for OA
 806 increases shown in Figure 6 do not include the nitrate mass.

plume number	plume time (UTC)	SOA molar yield (fraction) [± SD]	SOA mass yield (fraction) [± SD]	plume age from O ₃ / NO ₂ clock assuming S=1 (hours)	Likely NO _x origin & altitude (m)
1	7/2/13 2:18	0.09 [0.06]	0.25 [0.17]	2.5	Greene County @ 540 m
2	7/2/13 2:20	0.07	0.21	1.5	<i>ibid</i>
3	7/2/13 2:21	0.12 [0.10]	0.32 [0.25]	1.5	<i>ibid</i>
4	7/2/13 3:03	0.13	0.36	1.5	Gaston @ 720 m
5	7/2/13 3:55	0.06 [0.07]	0.17 [0.20]	1.4	Miller / Gorgas @ 690 m
6	7/2/13 4:34	0.05 [0.03]	0.15 [0.09]	2	<i>ibid</i>
7	7/2/13 4:37	0.10 [0.09]	0.26 [0.24]	5.5	<i>ibid</i>
8	7/2/13 4:39	0.16 [0.10]	0.45 [0.28]	5.8	Miller / Gorgas @ 1120 m
9	7/2/13 5:04	0.28 [0.19]	0.77 [0.52]	6.3	Gaston @ 1280 m

Juliane Fry 6/1/2018 3:38 PM

Deleted: 5

Juliane Fry 6/1/2018 3:38 PM

Deleted: 4

Juliane Fry 6/1/2018 3:38 PM

Deleted: 27

Juliane Fry 6/1/2018 3:38 PM

Deleted: 2

Juliane Fry 6/1/2018 3:39 PM

Deleted: 7

Juliane Fry 6/1/2018 3:39 PM

Deleted: 11

Juliane Fry 6/1/2018 3:39 PM

Deleted: 31

Juliane Fry 6/1/2018 3:39 PM

Deleted: 6

Juliane Fry 6/1/2018 3:39 PM

Deleted: 4

Juliane Fry 6/1/2018 3:39 PM

Deleted: 39

807
808

819 **Table 3.** Several caveats to the present SOA yields analysis are listed below, alongside the
 820 expected direction each would adjust the estimated yields. Because we do not know whether or
 821 how much each process may have occurred in the studied plumes, we cannot quantitatively
 822 assess the resulting uncertainties, so we simply list them here. See text above for more detailed
 823 discussion.

Process	Effect on determined SOA yield
Organic nitrate aerosol loses NO ₃ functional group	Larger, because the non-nitrate OA would not be counted in this analysis
Both double bonds in isoprene are oxidized by NO ₃ : two nitrates per condensing molecule	Smaller, because the assumed organic to nitrate mass ratio assumes one nitrate per molecule
NO ₃ oxidizes daytime isoprene oxidation products (e.g. ISOPOOH) to make new aerosol	Smaller, because this would produce organic nitrate aerosol without corresponding decrease in isoprene, so that some of existing SOA production is mis-attributed to isoprene + NO ₃
Assumed organic to nitrate mass ratio is incorrect	Unknown direction of effect, depends on whether assumed ratio is high or low
Daytime-produced IEPOX uptake onto acidic particles	No effect (only changes ΔOA, not nitrate)
Suppression of O ₃ + monoterpene or O ₃ + isoprene SOA in plumes	No effect (only changes ΔOA, not nitrate)

824
 825 Finally, the large range in observed yields can be interpreted by examining the relationship to
 826 estimated plume age. Using the slope of O₃ to NO₂ (Eq. 1) to estimate plume age as described
 827 above, a weak positive correlation is observed (Table 2, Fig. S4), suggesting that as the plume
 828 ages, later-generation chemistry results in greater partitioning to the condensed phase of NO₃ +
 829 isoprene organonitrate aerosol products. This is consistent with the observation by Rollins et al.
 830 (Rollins et al., 2009) that 2nd-generation oxidation produced substantially higher SOA yields
 831 than the oxidation of the first double bond alone, but we note that these mass yields (averaging
 832 27%, would be 18% using the organic mass only) are higher than even the largest yield found in
 833 that chamber study (14%, used organic mass only).

834
 835 We observe increasing SOA yield, from a molar yield of around 10% at 1.5 hours up to 30% at 6
 836 hours of aging. The lowest yields observed are found in the most recently emitted plumes,
 837 suggesting the interpretation of the higher yields as a consequence of longer aging timescales
 838 in the atmosphere.

839 4.3 Mechanistic considerations

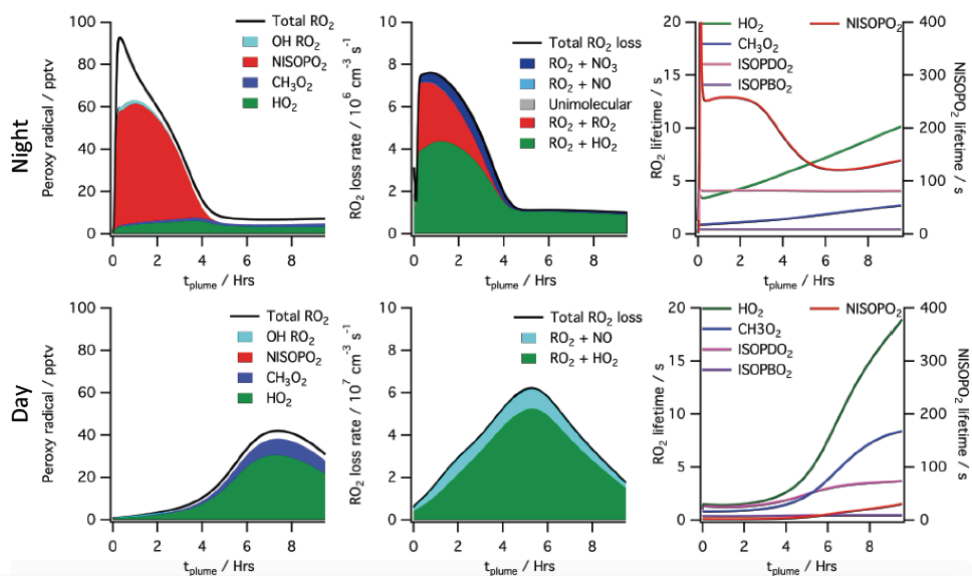
840
 841 These larger SOA mass yields from field determinations (average 27%) relative to chamber
 842 work (12 – 14%, see introduction) may arise for several reasons. We first assess the volatility of
 843 assumed first- and second-generation products using group contribution theory in order to
 844 predict partitioning. After a single oxidation step, with a representative product assumed to be a

845 C₅ hydroperoxynitrate, the saturation vapor pressure estimated by group contribution theory
846 (Pankow and Asher 2008) at 283 K would be 2.10×10^{-3} Torr ($C^* = 1.7 \times 10^4 \mu\text{g m}^{-3}$ for MW =
847 147 g mol^{-1}), while a double-oxidized isoprene molecule (assuming a C₅ dihydroxy dinitrate) has
848 an estimated vapor pressure of 7.95×10^{-8} Torr ($C^* = 1.01 \mu\text{g m}^{-3}$ for MW = 226 g mol^{-1}). This
849 supports the conclusion that while the first oxidation step produces compounds too volatile to
850 contribute appreciably to aerosol formation, oxidizing both double bonds of the isoprene
851 molecule is sufficient to produce substantial partitioning, consistent with Rollins et al. (Rollins et
852 al., 2009). This is also true if the second double bond is not oxidized by nitrate (group
853 contribution estimate P_{vap} for a C₅ tri-hydroxy nitrate is 7.7×10^{-8} Torr, $C^* = 0.79 \mu\text{g m}^{-3}$ for MW =
854 181 g mol^{-1}). These C^* saturation concentration values suggest that no dimer formation or
855 oligomerization is *required* to produce low-enough volatility products to condense to the aerosol
856 phase; however, such oligomerization would result in more efficient condensation. The fact that
857 Rollins et al. (Rollins et al., 2009) did not observe larger mass yields may indicate that it takes
858 longer than a typical chamber experiment timescale to reach equilibrium, or that this absorptive
859 partitioning model did not accurately capture those experiments, or that substantial loss of
860 semivolatiles to the chamber walls (e.g. (Krechmer et al., 2016)) suppressed apparent yields.

861
862 Determination of yields from ambient atmospheric data differs from chamber determinations in
863 several additional respects. First, ambient measurements do not suffer from wall loss effects,
864 such that no corrections are necessary for loss of aerosol or semi-volatile gases (Matsunaga
865 and Ziemann 2010, Krechmer et al., 2016). Second, ambient measurements take place on the
866 aging time scale of the atmosphere rather than a time scale imposed by the characteristics of
867 the chamber or the choice of oxidant addition. Third, the typical lifetime of the initially produced
868 nitrooxy-isoprene-RO₂ radical is more representative of the ambient atmosphere rather than a
869 chamber. The unique conditions of a high NO_x power plant plume affect lifetime and fates of
870 peroxy radicals, as described below.

871
872 To help interpret these in-plume peroxy radical lifetimes, a box model calculation using the
873 MCM v3.3.1 chemistry scheme was run (see details in Supplemental Information). This box
874 model shows substantially longer peroxy radical lifetimes during nighttime than daytime,
875 initializing with identical plume-observed conditions. These long peroxy radical lifetimes may
876 have consequences for comparison to chamber experiments: for example, in Schwantes'
877 (Schwantes et al., 2015) chamber experiment on the NO₃ + isoprene reaction mechanism, the
878 HO₂-limited nitrooxy-RO₂ lifetime was at maximum 30 s. In the plumes investigated in this study,
879 peroxy radical lifetimes are predicted to be substantially longer (>200 s early in the night, see
880 Fig. 7), allowing for the possibility of different bimolecular fates, or of unimolecular
881 transformations of the peroxy radicals that may result in lower-volatility products (e.g., auto-
882 oxidation to form highly oxidized molecules (Ehn et al., 2014)).

883
884



885
 886 **Figure 7.** Simulated peroxy radical concentration (left), loss rates (middle), and lifetime (right),
 887 using the MCM v3.3.1 chemical mechanism, for conditions typical of a nighttime intercepted
 888 power plant plume (top) and the same plume initial conditions run for daytime simulation
 889 (bottom, local noon occurs at 5 hrs). Included are total peroxy radical concentration and losses,
 890 as well as the highlighted subclasses HO₂, CH₃O₂, total nitrooxy-isoprene-RO₂, and the total
 891 hydroxy-isoprene-RO₂ produced from OH oxidation. The righthand panels show HO₂, CH₃O₂
 892 and the dominant hydroxy-isoprene-RO₂ ISOPBO₂ and ISOPDO₂ (β -hydroxy-peroxy radicals
 893 from OH attack at carbons 1 and 4 respectively) lifetime on the left axis and nitrooxy-isoprene-
 894 RO₂ on the right axis, showing nighttime lifetimes an order of magnitude longer than daytime for
 895 this NO₃ + isoprene derived RO₂ radical (NISOPO₂).

896
 897 The typically assumed major fate of nighttime RO₂ in the atmosphere is reaction with HO₂ to
 898 yield a hydroperoxide, NO₃-ROOH. This is shown in the model output above as the green
 899 reaction, and is responsible for half of early RO₂ losses in the MCM modeled plume. Schwantes
 900 *et al.* (Schwantes *et al.*, 2015) proposed reaction of these nighttime derived hydroperoxides with
 901 OH during the following day as a route to epoxides, which in turn can form SOA via reaction
 902 with acidic aerosol. Reaction of hydroperoxides with nighttime generated OH may similarly
 903 provide a route to SOA through epoxides, albeit more slowly than that due to photochemically
 904 generated OH.

905
 906 The predicted longer nighttime peroxy radical lifetimes may enable unique chemistry. For
 907 example, if nitrooxy-isoprene-RO₂ self-reactions are substantially faster than assumed in the
 908 MCM, as suggested by Schwantes *et al.* (Schwantes *et al.*, 2015), RO₂+RO₂ reactions may
 909 compete with the HO₂ reaction even more than shown in Fig. 7, and dimer formation may be
 910 favored at night, yielding lower volatility products. The 5:1 AMS Organic:Nitrate ratio observed in

911 the SOA formed in Rollins et al. (Rollins et al., 2009) , and consistent with aggregated
912 observations reported here, may suggest that in some isoprene units the nitrate is re-released
913 as NO₂ in such oligomerization reactions. We note that this larger organic to nitrate ratio would
914 mean higher SOA mass yields than estimated in Table 2.

915
916 Alternatively, longer nighttime peroxy radical lifetimes may allow sufficient time for
917 intramolecular reactions to produce condensable products. This unimolecular isomerization
918 (auto-oxidation) of initially formed peroxy radicals is a potentially efficient route to low-volatility,
919 highly functionalized products that could result in high aerosol yields. For OH-initiated oxidation
920 of isoprene, laboratory relative rate experiments found the fastest 1,6-H-shift isomerization
921 reaction to occur for the hydroxy-isoprene-RO₂ radical at a rate of 0.002 s⁻¹ (Crouse et al.,
922 2011), meaning that peroxy radicals must have an ambient lifetime of >500 s for this process to
923 be dominant. As shown in Fig. 7, the simulated power plant plume peroxy radical lifetimes are
924 long (>200 s), so an isomerization reaction at this rate may play a significant role. However, a
925 recent study has demonstrated that OH-initiated and NO₃-initiated RO₂ radicals from the same
926 precursor VOC can have very different unimolecular reactive fates due to highly structurally
927 sensitive varying rates of reactions of different product channels (Kurtén et al., 2017). A similar
928 theoretical study on the rate of unimolecular autooxidation reactions of nitrooxy-isoprene-RO₂
929 radicals would be valuable to help determine under what conditions such reactions might occur,
930 and this knowledge could be applied to comparing chamber and field SOA yields.

931 **4.4 Atmospheric implications and needs for future work**

932 Because this paper proposes higher SOA yield for the NO₃ + isoprene reaction than measured
933 in chamber studies, we conclude with some discussion of the implications for regional aerosol
934 burdens, and further needs for investigation in the NO₃ + isoprene system.

935
936 Using an isoprene + NO₃ yield parameterization that gave a 12% SOA mass yield at 10 µg m⁻³,
937 Pye et al. (2010) found that adding the NO₃ + isoprene oxidation pathway increased isoprene
938 SOA mass concentrations in the southeastern United States by about 30%, increases of 0.4 to
939 0.6 µg m⁻³. The larger NO₃ + isoprene SOA mass yields suggested in this paper, with average
940 value of 30%, could double this expected NO₃ radical enhancement of SOA production.
941 Edwards et al. (2017) concluded that the southeast U.S. is currently in transition between NO_x-
942 independent and NO_x-controlled nighttime BVOC oxidation regime. If NO₃-isoprene oxidation is
943 a larger aerosol source than currently understood, and if future NO_x reductions lead to a
944 stronger sensitivity in nighttime BVOC oxidation rates, regional SOA loadings could decrease by
945 a substantial fraction from the typical regional summertime OA loadings of 5 +/- 3 µg m⁻³ (Saha
946 et al., 2017).

947
948 Analysis of the degree of oxidation and chemical composition of NO₃ + isoprene SOA would
949 help to elucidate mechanistic reasons for the different field and lab SOA yields. For example,
950 the potential contribution of the uptake of morning-after OH + NISOPOOH produced epoxides,
951 discussed above in section 4.3, onto existing (acidic) aerosol could be quantified by
952 measurement of these intermediates or their products in the aerosol phase. Assessment of
953 degree of oxidation could help determine whether auto-oxidation mechanisms are active. [Future](#)

Juliane Fry 5/26/2018 10:23 PM

Deleted: 4.4 Two urban plume case studies ... [9]

Juliane Fry 5/26/2018 10:23 PM

Deleted: 5

958 [similar field studies would benefit from the co-deployment of the complementary tool of a](#)
959 [Chemical Ionization Mass Spectrometer \(CIMS\) to detect NO₃ + isoprene products such as](#)
960 [organic nitrates](#) (Lee et al., 2016, Slade et al., 2017). Because of the potentially large effect on
961 predicted SOA loading in regions of high isoprene emissions, a better mechanistic
962 understanding of these observed yields is crucial.

963

964 **Acknowledgements**

965 JLF gratefully acknowledges funding from the EPA STAR Program (no. RD-83539901) and from
966 the Fulbright U.S. Scholars Program in the Netherlands. PCJ, DAD, and JLJ were partially
967 supported by EPA STAR 83587701-0 and DOE (BER/ASR) DE-SC0016559. This paper has not
968 been formally reviewed by EPA. The views expressed in this document are solely those of the
969 authors, and do not necessarily reflect those of EPA. EPA does not endorse any products or
970 commercial services mentioned in this publication.

971 **5 References**

- 972 Allan, J. D., K. N. Bower, H. Coe, H. Boudries, J. T. Jayne, M. R. Canagaratna, D. B. Millet, A.
973 H. Goldstein, P. K. Quinn, R. J. Weber and D. R. Worsnop (2004). "Submicron aerosol
974 composition at Trinidad Head, California, during ITCT 2K2: Its relationship with gas phase
975 volatile organic carbon and assessment of instrument performance." *Journal of Geophysical*
976 *Research: Atmospheres* **109**(D23): n/a-n/a.
- 977 Allan, J. D., A. E. Delia, H. Coe, K. N. Bower, M. R. Alfarra, J. L. Jimenez, A. M. Middlebrook, F.
978 Drewnick, T. B. Onasch, M. R. Canagaratna, J. T. Jayne and D. R. Worsnop (2004). "A
979 generalised method for the extraction of chemically resolved mass spectra from Aerodyne
980 aerosol mass spectrometer data." *Journal of Aerosol Science* **35**(7): 909-922.
- 981 Atkinson, R., D. L. Baulch, R. A. Cox, J. N. Crowley, R. F. Hampson, R. G. Hynes, M. E. Jenkin,
982 M. J. Rossi and J. Troe (2004). "Evaluated kinetic and photochemical data for atmospheric
983 chemistry: Volume I - gas phase reactions of Ox, HOx, NOx and SOx species." *Atmos. Chem.*
984 *Phys.* **4**(6): 1461-1738.
- 985 Ayres, B. R., H. M. Allen, D. C. Draper, S. S. Brown, R. J. Wild, J. L. Jimenez, D. A. Day, P.
986 Campuzano-Jost, W. Hu, J. de Gouw, A. Koss, R. C. Cohen, K. C. Duffey, P. Romer, K.
987 Baumann, E. Edgerton, S. Takahama, J. A. Thornton, B. H. Lee, F. D. Lopez-Hilfiker, C. Mohr,
988 P. O. Wennberg, T. B. Nguyen, A. Teng, A. H. Goldstein, K. Olson and J. L. Fry (2015).
989 "Organic nitrate aerosol formation via NO₃ + biogenic volatile organic compounds
990 in the southeastern United States." *Atmos. Chem. Phys.* **15**(23): 13377-13392.
- 991 Bahreini, R., E. J. Dunlea, B. M. Matthew, C. Simons, K. S. Docherty, P. F. DeCarlo, J. L.
992 Jimenez, C. A. Brock and A. M. Middlebrook (2008). "Design and Operation of a Pressure-
993 Controlled Inlet for Airborne Sampling with an Aerodynamic Aerosol Lens." *Aerosol Science and*
994 *Technology* **42**(6): 465-471.
- 995 Bahreini, R., B. Ervens, A. M. Middlebrook, C. Warneke, J. A. de Gouw, P. F. DeCarlo, J. L.
996 Jimenez, C. A. Brock, J. A. Neuman, T. B. Ryerson, H. Stark, E. Atlas, J. Brioude, A. Fried, J. S.
997 Holloway, J. Peischl, D. Richter, J. Walega, P. Weibring, A. G. Wollny and F. C. Fehsenfeld
998 (2009). "Organic aerosol formation in urban and industrial plumes near Houston and Dallas,
999 Texas." *Journal of Geophysical Research: Atmospheres* **114**(D7): n/a-n/a.
- 1000 Boyd, C. M., J. Sanchez, L. Xu, A. J. Eugene, T. Nah, W. Y. Tuet, M. I. Guzman and N. L. Ng
1001 (2015). "Secondary organic aerosol formation from the β-pinene+NO₃ system: effect of humidity
1002 and peroxy radical fate." *Atmos. Chem. Phys.* **15**(13): 7497-7522.

1003 Brock, C. A., J. Cozic, R. Bahreini, K. D. Froyd, A. M. Middlebrook, A. McComiskey, J. Brioude,
1004 O. R. Cooper, A. Stohl, K. C. Aikin, J. A. de Gouw, D. W. Fahey, R. A. Ferrare, R. S. Gao, W.
1005 Gore, J. S. Holloway, G. Hübler, A. Jefferson, D. A. Lack, S. Lance, R. H. Moore, D. M. Murphy,
1006 A. Nenes, P. C. Novelli, J. B. Nowak, J. A. Ogren, J. Peischl, R. B. Pierce, P. Pilewskie, P. K.
1007 Quinn, T. B. Ryerson, K. S. Schmidt, J. P. Schwarz, H. Sodemann, J. R. Spackman, H. Stark,
1008 D. S. Thomson, T. Thornberry, P. Veres, L. A. Watts, C. Warneke and A. G. Wollny (2011).
1009 "Characteristics, sources, and transport of aerosols measured in spring 2008 during the aerosol,
1010 radiation, and cloud processes affecting Arctic Climate (ARCPAC) Project." Atmos. Chem.
1011 Phys. **11**(6): 2423-2453.
1012 Brock, C. A., N. L. Wagner, B. E. Anderson, A. R. Attwood, A. Beyersdorf, P. Campuzano-Jost,
1013 A. G. Carlton, D. A. Day, G. S. Diskin, T. D. Gordon, J. L. Jimenez, D. A. Lack, J. Liao, M. Z.
1014 Markovic, A. M. Middlebrook, N. L. Ng, A. E. Perring, M. S. Richardson, J. P. Schwarz, R. A.
1015 Washenfelder, A. Welti, L. Xu, L. D. Ziemba and D. M. Murphy (2016). "Aerosol optical
1016 properties in the southeastern United States in summer – Part 1: Hygroscopic growth." Atmos.
1017 Chem. Phys. **16**(8): 4987-5007.
1018 Brown, S. S., J. A. deGouw, C. Warneke, T. B. Ryerson, W. P. Dubé, E. Atlas, R. J. Weber, R.
1019 E. Peltier, J. A. Neuman, J. M. Roberts, A. Swanson, F. Flocke, S. A. McKeen, J. Brioude, R.
1020 Sommariva, M. Trainer, F. C. Fehsenfeld and A. R. Ravishankara (2009). "Nocturnal isoprene
1021 oxidation over the Northeast United States in summer and its impact on reactive nitrogen
1022 partitioning and secondary organic aerosol." Atmos. Chem. Phys. **9**(9): 3027-3042.
1023 Brown, S. S., W. P. Dubé, R. Bahreini, A. M. Middlebrook, C. A. Brock, C. Warneke, J. A. de
1024 Gouw, R. A. Washenfelder, E. Atlas, J. Peischl, T. B. Ryerson, J. S. Holloway, J. P. Schwarz, R.
1025 Spackman, M. Trainer, D. D. Parrish, F. C. Fehshenfeld and A. R. Ravishankara (2013).
1026 "Biogenic VOC oxidation and organic aerosol formation in an urban nocturnal boundary layer:
1027 aircraft vertical profiles in Houston, TX." Atmos. Chem. Phys. **13**(22): 11317-11337.
1028 Brown, S. S., W. P. Dubé, P. Karamchandani, G. Yarwood, J. Peischl, T. B. Ryerson, J. A.
1029 Neuman, J. B. Nowak, J. S. Holloway, R. A. Washenfelder, C. A. Brock, G. J. Frost, M. Trainer,
1030 D. D. Parrish, F. C. Fehsenfeld and A. R. Ravishankara (2012). "Effects of NO_x control and
1031 plume mixing on nighttime chemical processing of plumes from coal-fired power plants." Journal
1032 of Geophysical Research: Atmospheres **117**(D7): n/a-n/a.
1033 Brown, S. S., J. A. Neuman, T. B. Ryerson, M. Trainer, W. P. Dubé, J. S. Holloway, C.
1034 Warneke, J. A. de Gouw, S. G. Donnelly, E. Atlas, B. Matthew, A. M. Middlebrook, R. Peltier, R.
1035 J. Weber, A. Stohl, J. F. Meagher, F. C. Fehsenfeld and A. R. Ravishankara (2006). "Nocturnal
1036 odd-oxygen budget and its implications for ozone loss in the lower troposphere." Geophysical
1037 Research Letters **33**(8): n/a-n/a.
1038 Brown, S. S. and J. Stutz (2012). "Nighttime radical observations and chemistry." Chemical
1039 Society Reviews **41**(19): 6405-6447.
1040 Bruns, E. A., V. Perraud, A. Zelenyuk, M. J. Ezell, S. N. Johnson, Y. Yu, D. Imre, B. J.
1041 Finlayson-Pitts and M. L. Alexander (2010). "Comparison of FTIR and Particle Mass
1042 Spectrometry for the Measurement of Particulate Organic Nitrates." Environmental Science &
1043 Technology **44**(3): 1056-1061.
1044 Cai, Y., D. C. Montague, W. Mooiweer-Bryan and T. Deshler (2008). Performance
1045 characteristics of the ultra high sensitivity aerosol spectrometer for particles between 55 and
1046 800 nm: Laboratory and field studies.
1047 Calvert, J. G., J. A. Atkinson, J. A. Kerr, S. Madronich, G. K. Moortgat, T. J. Wallington and G.
1048 Yarwood (2000). Mechanisms of the atmospheric oxidation of the alkenes. New York, NY,
1049 Oxford University Press.
1050 Carlton, A. G., R. W. Pinder, P. V. Bhave and G. A. Pouliot (2010). "To What Extent Can
1051 Biogenic SOA be Controlled?" Environmental Science & Technology **44**(9): 3376-3380.
1052 Carlton, A. G., C. Wiedinmyer and J. H. Kroll (2009). "A review of Secondary Organic Aerosol
1053 (SOA) formation from isoprene." Atmos. Chem. Phys. **9**(14): 4987-5005.

1054 Crounse, J. D., F. Paulot, H. G. Kjaergaard and P. O. Wennberg (2011). "Peroxy radical
1055 isomerization in the oxidation of isoprene." *Physical Chemistry Chemical Physics* **13**(30): 13607-
1056 13613.

1057 D'Ambro, E. L., K. H. Møller, F. D. Lopez-Hilfiker, S. Schobesberger, J. Liu, J. E. Shilling, B. H.
1058 Lee, H. G. Kjaergaard and J. A. Thornton (2017). "Isomerization of Second-Generation Isoprene
1059 Peroxy Radicals: Epoxide Formation and Implications for Secondary Organic Aerosol Yields."
1060 *Environmental Science & Technology* **51**(9): 4978-4987.

1061 Darer, A. I., N. C. Cole-Filipiak, A. E. O'Connor and M. J. Elrod (2011). "Formation and Stability
1062 of Atmospherically Relevant Isoprene-Derived Organosulfates and Organonitrates."
1063 *Environmental Science & Technology* **45**(5): 1895-1902.

1064 Day, D. A., P. Campuzano-Jost, B. B. Palm, W. W. Hu, B. A. Nault, P. J. Wooldridge, R. C.
1065 Cohen, K. S. Docherty, J. A. Huffman and J. L. Jimenez (2017). "Evaluation of methods for
1066 quantification of bulk particle-phase organic nitrates using real-time aerosol mass spectrometry."
1067 *in preparation*.

1068 Dommen, J., H. Hellén, M. Saurer, M. Jaeggi, R. Siegwolf, A. Metzger, J. Duplissy, M. Fierz and
1069 U. Baltensperger (2009). "Determination of the Aerosol Yield of Isoprene in the Presence of an
1070 Organic Seed with Carbon Isotope Analysis." *Environmental Science & Technology* **43**(17):
1071 6697-6702.

1072 Drewnick, F., S. S. Hings, P. DeCarlo, J. T. Jayne, M. Gonin, K. Fuhrer, S. Weimer, J. L.
1073 Jimenez, K. L. Demerjian, S. Borrmann and D. R. Worsnop (2005). "A New Time-of-Flight
1074 Aerosol Mass Spectrometer (TOF-AMS)—Instrument Description and First Field Deployment."
1075 *Aerosol Science and Technology* **39**(7): 637-658.

1076 Dunlea, E. J., P. F. DeCarlo, A. C. Aiken, J. R. Kimmel, R. E. Peltier, R. J. Weber, J. Tomlinson,
1077 D. R. Collins, Y. Shinozuka, C. S. McNaughton, S. G. Howell, A. D. Clarke, L. K. Emmons, E. C.
1078 Apel, G. G. Pfister, A. van Donkelaar, R. V. Martin, D. B. Millet, C. L. Heald and J. L. Jimenez
1079 (2009). "Evolution of Asian aerosols during transpacific transport in INTEX-B." *Atmos. Chem.*
1080 *Phys.* **9**(19): 7257-7287.

1081 Edwards, P. M., K. C. Aikin, W. P. Dube, J. L. Fry, J. B. Gilman, J. A. de Gouw, M. G. Graus, T.
1082 F. Hanisco, J. Holloway, G. Hubler, J. Kaiser, F. N. Keutsch, B. M. Lerner, J. A. Neuman, D. D.
1083 Parrish, J. Peischl, I. B. Pollack, A. R. Ravishankara, J. M. Roberts, T. B. Ryerson, M. Trainer,
1084 P. R. Veres, G. M. Wolfe, C. Warneke and S. S. Brown (2017). "Transition from high- to low-
1085 NO_x control of night-time oxidation in the southeastern US." *Nature Geosci* **10**(7): 490-495.

1086 Ehn, M., J. A. Thornton, E. Kleist, M. Sipila, H. Junninen, I. Pullinen, M. Springer, F. Rubach, R.
1087 Tillmann, B. Lee, F. Lopez-Hilfiker, S. Andres, I.-H. Acir, M. Rissanen, T. Jokinen, S.
1088 Schobesberger, J. Kangasluoma, J. Kontkanen, T. Nieminen, T. Kurten, L. B. Nielsen, S.
1089 Jorgensen, H. G. Kjaergaard, M. Canagaratna, M. D. Maso, T. Berndt, T. Petaja, A. Wahner, V.-
1090 M. Kerminen, M. Kulmala, D. R. Worsnop, J. Wildt and T. F. Mentel (2014). "A large source of
1091 low-volatility secondary organic aerosol." *Nature* **506**(7489): 476-479.

1092 Emmerson, K. M. and M. J. Evans (2009). "Comparison of tropospheric gas-phase chemistry
1093 schemes for use within global models." *Atmos. Chem. Phys.* **9**(5): 1831-1845.

1094 Farmer, D. K., A. Matsunaga, K. S. Docherty, J. D. Surratt, J. H. Seinfeld, P. J. Ziemann and J.
1095 L. Jimenez (2010). "Response of an aerosol mass spectrometer to organonitrates and
1096 organosulfates and implications for atmospheric chemistry." *Proceedings of the National*
1097 *Academy of Sciences* **107**(15): 6670-6675.

1098 Fisher, J. A., D. J. Jacob, K. R. Travis, P. S. Kim, E. A. Marais, C. Chan Miller, K. Yu, L. Zhu, R.
1099 M. Yantosca, M. P. Sulprizio, J. Mao, P. O. Wennberg, J. D. Crounse, A. P. Teng, T. B. Nguyen,
1100 J. M. St. Clair, R. C. Cohen, P. Romer, B. A. Nault, P. J. Wooldridge, J. L. Jimenez, P.
1101 Campuzano-Jost, D. A. Day, W. Hu, P. B. Shepson, F. Xiong, D. R. Blake, A. H. Goldstein, P.
1102 K. Misztal, T. F. Hanisco, G. M. Wolfe, T. B. Ryerson, A. Wisthaler and T. Mikoviny (2016).
1103 "Organic nitrate chemistry and its implications for nitrogen budgets in an isoprene- and

1104 monoterpene-rich atmosphere: constraints from aircraft (SEAC4RS) and ground-based (SOAS)
1105 observations in the Southeast US." *Atmos. Chem. Phys.* **16**(9): 5969-5991.
1106 Fry, J. L., D. C. Draper, K. J. Zarzana, P. Campuzano-Jost, D. A. Day, J. L. Jimenez, S. S.
1107 Brown, R. C. Cohen, L. Kaser, A. Hansel, L. Cappellin, T. Karl, A. Hodzic Roux, A. Turnipseed,
1108 C. Cantrell, B. L. Lefer and N. Grossberg (2013). "Observations of gas- and aerosol-phase
1109 organic nitrates at BEACHON-RoMBAS 2011." *Atmos. Chem. Phys.* **13**(1): 8585-8605.
1110 Fry, J. L., A. Kiendler-Scharr, A. W. Rollins, T. Brauers, S. S. Brown, H.-P. Dorn, W. P. Dube, H.
1111 Fuchs, A. Mensah, F. Rohrer, R. Tillmann, A. Wahner, P. J. Wooldridge and R. C. Cohen
1112 (2011). "SOA from limonene: role of NO₃ in its generation and degradation." *Atmospheric
1113 Chemistry and Physics* **11**(8): 3879-3894.
1114 Fry, J. L., A. Kiendler-Scharr, A. W. Rollins, P. J. Wooldridge, S. S. Brown, H. Fuchs, W. Dube,
1115 A. Mensah, M. dal Maso, R. Tillmann, H. P. Dorn, T. Brauers and R. C. Cohen (2009). "Organic
1116 nitrate and secondary organic aerosol yield from NO₃ oxidation of beta-pinene evaluated using
1117 a gas-phase kinetics/aerosol partitioning model." *Atmospheric Chemistry and Physics* **9**(4):
1118 1431-1449.
1119 Fry, J. L., C. Koski, K. Bott, R. Hsu-Flanders and M. Hazell (2015). "Downwind particulate
1120 matters: Regulatory implications of secondary aerosol formation from the interaction of nitrogen
1121 oxides and tree emissions." *Environmental Science & Policy* **50**: 180-190.
1122 Goldstein, A. H., C. D. Koven, C. L. Heald and I. Y. Fung (2009). "Biogenic carbon and
1123 anthropogenic pollutants combine to form a cooling haze over the southeastern United States."
1124 *Proceedings of the National Academy of Sciences* **106**(22): 8835-8840.
1125 Guenther, A., T. Karl, P. Harley, C. Wiedinmyer, P. I. Palmer and C. Geron (2006). "Estimates
1126 of global terrestrial isoprene emissions using MEGAN (Model of Emissions of Gases and
1127 Aerosols from Nature)." *Atmos. Chem. Phys.* **6**: 3181-3210.
1128 Guo, H., L. Xu, A. Bougiatioti, K. M. Cerully, S. L. Capps, J. R. Hite Jr, A. G. Carlton, S. H. Lee,
1129 M. H. Bergin, N. L. Ng, A. Nenes and R. J. Weber (2015). "Fine-particle water and pH in the
1130 southeastern United States." *Atmos. Chem. Phys.* **15**(9): 5211-5228.
1131 Hallquist, M., J. C. Wenger, U. Baltensperger, Y. Rudich, D. Simpson, M. Claeys, J. Dommen,
1132 N. M. Donahue, C. George, A. H. Goldstein, J. F. Hamilton, H. Herrmann, T. Hoffmann, Y.
1133 Iinuma, M. Jang, M. E. Jenkin, J. L. Jimenez, A. Kiendler-Scharr, W. Maenhaut, G. McFiggans,
1134 T. F. Mentel, A. Monod, A. S. H. Prévôt, J. H. Seinfeld, J. D. Surratt, R. Szmigielski and J. Wildt
1135 (2009). "The formation, properties and impact of secondary organic aerosol: current and
1136 emerging issues." *Atmospheric Chemistry & Physics* **9**: 5155-5235.
1137 Hayes, P. L., A. M. Ortega, M. J. Cubison, K. D. Froyd, Y. Zhao, S. S. Cliff, W. W. Hu, D. W.
1138 Toohey, J. H. Flynn, B. L. Lefer, N. Grossberg, S. Alvarez, B. Rappenglück, J. W. Taylor, J. D.
1139 Allan, J. S. Holloway, J. B. Gilman, W. C. Kuster, J. A. de Gouw, P. Massoli, X. Zhang, J. Liu, R.
1140 J. Weber, A. L. Corrigan, L. M. Russell, G. Isaacman, D. R. Worton, N. M. Kreisberg, A. H.
1141 Goldstein, R. Thalman, E. M. Waxman, R. Volkamer, Y. H. Lin, J. D. Surratt, T. E. Kleindienst,
1142 J. H. Offenberg, S. Dusanter, S. Griffith, P. S. Stevens, J. Brioude, W. M. Angevine and J. L.
1143 Jimenez (2013). "Organic aerosol composition and sources in Pasadena, California, during the
1144 2010 CalNex campaign." *Journal of Geophysical Research: Atmospheres* **118**(16): 9233-9257.
1145 Heald, C. L., D. K. Henze, L. W. Horowitz, J. Feddema, J. F. Lamarque, A. Guenther, P. G.
1146 Hess, F. Vitt, J. H. Seinfeld, A. H. Goldstein and I. Fung (2008). "Predicted change in global
1147 secondary organic aerosol concentrations in response to future climate, emissions, and land
1148 use change." *Journal of Geophysical Research: Atmospheres* **113**(D5): n/a-n/a.
1149 Henze, D. K. and J. H. Seinfeld (2006). "Global secondary organic aerosol from isoprene
1150 oxidation." *Geophysical Research Letters* **33**(9).
1151 Hoyle, C., M. Boy, N. Donahue, J. Fry, M. Glasius, A. Guenther, A. Hallar, K. H. Hartz, M.
1152 Petters and T. Petaja (2011). "A review of the anthropogenic influence on biogenic secondary
1153 organic aerosol." *Atmospheric Chemistry and Physics* **11**(1): 321-343.

1154 Hoyle, C. R., T. Berntsen, G. Myhre and I. S. A. Isaksen (2007). "Secondary organic aerosol in
1155 the global aerosol - chemical transport model Oslo CTM2." *Atmospheric Chemistry and Physics*
1156 **7**(21): 5675-5694.

1157 Hu, K. S., A. I. Darer and M. J. Elrod (2011). "Thermodynamics and kinetics of the hydrolysis of
1158 atmospherically relevant organonitrates and organosulfates." *Atmos. Chem. Phys.* **11**(16):
1159 8307-8320.

1160 Hu, W. W., P. Campuzano-Jost, B. B. Palm, D. A. Day, A. M. Ortega, P. L. Hayes, J. E.
1161 Krechmer, Q. Chen, M. Kuwata, Y. J. Liu, S. S. de Sá, K. McKinney, S. T. Martin, M. Hu, S. H.
1162 Budisulistiorini, M. Riva, J. D. Surratt, J. M. St. Clair, G. Isaacman-Van Wertz, L. D. Yee, A. H.
1163 Goldstein, S. Carbone, J. Brito, P. Artaxo, J. A. de Gouw, A. Koss, A. Wisthaler, T. Mikoviny, T.
1164 Karl, L. Kaser, W. Jud, A. Hansel, K. S. Docherty, M. L. Alexander, N. H. Robinson, H. Coe, J.
1165 D. Allan, M. R. Canagaratna, F. Paulot and J. L. Jimenez (2015). "Characterization of a real-
1166 time tracer for isoprene epoxydiols-derived secondary organic aerosol (IEPOX-SOA) from
1167 aerosol mass spectrometer measurements." *Atmos. Chem. Phys.* **15**(20): 11807-11833.

1168 Jenkin, M. E., J. C. Young and A. R. Rickard (2015). "The MCM v3.3.1 degradation scheme for
1169 isoprene." *Atmos. Chem. Phys.* **15**(20): 11433-11459.

1170 Jimenez, J. L., M. R. Canagaratna, N. M. Donahue, A. S. H. Prevot, Q. Zhang, J. H. Kroll, P. F.
1171 DeCarlo, J. D. Allan, H. Coe, N. L. Ng, A. C. Aiken, K. S. Docherty, I. M. Ulbrich, A. P. Grieshop,
1172 A. L. Robinson, J. Duplissy, J. D. Smith, K. R. Wilson, V. A. Lanz, C. Hueglin, Y. L. Sun, J. Tian,
1173 A. Laaksonen, T. Raatikainen, J. Rautiainen, P. Vaattovaara, M. Ehn, M. Kulmala, J. M.
1174 Tomlinson, D. R. Collins, M. J. Cubison, E., J. Dunlea, J. A. Huffman, T. B. Onasch, M. R.
1175 Alfarra, P. I. Williams, K. Bower, Y. Kondo, J. Schneider, F. Drewnick, S. Borrmann, S. Weimer,
1176 K. Demerjian, D. Salcedo, L. Cottrell, R. Griffin, A. Takami, T. Miyoshi, S. Hatakeyama, A.
1177 Shimono, J. Y. Sun, Y. M. Zhang, K. Dzepina, J. R. Kimmel, D. Sueper, J. T. Jayne, S. C.
1178 Herndon, A. M. Trimborn, L. R. Williams, E. C. Wood, A. M. Middlebrook, C. E. Kolb, U.
1179 Baltensperger and D. R. Worsnop (2009). "Evolution of Organic Aerosols in the Atmosphere."
1180 *Science*(5959): 1525-1529.

1181 Kanakidou, M., J. H. Seinfeld, S. N. Pandis, I. Barnes, F. J. Dentener, M. C. Facchini, R. Van
1182 Dingenen, B. Ervens, A. Nenes, C. J. Nielsen, E. Swietlicki, J. P. Putaud, Y. Balkanski, S. Fuzzi,
1183 J. Horth, G. K. Moortgat, R. Winterhalter, C. E. L. Myhre, K. Tsigaridis, E. Vignati, E. G.
1184 Stephanou and J. Wilson (2005). "Organic aerosol and global climate modelling: a review."
1185 *Atmospheric Chemistry and Physics* **5**: 1053-1123.

1186 Kiendler-Scharr, A., A. A. Mensah, E. Friese, D. Topping, E. Nemitz, A. S. H. Prevot, M. Äijälä,
1187 J. Allan, F. Canonaco, M. Canagaratna, S. Carbone, M. Crippa, M. Dall'Osto, D. A. Day, P. De
1188 Carlo, C. F. Di Marco, H. Elbern, A. Eriksson, E. Freney, L. Hao, H. Herrmann, L. Hildebrandt,
1189 R. Hillamo, J. L. Jimenez, A. Laaksonen, G. McFiggans, C. Mohr, C. O'Dowd, R. Otjes, J.
1190 Ovadnevaite, S. N. Pandis, L. Poulain, P. Schlag, K. Sellegri, E. Swietlicki, P. Tiitta, A.
1191 Vermeulen, A. Wahner, D. Worsnop and H. C. Wu (2016). "Ubiquity of organic nitrates from
1192 nighttime chemistry in the European submicron aerosol." *Geophysical Research Letters* **43**(14):
1193 7735-7744.

1194 Kim, P. S., D. J. Jacob, J. A. Fisher, K. Travis, K. Yu, L. Zhu, R. M. Yantosca, M. P. Sulprizio, J.
1195 L. Jimenez, P. Campuzano-Jost, K. D. Froyd, J. Liao, J. W. Hair, M. A. Fenn, C. F. Butler, N. L.
1196 Wagner, T. D. Gordon, A. Welti, P. O. Wennberg, J. D. Crouse, J. M. St. Clair, A. P. Teng, D.
1197 B. Millet, J. P. Schwarz, M. Z. Markovic and A. E. Perring (2015). "Sources, seasonality, and
1198 trends of southeast US aerosol: an integrated analysis of surface, aircraft, and satellite
1199 observations with the GEOS-Chem chemical transport model." *Atmos. Chem. Phys.* **15**(18):
1200 10411-10433.

1201 Kleindienst, T. E., M. Lewandowski, J. H. Offenberg, M. Jaoui and E. O. Edney (2007). "Ozone-
1202 isoprene reaction: Re-examination of the formation of secondary organic aerosol." *Geophysical*
1203 *Research Letters* **34**(1): n/a-n/a.

1204 Krechmer, J. E., D. Pagonis, P. J. Ziemann and J. L. Jimenez (2016). "Quantification of Gas-
1205 Wall Partitioning in Teflon Environmental Chambers Using Rapid Bursts of Low-Volatility
1206 Oxidized Species Generated in Situ." *Environmental Science & Technology* **50**(11): 5757-5765.
1207 Kroll, J. H., N. L. Ng, S. M. Murphy, R. C. Flagan and J. H. Seinfeld (2006). "Secondary Organic
1208 Aerosol Formation from Isoprene Photooxidation." *Environmental Science & Technology* **40**(6):
1209 1869-1877.
1210 Kurtén, T., K. H. Møller, T. B. Nguyen, R. H. Schwantes, P. K. Misztal, L. Su, P. O. Wennberg,
1211 J. L. Fry and H. G. Kjaergaard (2017). "Alkoxy Radical Bond Scissions Explain the Anomalously
1212 Low Secondary Organic Aerosol and Organonitrate Yields From α -Pinene + NO₃." *The Journal*
1213 *of Physical Chemistry Letters*: 2826-2834.
1214 Lee, B. H., C. Mohr, F. D. Lopez-Hilfiker, A. Lutz, M. Hallquist, L. Lee, P. Romer, R. C. Cohen,
1215 S. Iyer, T. Kurtén, W. Hu, D. A. Day, P. Campuzano-Jost, J. L. Jimenez, L. Xu, N. L. Ng, H.
1216 Guo, R. J. Weber, R. J. Wild, S. S. Brown, A. Koss, J. de Gouw, K. Olson, A. H. Goldstein, R.
1217 Seco, S. Kim, K. McAvey, P. B. Shepson, T. Starn, K. Baumann, E. S. Edgerton, J. Liu, J. E.
1218 Shilling, D. O. Miller, W. Brune, S. Schobesberger, E. L. D'Ambro and J. A. Thornton (2016).
1219 "Highly functionalized organic nitrates in the southeast United States: Contribution to secondary
1220 organic aerosol and reactive nitrogen budgets." *Proceedings of the National Academy of*
1221 *Sciences* **113**(6): 1516-1521.
1222 Lelieveld, J., J. S. Evans, M. Fnais, D. Giannadaki and A. Pozzer (2015). "The contribution of
1223 outdoor air pollution sources to premature mortality on a global scale." *Nature* **525**(7569): 367-
1224 371.
1225 Lerner, B. M., J. B. Gilman, K. C. Aikin, E. L. Atlas, P. D. Goldan, M. Graus, R. Hendershot, G.
1226 A. Isaacman-VanWertz, A. Koss, W. C. Kuster, R. A. Lueb, R. J. McLaughlin, J. Peischl, D.
1227 Sueper, T. B. Ryerson, T. W. Tokarek, C. Warneke, B. Yuan and J. A. de Gouw (2017). "An
1228 improved, automated whole air sampler and gas chromatography mass spectrometry analysis
1229 system for volatile organic compounds in the atmosphere." *Atmos. Meas. Tech.* **10**(1): 291-313.
1230 Liu, J., E. L. D'Ambro, B. H. Lee, F. D. Lopez-Hilfiker, R. A. Zaveri, J. C. Rivera-Rios, F. N.
1231 Keutsch, S. Iyer, T. Kurten, Z. Zhang, A. Gold, J. D. Surratt, J. E. Shilling and J. A. Thornton
1232 (2016). "Efficient Isoprene Secondary Organic Aerosol Formation from a Non-IEPOX Pathway."
1233 *Environmental Science & Technology* **50**(18): 9872-9880.
1234 Marais, E. A., D. J. Jacob, J. L. Jimenez, P. Campuzano-Jost, D. A. Day, W. Hu, J. Krechmer,
1235 L. Zhu, P. S. Kim, C. C. Miller, J. A. Fisher, K. Travis, K. Yu, T. F. Hanisco, G. M. Wolfe, H. L.
1236 Arkinson, H. O. T. Pye, K. D. Froyd, J. Liao and V. F. McNeill (2016). "Aqueous-phase
1237 mechanism for secondary organic aerosol formation from isoprene: application to the southeast
1238 United States and co-benefit of SO₂ emission controls." *Atmos. Chem. Phys.* **16**(3): 1603-1618.
1239 Marcolli, C., M. R. Canagaratna, D. R. Worsnop, R. Bahreini, J. A. de Gouw, C. Warneke, P. D.
1240 Goldan, W. C. Kuster, E. J. Williams, B. M. Lerner, J. M. Roberts, J. F. Meagher, F. C.
1241 Fehsenfeld, M. Marchewka, S. B. Bertman and A. M. Middlebrook (2006). "Cluster Analysis of
1242 the Organic Peaks in Bulk Mass Spectra Obtained During the 2002 New England Air Quality
1243 Study with an Aerodyne Aerosol Mass Spectrometer." *Atmos. Chem. Phys.* **6**(12): 5649-5666.
1244 Matsunaga, A. and P. J. Ziemann (2010). "Gas-Wall Partitioning of Organic Compounds in a
1245 Teflon Film Chamber and Potential Effects on Reaction Product and Aerosol Yield
1246 Measurements." *Aerosol Science and Technology* **44**(10): 881-892.
1247 Middlebrook, A. M., R. Bahreini, J. L. Jimenez and M. R. Canagaratna (2012). "Evaluation of
1248 Composition-Dependent Collection Efficiencies for the Aerodyne Aerosol Mass Spectrometer
1249 using Field Data." *Aerosol Science and Technology* **46**(3): 258-271.
1250 Myhre, G., D. Shindell, F.-M. Bréon, W. Collins, J. Fuglestedt, J. Huang, D. Koch, J.-F.
1251 Lamarque, D. Lee, B. Mendoza, T. Nakajima, A. Robock, G. Stephens, T. Takemura and H.
1252 Zhang (2013). Anthropogenic And Natural Radiative Forcing, in *Climate Change 2013: The*
1253 *Physical Science Basis. Contribution of Working Group I to the Fifth Assessment Report of the*

1254 Intergovernmental Panel on Climate Change. T. F. Stocker, D. Qin, G.-K. Plattner et al. New
1255 York, NY, USA, Cambridge University Press: 659-740.
1256 NASA. (2018). "SEAC4RS data site." from DOI: 10.5067/Aircraft/SEAC4RS/Aerosol-TraceGas-
1257 Cloud.
1258 Ng, N. L., S. S. Brown, A. T. Archibald, E. Atlas, R. C. Cohen, J. N. Crowley, D. A. Day, N. M.
1259 Donahue, J. L. Fry, H. Fuchs, R. J. Griffin, M. I. Guzman, H. Herrmann, A. Hodzic, Y. Iinuma, J.
1260 L. Jimenez, A. Kiendler-Scharr, B. H. Lee, D. J. Luecken, J. Mao, R. McLaren, A. Mutzel, H. D.
1261 Osthoff, B. Ouyang, B. Picquet-Varrault, U. Platt, H. O. T. Pye, Y. Rudich, R. H. Schwantes, M.
1262 Shiraiwa, J. Stutz, J. A. Thornton, A. Tilgner, B. J. Williams and R. A. Zaveri (2017). "Nitrate
1263 radicals and biogenic volatile organic compounds: oxidation, mechanisms, and organic aerosol."
1264 *Atmos. Chem. Phys.* **17**(3): 2103-2162.
1265 Ng, N. L., A. J. Kwan, J. D. Surratt, A. W. H. Chan, P. S. Chhabra, A. Sorooshian, H. O. T. Pye,
1266 J. D. Crouse, P. O. Wennberg, R. C. Flagan and J. H. Seinfeld (2008). "Secondary organic
1267 aerosol (SOA) formation from reaction of isoprene with nitrate radicals (NO₃)."
1268 *Atmos. Chem. Phys.* **8**: 4117-4140.
1269 Palm, B. B., P. Campuzano-Jost, D. A. Day, A. M. Ortega, J. L. Fry, S. S. Brown, K. J. Zarzana,
1270 W. Dube, N. L. Wagner, D. C. Draper, L. Kaser, W. Jud, T. Karl, A. Hansel, C. Gutiérrez-Montes
1271 and J. L. Jimenez (2017). "Secondary organic aerosol formation from in situ OH, O₃, and NO₃
1272 oxidation of ambient forest air in an oxidation flow reactor." *Atmos. Chem. Phys.* **17**(8): 5331-
1273 5354.
1274 Pankow, J. F. and W. E. Asher (2008). "SIMPOL.1: a simple group contribution method for
1275 predicting vapor pressures and enthalpies of vaporization of multifunctional organic
1276 compounds." *Atmospheric Chemistry and Physics* **8**(10): 2773-2796.
1277 Peischl, J., T. B. Ryerson, J. S. Holloway, D. D. Parrish, M. Trainer, G. J. Frost, K. C. Aikin, S.
1278 S. Brown, W. P. Dubé, H. Stark and F. C. Fehsenfeld (2010). "A top-down analysis of emissions
1279 from selected Texas power plants during TexAQS 2000 and 2006." *Journal of Geophysical*
1280 *Research: Atmospheres* **115**(D16): n/a-n/a.
1281 Pye, H., A. Chan, M. Barkley and J. Seinfeld (2010). "Global modeling of organic aerosol: the
1282 importance of reactive nitrogen (NO_x and NO₃)."
1283 *Atmospheric Chemistry and Physics* **10**(22): 11261-11276.
1284 Pye, H. O. T., D. J. Luecken, L. Xu, C. M. Boyd, N. L. Ng, K. R. Baker, B. R. Ayres, J. O. Bash,
1285 K. Baumann, W. P. L. Carter, E. Edgerton, J. L. Fry, W. T. Hutzell, D. B. Schwede and P. B.
1286 Shepson (2015). "Modeling the Current and Future Roles of Particulate Organic Nitrates in the
1287 Southeastern United States." *Environmental Science & Technology* **49**(24): 14195-14203.
1288 Rollins, A. W., E. C. Browne, K. E. Min, S. E. Pusede, P. J. Wooldridge, D. R. Gentner, A. H.
1289 Goldstein, S. Liu, D. A. Day, L. M. Russell and R. C. Cohen (2012). "Evidence for NO_x Control
1290 over Nighttime SOA Formation." *Science* **337**(6099): 1210.
1291 Rollins, A. W., A. Kiendler-Scharr, J. L. Fry, T. Brauers, S. S. Brown, H.-P. Dorn, W. P. Dube, H.
1292 Fuchs, A. Mensah, T. F. Mentel, F. Rohrer, R. Tillmann, R. Wegener, P. J. Wooldridge and R.
1293 C. Cohen (2009). "Isoprene oxidation by nitrate radical: alkyl nitrate and secondary organic
1294 aerosol yields." *Atmos. Chem. Phys.* **9**: 6685-6703.
1295 Romer, P. S., K. C. Duffey, P. J. Wooldridge, H. M. Allen, B. R. Ayres, S. S. Brown, W. H.
1296 Brune, J. D. Crouse, J. de Gouw, D. C. Draper, P. A. Feiner, J. L. Fry, A. H. Goldstein, A.
1297 Koss, P. K. Misztal, T. B. Nguyen, K. Olson, A. P. Teng, P. O. Wennberg, R. J. Wild, L. Zhang
1298 and R. C. Cohen (2016). "The lifetime of nitrogen oxides in an isoprene-dominated forest."
1299 *Atmos. Chem. Phys.* **16**(12): 7623-7637.
1300 Saha, P. K., A. Khlystov, K. Yahya, Y. Zhang, L. Xu, N. L. Ng and A. P. Grieshop (2017).
1301 "Quantifying the volatility of organic aerosol in the southeastern US." *Atmos. Chem. Phys.* **17**(1):
1302 501-520.

1303 Sato, K., A. Takami, T. Isozaki, T. Hikida, A. Shimono and T. Imamura (2010). "Mass
1304 spectrometric study of secondary organic aerosol formed from the photo-oxidation of aromatic
1305 hydrocarbons." Atmospheric Environment **44**(8): 1080-1087.

1306 Schwantes, R. H., A. P. Teng, T. B. Nguyen, M. M. Coggon, J. D. Crouse, J. M. St. Clair, X.
1307 Zhang, K. A. Schilling, J. H. Seinfeld and P. O. Wennberg (2015). "Isoprene NO₃ Oxidation
1308 Products from the RO₂ + HO₂ Pathway." The Journal of Physical Chemistry A **119**(40): 10158-
1309 10171.

1310 Slade, J. H., C. de Perre, L. Lee and P. B. Shepson (2017). "Nitrate radical oxidation of γ -
1311 terpinene: hydroxy nitrate, total organic nitrate, and secondary organic aerosol yields." Atmos.
1312 Chem. Phys. **17**(14): 8635-8650.

1313 Spracklen, D. V., J. L. Jimenez, K. S. Carslaw, D. R. Worsnop, M. J. Evans, G. W. Mann, Q.
1314 Zhang, M. R. Canagaratna, J. Allan, H. Coe, G. McFiggans, A. Rap and P. Forster (2011).
1315 "Aerosol mass spectrometer constraint on the global secondary organic aerosol budget." Atmos.
1316 Chem. Phys. **11**(23): 12109-12136.

1317 Surratt, J. D., A. W. H. Chan, N. C. Eddingsaas, M. N. Chan, C. L. Loza, A. J. Kwan, S. P.
1318 Hersey, R. C. Flagan, P. O. Wennberg and J. H. Seinfeld (2010). "Reactive intermediates
1319 revealed in secondary organic aerosol formation from isoprene." Proceedings of the National
1320 Academy of Sciences **107**(15): 6640-6645.

1321 Takegawa, N., T. Miyakawa, K. Kawamura and Y. Kondo (2007). "Contribution of Selected
1322 Dicarboxylic and ω -Oxocarboxylic Acids in Ambient Aerosol to the m/z 44 Signal of an
1323 Aerodyne Aerosol Mass Spectrometer." Aerosol Science and Technology **41**(4): 418-437.

1324 Toon, O. B., H. Maring, J. Dibb, R. Ferrare, D. J. Jacob, E. J. Jensen, Z. J. Luo, G. G. Mace, L.
1325 L. Pan, L. Pfister, K. H. Rosenlof, J. Redemann, J. S. Reid, H. B. Singh, A. M. Thompson, R.
1326 Yokelson, P. Minnis, G. Chen, K. W. Jucks and A. Pszenny (2016). "Planning, implementation,
1327 and scientific goals of the Studies of Emissions and Atmospheric Composition, Clouds and
1328 Climate Coupling by Regional Surveys (SEAC4RS) field mission." Journal of Geophysical
1329 Research: Atmospheres **121**(9): 4967-5009.

1330 Warneke, C., M. Trainer, J. A. de Gouw, D. D. Parrish, D. W. Fahey, A. R. Ravishankara, A. M.
1331 Middlebrook, C. A. Brock, J. M. Roberts, S. S. Brown, J. A. Neuman, B. M. Lerner, D. Lack, D.
1332 Law, G. Hübler, I. Pollack, S. Sjostedt, T. B. Ryerson, J. B. Gilman, J. Liao, J. Holloway, J.
1333 Peischl, J. B. Nowak, K. C. Aikin, K. E. Min, R. A. Washenfelder, M. G. Graus, M. Richardson,
1334 M. Z. Markovic, N. L. Wagner, A. Welti, P. R. Veres, P. Edwards, J. P. Schwarz, T. Gordon, W.
1335 P. Dube, S. A. McKeen, J. Brioude, R. Ahmadov, A. Bougiatioti, J. J. Lin, A. Nenes, G. M.
1336 Wolfe, T. F. Hanisco, B. H. Lee, F. D. Lopez-Hilfiker, J. A. Thornton, F. N. Keutsch, J. Kaiser, J.
1337 Mao and C. D. Hatch (2016). "Instrumentation and measurement strategy for the NOAA SENEX
1338 aircraft campaign as part of the Southeast Atmosphere Study 2013." Atmos. Meas. Tech. **9**(7):
1339 3063-3093.

1340 Wilson, J. C., B. G. Lafleu, H. Hilbert, W. R. Seebaugh, J. Fox, D. W. Gesler, C. A. Brock, B. J.
1341 Huebert and J. Mullen (2004). "Function and Performance of a Low Turbulence Inlet for
1342 Sampling Supermicron Particles from Aircraft Platforms." Aerosol Science and Technology
1343 **38**(8): 790-802.

1344 Worton, D. R., J. D. Surratt, B. W. LaFranchi, A. W. H. Chan, Y. Zhao, R. J. Weber, J.-H. Park,
1345 J. B. Gilman, J. de Gouw, C. Park, G. Schade, M. Beaver, J. M. S. Clair, J. Crouse, P.
1346 Wennberg, G. M. Wolfe, S. Harrold, J. A. Thornton, D. K. Farmer, K. S. Docherty, M. J.
1347 Cubison, J.-L. Jimenez, A. A. Frossard, L. M. Russell, K. Kristensen, M. Glasius, J. Mao, X.
1348 Ren, W. Brune, E. C. Browne, S. E. Pusede, R. C. Cohen, J. H. Seinfeld and A. H. Goldstein
1349 (2013). "Observational Insights into Aerosol Formation from Isoprene." Environmental Science
1350 & Technology **47**(20): 11403-11413.

1351 Xie, Y., F. Paulot, W. P. L. Carter, C. G. Nolte, D. J. Luecken, W. T. Hutzell, P. O. Wennberg, R.
1352 C. Cohen and R. W. Pinder (2013). "Understanding the impact of recent advances in isoprene
1353 photooxidation on simulations of regional air quality." Atmos. Chem. Phys. **13**(16): 8439-8455.

1354 Xu, L., S. Suresh, H. Guo, R. J. Weber and N. L. Ng (2015). "Aerosol characterization over the
1355 southeastern United States using high-resolution aerosol mass spectrometry: spatial and
1356 seasonal variation of aerosol composition and sources with a focus on organic nitrates." Atmos.
1357 Chem. Phys. **15**(13): 7307-7336.

1358 Zhang, H., L. D. Yee, B. H. Lee, M. P. Curtis, D. R. Worton, G. Isaacman-VanWertz, J. H.
1359 Offenberg, M. Lewandowski, T. E. Kleindienst, M. R. Beaver, A. L. Holder, W. A. Lonneman, K.
1360 S. Docherty, M. Jaoui, H. O. T. Pye, W. Hu, D. A. Day, P. Campuzano-Jost, J. L. Jimenez, H.
1361 Guo, R. J. Weber, J. de Gouw, A. R. Koss, E. S. Edgerton, W. Brune, C. Mohr, F. D. Lopez-
1362 Hilfiker, A. Lutz, N. M. Kreisberg, S. R. Spielman, S. V. Hering, K. R. Wilson, J. A. Thornton and
1363 A. H. Goldstein (2018). "Monoterpenes are the largest source of summertime organic aerosol in
1364 the southeastern United States." Proceedings of the National Academy of Sciences **115**(9):
1365 2038.

1366 Zhang, Q., M. R. Alfarra, D. R. Worsnop, J. D. Allan, H. Coe, M. R. Canagaratna and J. L.
1367 Jimenez (2005). "Deconvolution and Quantification of Hydrocarbon-like and Oxygenated
1368 Organic Aerosols Based on Aerosol Mass Spectrometry." Environmental Science & Technology
1369 **39**(13): 4938-4952.

1370 Zhang, Q., J. L. Jimenez, M. R. Canagaratna, J. D. Allan, H. Coe, I. Ulbrich, M. R. Alfarra, A.
1371 Takami, A. M. Middlebrook, Y. L. Sun, K. Dzepina, E. Dunlea, K. Docherty, P. F. DeCarlo, D.
1372 Salcedo, T. Onasch, J. T. Jayne, T. Miyoshi, A. Shimono, S. Hatakeyama, N. Takegawa, Y.
1373 Kondo, J. Schneider, F. Drewnick, S. Borrmann, S. Weimer, K. Demerjian, P. Williams, K.
1374 Bower, R. Bahreini, L. Cottrell, R. J. Griffin, J. Rautiainen, J. Y. Sun, Y. M. Zhang and D. R.
1375 Worsnop (2007). "Ubiquity and dominance of oxygenated species in organic aerosols in
1376 anthropogenically-influenced Northern Hemisphere midlatitudes." Geophysical Research Letters
1377 **34**(13): L13801.

1378 Zhang, Q., C. O. Stanier, M. R. Canagaratna, J. T. Jayne, D. R. Worsnop, S. N. Pandis and J.
1379 L. Jimenez (2004). "Insights into the Chemistry of New Particle Formation and Growth Events in
1380 Pittsburgh Based on Aerosol Mass Spectrometry." Environmental Science & Technology **38**(18):
1381 4797-4809.

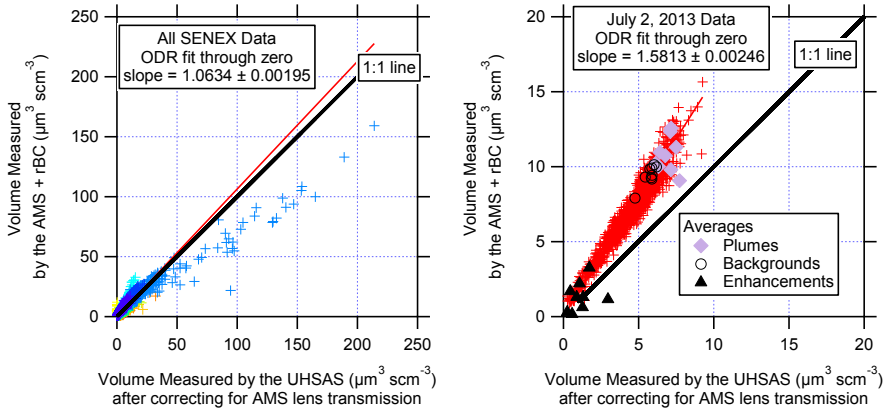
1382 Zheng, Y., N. Unger, A. Hodzic, L. Emmons, C. Knote, S. Tilmes, J. F. Lamarque and P. Yu
1383 (2015). "Limited effect of anthropogenic nitrogen oxides on secondary organic aerosol
1384 formation." Atmos. Chem. Phys. **15**(23): 13487-13506.

1385
1386
1387

1388 **Supplemental Information**

1389 In the main text, we noted a discrepancy between overall average aerosol volume estimates
1390 based on size measurements vs. AMS for the flight analyzed here (see Figure S1). We checked
1391 to see if this bias was also present in the individual plumes studied here by calculating the
1392 volume changes from the sizing instruments and the derived volume changes from the
1393 AMS+rBC mass. There is quite a bit of scatter in the volume enhancements, with with some of
1394 the points falling along the same line as the data for this flight and some falling significantly
1395 below the line. It is unclear why the two types of volume measurements disagree more for this
1396 flight. Therefore, the bias in volume changes introduces additional uncertainty in the magnitude
1397 of the plume enhancements, which is not included in the uncertainty propagation.
1398

Juliane Fry 7/30/2018 10:46 PM
Deleted: most of the points falling along the same line as the data for this flight



1399 **Figure S1.** Aerosol volume measured using the total aerosol mass from the AMS plus refractory
1400 black carbon (rBC) and mass-weighted densities versus the aerosol volume measured by
1401 optical size with the UHSAS after correcting for AMS lens transmission. The procedure for
1402 calculating the mass-weighted density is described by [Bahreini et al. \(2009\)](#). On average, the
1403 measured aerosol volume from composition is roughly equal to the measured aerosol volume
1404 from size for the entire SENEX study (left hand panel) and is higher than one for the flight
1405 analyzed here (July 2, 2013, right hand panel).
1406
1407

Juliane Fry 5/26/2018 6:45 PM
Deleted: Bahreini
Juliane Fry 5/26/2018 6:46 PM
Deleted: [65]

1408 **Corrections for AMS UMR nitrate data and applicability to pRONO₂ estimation**

1409
1410 Nitrate in the AMS is quantified in unit mass resolution mode (UMR) as the sum of the estimated
1411 NO⁺ at *m/z* 30 and NO₂⁺ at *m/z* 46, with a correction factor to account for the smaller ions (N⁺
1412 and HNO₃⁺, mostly) produced from nitrate (Allan et al., 2004). The default AMS UMR
1413 quantification algorithm (documented in the AMS “fragmentation table”) estimates NO⁺ as the
1414 total signal at *m/z* 30 minus a small (2.2% of OA at *m/z* 29, “Org29” in AMS parlance)
1415 subtraction to account for organic interferences and an isotopic correction for naturally-occurring
1416 ¹⁵N₂ from nitrogen in air. The default UMR fragmentation table was developed for mixed ambient
1417 aerosols, in particular in urban studies, and it is the responsibility of each AMS user to correct it
1418 as needed for each study. In environments with high biogenic contributions to total OA, and/or

1423 low total nitrate concentrations, the contribution of the CH_2O^+ ion can be much larger than the
1424 default subtraction at m/z 30. Similarly, the CH_2O_2^+ ion at m/z 46 becomes non-negligible, and
1425 hence nitrate reported from AMS data with UMR resolution will frequently be overestimated in
1426 these situations. The poor performance of the default AMS correction is likely due to the initial
1427 focus on urban OA with high nitrate fractions when deriving those corrections (Allan et al., 2004,
1428 Zhang et al., 2004).

1429
1430 Here we derive a set of corrections based on an aircraft high-resolution (HR) dataset acquired
1431 with the University of Colorado HR-AMS (Dunlea et al., 2009) on the NASA DC-8 during the
1432 SEAC⁴RS campaign (Toon et al., 2016). SEAC⁴RS took place with a strong emphasis on the
1433 SEUS 6 weeks after the SENEX flight analyzed in this manuscript. Based on an initial screening
1434 of the correlations of the CH_2O^+ and CH_2O_2^+ ions with UMR signals, 10 potential UMR m/z
1435 between m/z 29 and m/z 53 were selected as viable for deriving suitable corrections. Further
1436 analysis using three specific SEAC⁴RS flights (RF11 on 30 Aug 30th, 2013, RF16 on Sep 11th,
1437 2013 and RF18 on Sep 16th, 2013) that covered a wide range of OA composition with both
1438 strong biogenic contributions and fresh and aged biomass plumes showed that only four m/z
1439 (29, 42, 43 and 45) had good enough S/N and robust enough correlations to be used as
1440 corrections. Table S1 summarizes the correction coefficients obtained in this analysis, and
1441 Figure S2 shows the ability of matching the actual NO^+ and NO_2^+ signals (as obtained from
1442 high-resolution analysis of these flights) with the corrected UMR procedure. These corrections
1443 are applied as:

$$\begin{aligned} \text{UMR NO} &= \text{Signal}(m/z30) - a_i * \text{Signal}(\text{Variable}_i) \\ \text{UMR NO}_2 &= \text{Signal}(m/z 46) - b_i * \text{Signal}(\text{Variable}_i) \end{aligned}$$

1444
1445
1446
1447
1448 with the coefficients a_i and b_i as reported in Table S1. It should be noted that in all cases the
1449 contributions of C^{18}O^+ to m/z 30 need to be subtracted first before applying the correction (which
1450 is constrained to the organic CO_2^+ signal, measured at m/z 44, by the naturally-occurring
1451 isotopic ratio and assuming that OA produces $\text{CO}^+ = \text{CO}_2^+$ (Zhang et al., 2005, Takegawa et al.,
1452 2007). Likewise, the contribution of $^{13}\text{CO}^+$ to Org29 needs to be subtracted first. It is hence very
1453 important for this analysis that the corrections to the AMS frag table to suitably estimate the
1454 contribution of gas phase CO_2^+ to total UMR m/z 44 as well as the baseline correction for m/z 29
1455 be properly applied first (Allan et al., 2004). Finally, also note that the corrections using m/z 29
1456 and 43 are rather based on Org29 and Org43, which are standard AMS products that take the
1457 OA relative ionization efficiency (RIE) into account.

1458
1459 For the SEAC⁴RS dataset, the corrections amounted to on average subtracting 55% from UMR
1460 m/z 30 and 33% from UMR m/z 46. Despite this large subtraction, the corrected data correlates
1461 very well with the HR AMS results, with less than 5% deviation in the regression slope between
1462 the two datasets.

1463
1464 Although all of the corrections in Table S1 were valid for the SEAC⁴RS data set, for the flight
1465 analyzed here we chose Org29 to correct m/z 30 and mz 45 correction to correct m/z 46
1466 because they were the closest organic signals to the UMR nitrate peaks with organic

1467 interferences and may be more valid for other field studies where different types of OA are
1468 sampled. After these UMR signals were corrected and the appropriate RIEs and CE were
1469 applied, the nitrate mass concentrations in the final data archive for the flight analyzed here
1470 were reduced by 0-0.24 $\mu\text{g sm}^{-3}$, averaging 0.11 $\mu\text{g sm}^{-3}$ or 32%. The corresponding increase in
1471 OA due to the organic interferences in the UMR nitrate had linear dependence on the reported
1472 OA mass concentrations ($r^2 = 0.89$) with a slope of 1.3%.

1473
1474 To estimate the fraction of nitrate that is organic nitrate (pRONO₂) the use of the NO₂⁺/NO⁺ ratio
1475 with an empirically determined pRONO₂ calibration ratio has been successfully used previously
1476 with HR-AMS data (Farmer et al., 2010, Fry et al., 2013, Ayres et al., 2015, Fisher et al., 2016,
1477 Lee et al., 2016, Day et al., 2017, Palm et al., 2017). Figure S2 summarizes how well the ratio of
1478 the corrected UMR *m/z* 30 and 46 signals correlate with the NO₂⁺ and NO⁺ (and ratios)
1479 determined using HR data. As expected, there is considerable scatter at very low nitrate
1480 concentrations (which is a considerable part of the dataset, as the time series shows, since the
1481 free troposphere was sampled extensively). However, for the predicted pRONO₂ (which is
1482 mass-weighted), most of this scatter disappears, and for concentrations above 0.1 $\mu\text{g sm}^{-3}$ of
1483 nitrate there is good agreement between the HR results and the UMR-corrected pRONO₂,
1484 regardless of the correction chosen. For lower concentrations the scatter is considerable larger,
1485 with the Org29 correction providing the best overall agreement. Based on the variability in this
1486 dataset for this correction (Org29), we estimate the uncertainty in pRONO₂ fraction
1487 apportionment using UMR to be about 30%, in addition to an estimated uncertainty for the
1488 apportionment method using HR of 20%. From the comparison of UMR-corrected total nitrate
1489 to HR nitrate (not shown), we estimate an additional error of 5% for total nitrate error using
1490 these corrections.

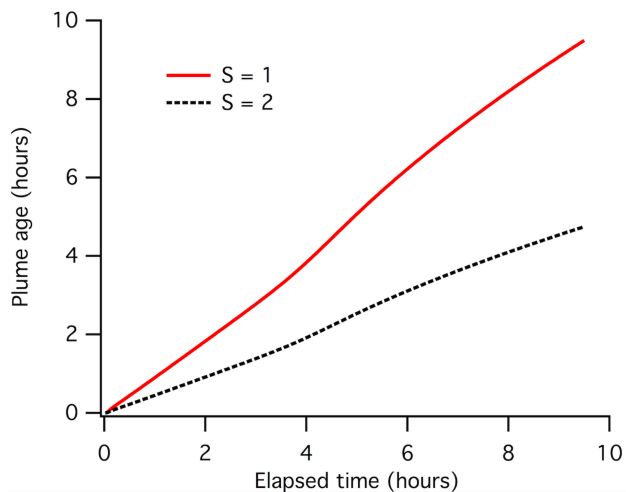
1491
1492 As mentioned in the main text, the empirically determined pRONO₂ calibration ratio used for the
1493 flight data analyzed here was the ratio of NO₂⁺/NO⁺ from the ammonium nitrate calibration
1494 aerosols divided by 2.8. This factor was determined as the average of several literature studies
1495 (Fry et al., 2009, Rollins et al., 2009, Farmer et al., 2010, Sato et al., 2010, Fry et al., 2011,
1496 Boyd et al., 2015) and applied according to the "ratio of ratios" method (Fry et al., 2013). The
1497 ammonium nitrate NO₂⁺/NO⁺ ratio was obtained from the two calibrations on 30 June and 7 July
1498 that bracketed the flight on 2 July, as described above. This ratio averaged 0.490. Hence, the
1499 organic nitrate NO₂⁺/NO⁺ ratio was estimated to be 0.175. The ratio of NO₂⁺/NO⁺ from the flight
1500 data was then used with the pRONO₂ and ammonium nitrate NO₂⁺/NO⁺ calibration ratios to
1501 estimate the fraction of the total corrected nitrate mass concentrations that was organic
1502 (pRONO₂) or inorganic (nitrate associated with ammonium or NH₄NO₃). Propagating the 30%
1503 UMR vs HR uncertainty and 20% apportionment (see above) error on top of the 34% AMS total
1504 nitrate measurement uncertainty results in $\pm 50\%$ uncertainties in the derived organic nitrate
1505 mass concentrations (and similar for NH₄NO₃; however it will depend on the relative
1506 contributions of pRONO₂ and NH₄NO₃ to total nitrate since the absolute concentration errors
1507 associated with pRONO₂ - NH₄NO₃ apportionment should be similar [64]).
1508

Juliane Fry 5/26/2018 9:58 PM
Deleted: (Day et al., 2017).

Juliane Fry 5/26/2018 10:16 PM
Formatted: Normal

Juliane Fry 5/26/2018 10:11 PM
Deleted: (Boyd et al., 2015)

1534



1535

1536

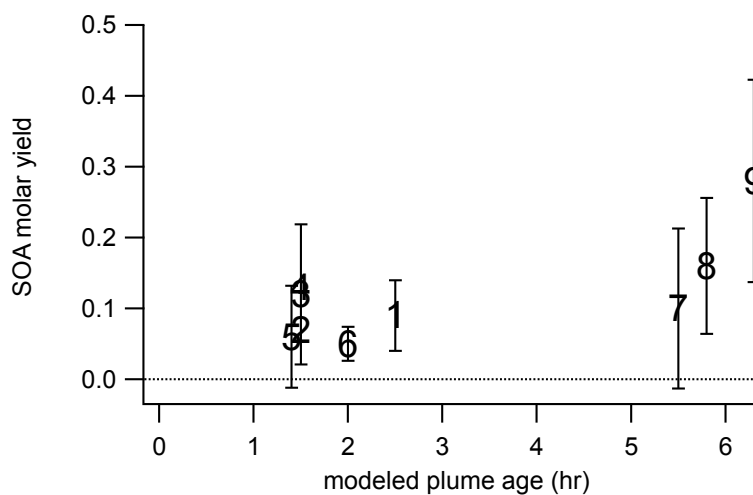
1537

1538

1539

1540

Figure S3. Calculated plume age vs. elapsed time in a box model run for a single representative night. Plume ages on the y-axis are calculated based on Equation 1 in the main text but using model NO_2 and O_3 data. Time since sunset on the x-axis is the model elapsed time (i.e., run time of the model during darkness).



1541

1542

1543

1544

1545

Figure S4. SOA molar yield is positively correlated with estimated plume age. This SOA molar yield is based on Eq. 3, with error bars determined by propagation of observed variability in pRONO_2 and isoprene, where multiple point averaging was possible. Markers correspond to

1546 plume numbers.). Based on the box model described in more detail below, the first-generation
1547 isoprene products peak at a approximately 4 hours plume age and then begin to decay.

1548

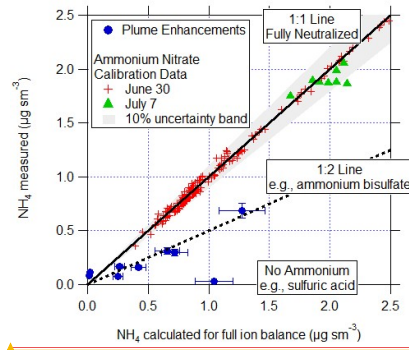
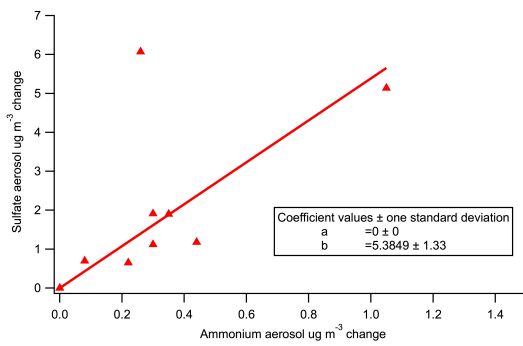
1549 **Table S2.** Peak ambient (wet) aerosol surface area during each plume used in the yield
1550 analysis (plume numbers 1 – 9), and for the two longer urban plumes transected at the end of
1551 the flight.

plume number	7/2/13 plume time (UTC)	Peak aerosol surface area ($\mu\text{m}^2 \text{cm}^{-3}$)
1	2:18	280
2	2:20	370
3	2:21	470
4	3:03	340
5	3:55	800
6	4:34	470
7	4:37	370
8	4:39	420
9	5:04	490
Urban plume	5:36	340
Urban plume	6:37	300

1552

1553

1554



Juliane Fry 6/1/2018 8:36 AM
Formatted: Normal1

Unknown
Formatted: Font:Font color: Blue

Juliane Fry 6/1/2018 8:36 AM
Formatted: Font:(Default) Arial, 11 pt, Font color: Black

1555
1556
1557
1558
1559
1560
1561
1562
1563
1564
1565
1566
1567
1568
1569
1570
1571

Figure S5. (a) In-plume change in sulfate mass concentration vs. change in ammonium aerosol mass concentration is generally well correlated, with a slope of 5.4. The masses of the cations and anions would give an ion balance for pure $(\text{NH}_4)_2\text{SO}_4$ of $\text{MW}(\text{SO}_4)/(\text{2 x MW}(\text{NH}_4)) = 2.7$, and for $(\text{NH}_4)\text{HSO}_4$ of $\text{MW}(\text{SO}_4)/(\text{MW}(\text{NH}_4)) = 5.4$. Hence, this slope provides support for a mix of these two ammonium sulfate salts, with sometimes exclusively $(\text{NH}_4)\text{HSO}_4$. This is consistent with incomplete neutralization of the sulfate mass by ammonium. The one clear outlier (sulfate increase of $6 \mu\text{g m}^{-3}$ for Plume #5) suggests excess sulfate, rendering ammonium or other inorganic nitrate formation even less likely. Points with ammonium aerosol below $0.1 \mu\text{g m}^{-3}$ are within the variability of that measurement; their omission does not change the slope. (b) Measured vs. calculated (ion balanced) NH_4 for calibration data and plume enhancements. This also shows that plumes are acidic than ammonium sulfate, ruling out the possibility of inorganic nitrate formation.

Juliane Fry 6/1/2018 8:34 AM
Formatted: Subscript

1572 **Additional AMS and auxiliary data from plumes**

1573

1574 **Table S3.** Additional information for the list of plumes used in this NO₃ + isoprene SOA yield
 1575 analysis, for which key yield-related data is presented in Table 1. For each plume, the delta-
 1576 values listed indicate the difference between in-plume and outside-plume background in
 1577 average observed concentration. After each plume number, the numbers of points averaged for
 1578 isoprene and AMS, respectively, are listed. Plume numbers annotated with * indicate brief
 1579 plumes for which only single-point measurements of in-plume aerosol composition were
 1580 possible. Also shown are the plume changes in isoprene used in the present analysis (Δ_{isop} ,
 1581 the difference between in-plume and background isoprene concentration, reproduced from
 1582 Table 1), alongside for comparison the Δ_{isop} determined as the difference between in-plume
 1583 isoprene and the modeled sunset (initial) concentration of isoprene present at that location
 1584 outside of the plume, determined using an iterative box model (Edwards et al., 2017). The
 1585 similarity between these two values for most points suggests that the isoprene just outside of
 1586 each plume transect was largely unperturbed from the sunset initial value.

plume number [#isop/#AMS]	7/2/13 plume time (UTC)	$\Delta_{ORG,aero}$ ($\mu\text{g m}^{-3}$)	$\Delta_{NH_4,aero}$ ($\mu\text{g m}^{-3}$)	$\Delta_{SO_4,aero}$ ($\mu\text{g m}^{-3}$)	Temp (C)	%RH	Δ_{isop} (pptv)	Δ_{isop} from model (pptv)	Is Mo
Typical variability ($\mu\text{g m}^{-3}$):		0.75	0.1	0.5					
1 [2/3]	2:18	0.35	0	0	23.6	66.5	-335	-327	
2 [*]	2:20	0.89	0.3	1.91	23.6	65	-404	-453	
3 [4/5]	2:21	1.25	1.05	5.14	23.6	65.2	-228	-337	
4 [*]	3:03	0.16	0.08	0.7	21.2	68.1	-453	-391	
5 [3/4]	3:55	0.32	0.26	6.07	21.9	65.5	-255	-376	
6 [2/2]	4:34	0.57	0.3	1.12	19.9	74.6	-713	-233	
7 [5/6]	4:37	1.05	0.22	0.65	19.7	76.2	-298	-221	
8 [2/3]	4:39	1.26	0.44	1.18	18.3	82.2	-443	-353	
9 [7/8]	5:04	1.45	0.35	1.9	17.2	84.8	-293	-434	

1587

1588

1589

1590 **Box model calculations**

- Juliane Fry 6/1/2018 8:26 AM
Formatted ... [10]
- Juliane Fry 5/26/2018 8:10 PM
Formatted ... [11]
- Juliane Fry 5/26/2018 8:10 PM
Formatted ... [12]
- Juliane Fry 5/26/2018 8:10 PM
Formatted ... [13]
- Juliane Fry 6/1/2018 8:25 AM
Formatted ... [14]
- Juliane Fry 6/1/2018 8:25 AM
Formatted ... [15]
- Juliane Fry 6/1/2018 8:26 AM
Formatted ... [16]
- Juliane Fry 5/26/2018 6:54 PM
Formatted Table ... [17]
- Juliane Fry 5/26/2018 8:07 PM
Formatted ... [19]
- Juliane Fry 5/26/2018 7:59 PM
Formatted ... [18]
- Juliane Fry 5/26/2018 8:07 PM
Formatted ... [21]
- Juliane Fry 5/26/2018 7:59 PM
Formatted ... [20]
- Juliane Fry 5/26/2018 8:07 PM
Formatted ... [23]
- Juliane Fry 5/26/2018 7:59 PM
Formatted ... [22]
- Juliane Fry 5/26/2018 8:07 PM
Formatted ... [25]
- Juliane Fry 5/26/2018 7:59 PM
Formatted ... [24]
- Juliane Fry 5/26/2018 8:07 PM
Formatted ... [27]
- Juliane Fry 5/26/2018 7:59 PM
Formatted ... [26]
- Juliane Fry 5/26/2018 8:07 PM
Formatted ... [29]
- Juliane Fry 5/26/2018 7:59 PM
Formatted ... [28]
- Juliane Fry 5/26/2018 8:07 PM
Formatted ... [31]
- Juliane Fry 5/26/2018 7:59 PM
Formatted ... [30]
- Juliane Fry 5/26/2018 8:07 PM
Formatted ... [33]
- Juliane Fry 5/26/2018 7:59 PM
Formatted ... [32]
- Juliane Fry 5/26/2018 8:07 PM
Formatted ... [35]
- Juliane Fry 5/26/2018 7:59 PM
Formatted ... [34]

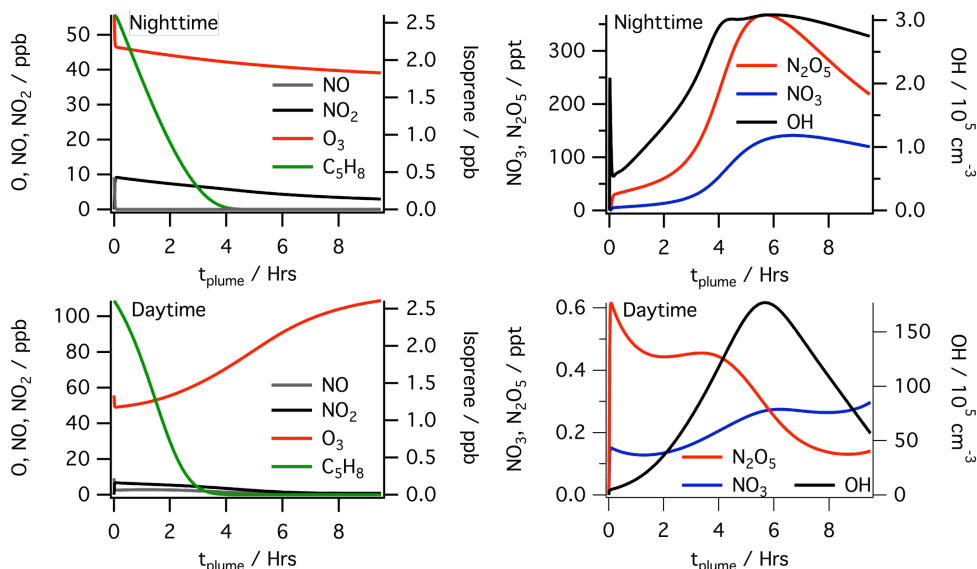
1591 Box model simulations were performed using the Dynamically Simple Model of Atmospheric
 1592 Chemical Complexity (DSMACC, [http://wiki.seas.harvard.edu/geos-](http://wiki.seas.harvard.edu/geos-chem/index.php/DSMACC_chemical_box_model)
 1593 [chem/index.php/DSMACC_chemical_box_model](http://wiki.seas.harvard.edu/geos-chem/index.php/DSMACC_chemical_box_model)), containing the Master Chemical Mechanism
 1594 v3.3.1 chemistry scheme (<http://mcm.leeds.ac.uk/MCM/>). The model approach is similar to that
 1595 described in detail in Edwards et al. 2017, and the accompanying supplement, with the model
 1596 run over a 9.5 hour night to simulate the nocturnal residual layer. For the nocturnal simulation
 1597 used in this work (for both the plume lifetime calculation and the peroxy radical lifetime analysis
 1598 in Sect. 4.3) the model was initialized with concentrations of the constraining species
 1599 representative of the SENEX observations (Table S4). As the model is simulating power plant
 1600 plume evolution from point of emission, a starting NO mixing ratio of 10 ppb was used to
 1601 constrain NO_x, and the chemistry scheme was subsequently allowed to partition the reactive
 1602 nitrogen. The top panels in Figure S7 show the evolution of key species during this nocturnal
 1603 simulation.

1604 **Table S4:** Species constrained (MCM v3.3.1 names) during model simulations and constraining
 1605 values. Constraint column indicates if species concentrations were held at the constrained value
 1606 throughout the simulation (Fixed) or allowed to vary after initialization (Initial).

Species	Mixing ratio	Units	Constraint
NO	9.28	ppb	Initial
O3	55.72	ppb	Initial
CO	134.00	ppb	Fixed
CH4	1920.00	ppb	Fixed
C5H8	2606.80	ppt	Initial
APINENE	38.87	ppt	Initial
BPINENE	195.50	ppt	Initial
LIMONENE	12.42	ppt	Initial
MACR	454.13	ppt	Initial
MVK	1006.00	ppt	Initial
IC4H10	47.00	ppt	Fixed
NC4H10	128.00	ppt	Fixed
C2H6	1199.00	ppt	Fixed
C2H4	117.00	ppt	Fixed
C2H2	145.00	ppt	Fixed
NC6H14	20.00	ppt	Fixed
IC5H12	120.00	ppt	Fixed
NC5H12	76.00	ppt	Fixed
C3H8	344.00	ppt	Fixed
C3H6	26.00	ppt	Fixed
CH3COCH3	2556.00	ppt	Fixed
BENZENE	35.90	ppt	Fixed
C2H5OH	2239.00	ppt	Fixed
MEK	309.00	ppt	Fixed
CH3OH	5560.00	ppt	Fixed

1607 The daytime simulation used for comparison in Sect. 4.3 of the main manuscript (lower panels
 1608 of Figure S7) uses the same initialization as the nocturnal simulation; with the only difference
 1609 being the model is run during the daytime. Photolysis rates are calculated using TUV
 1610 (<https://www2.acom.ucar.edu/modeling/tropospheric-ultraviolet-and-visible-tuv-radiation-model>).
 1611 The daytime simulation does not accurately simulate daytime mixing ratios of species such as
 1612 O₃ representative of SENEX observations. However, the intent of this simulation is to compare
 1613 model daytime peroxy radical fate and lifetime with the nocturnal simulation. The presence of

1614 intense convective mixing in the daytime planetary boundary layer of the Southeast US makes
1615 accurately modeling these concentrations difficult with a zero dimensional model.
1616



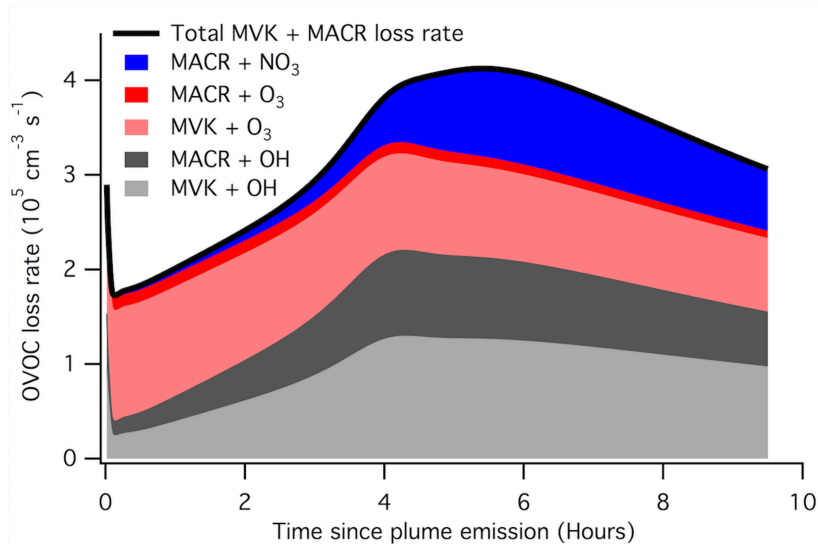
1617
1618 **Fig. S6.** Model calculated NO, NO₂, O₃, and isoprene (left) and NO₃, N₂O₅ and OH (right for the
1619 nocturnal (top) and daytime (bottom) simulations shown in Sect. 4.3.

1620

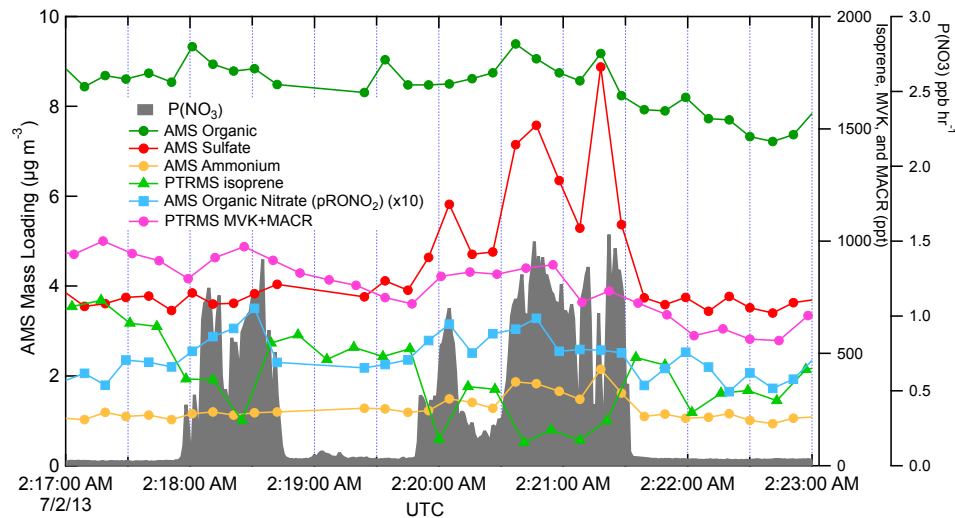
1621 **Additional considerations investigated via RO₂ fate box modeling**

1622

1623 Based on the potentially larger than previously estimated contribution of RO₂+RO₂ reactions at
1624 night, we considered a related possible source of a high bias in the determined SOA yields. If
1625 NO₃ reaction with the major daytime isoprene oxidation products MVK and/or MACR produces
1626 RO₂ radicals that can cross-react with NO₃ + isoprene products to produce condensable
1627 products, this would be a mechanism of recruiting isoprene-derived organic mass into the
1628 aerosol, but that original isoprene oxidation would not be counted in the denominator of the yield
1629 calculation, since its interaction with NO₃ began as MACR or MVK. In the box model, substantial
1630 MVK and MACR are available in the plume at nighttime, but only MACR reacts with NO₃, and a
1631 maximum fraction of one-quarter of MVK+MACR losses go to reaction with NO₃ overnight (see
1632 Figure S8). In addition, in our power plant plume observations, MVK+MACR are not observed to
1633 be appreciably depleted by the large NO₃ injection, further suggesting that this chemistry is not
1634 a substantial additional source of SOA (see Figure S9).
1635



1636
 1637 **Figure S7.** Calculated (via MCM) loss rate contributions for the daytime isoprene products
 1638 methyl vinyl ketone (MVK) and methacrolein (MACR) in the simulated nighttime plume used in
 1639 the text. Only MACR reacts with NO_3 , and the contribution of this process to total losses (green
 1640 stack) is relatively minor.



1641
 1642 **Figure S8.** MVK and MACR are not titrated on the timescale of these yield estimates in power
 1643 plant plumes.
 1644

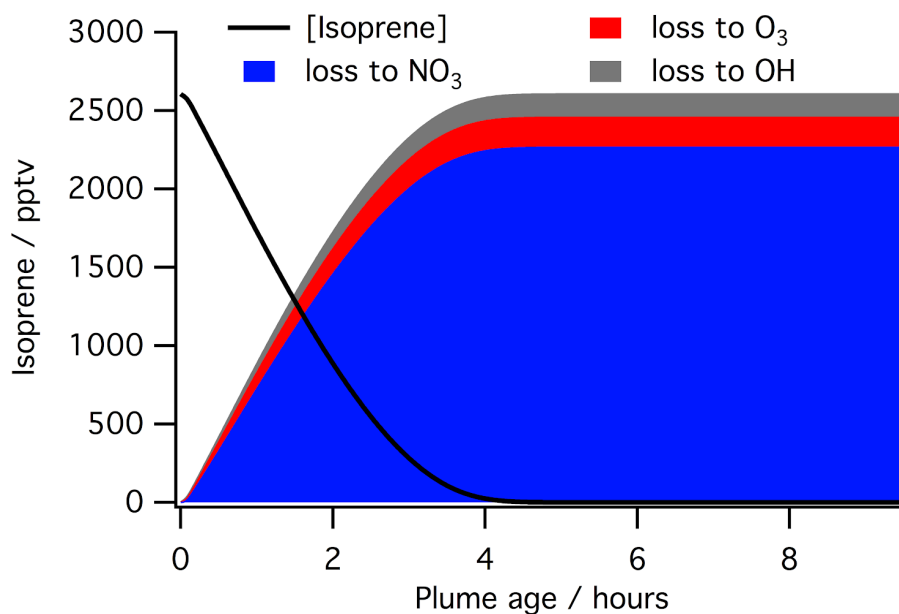


Figure S9. Model simulation of typical in-plume consumption of isoprene (black line), and stacked plot showing the contributions to this from the NO₃, O₃, and OH. Modeled plume was emitted at sunset, so this represents nocturnal processing under power plant plume conditions.

Unknown
Formatted: Font:

Juliane Fry 6/1/2018 8:30 AM
Formatted: Font color: Auto

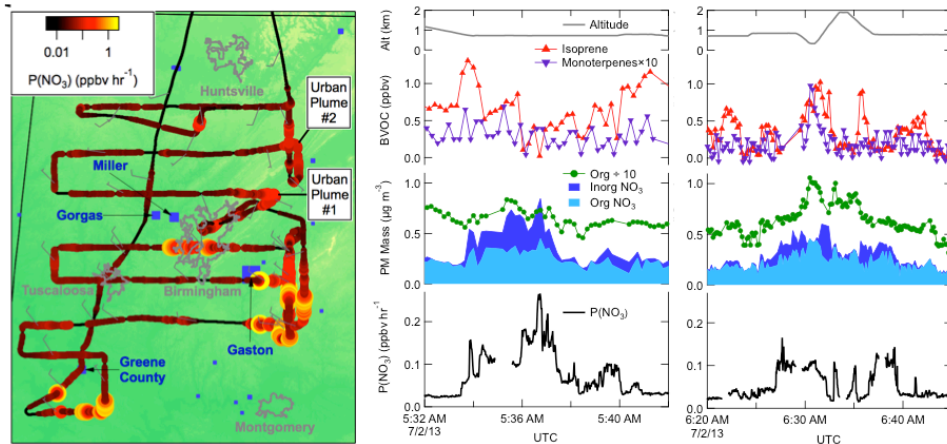
1645
1646
1647
1648
1649
1650

Two urban plume case studies

1651
1652
1653
1654
1655
1656
1657
1658
1659
1660
1661
1662
1663
1664
1665
1666
1667
1668

In addition to the nine power plant plumes analyzed above to determine the NO₃ + isoprene SOA molar yield, towards the end of the July 2 flight, the Birmingham urban plume was intercepted twice (around 5:36 am and 6:37 am UTC, Fig. 8). These downwind urban plumes are among the most aged plumes (estimated at 5.2 and 5.8 hours, respectively), but are also substantially more diffuse than the narrow power plant plume intercepts and have lower peak $P(\text{NO}_3)$. Nevertheless, we note that these two plumes contain periods of apparent anti-correlation of isoprene and organic nitrate aerosol time series and high apparent SOA molar yields (23%, 19%) and mass yields (62%, 51%), if calculated by the same method as above and omitting the period of vertical profiling in the second plume. Potentially complicating these urban SOA yield determinations is the fact that the inorganic fraction of nitrate was much larger than in the power plant plumes (see Fig. 8). The background isoprene is also somewhat lower in these urban plumes, potentially shifting the NO₃/N₂O₅ fate to reactions other than NO₃ + isoprene (see Fig. S4 in Edwards et al. (Edwards et al., 2017)). The aerosol surface area is not noticeably higher in these urban plumes, which one might expect to lead to a larger contribution of N₂O₅ uptake and hydrolysis. In the more complex mix of gases characteristic of an urban plume, we hesitate to attribute these apparent yields exclusively to the NO₃ + isoprene reaction.

1669



1670
1671
1672
1673
1674
1675
1676
1677

Figure S10. Flight map and time series of two urban plume intercepts, showing anticorrelation of organic nitrate and isoprene. These more diffuse plumes, with lower $P(\text{NO}_3)$ and larger inorganic nitrate contribution, make yield determination more uncertain, so we do not include them in the overall yield determination. However, using the same methodology as for the power plant plumes would give similarly high yields for these very aged plumes.

Page 19: [1] Deleted	Juliane Fry	5/26/18 5:14 PM
	Δ ISOP (ppt)	
	[\pm SD]	
Page 19: [2] Deleted	Juliane Fry	5/26/18 5:14 PM
		-335
		[128]
Page 19: [3] Deleted	Juliane Fry	5/26/18 5:14 PM
		-228
		[121]
Page 19: [4] Deleted	Juliane Fry	5/26/18 5:14 PM
		-255
		[251]
Page 19: [5] Deleted	Juliane Fry	5/26/18 5:14 PM
		-713
		[219]
Page 19: [6] Deleted	Juliane Fry	5/26/18 5:14 PM
		-298
		[197]
Page 19: [7] Deleted	Juliane Fry	5/26/18 5:14 PM
		-443
		[75]
Page 19: [8] Deleted	Juliane Fry	5/26/18 5:14 PM
		-293
		[131]
Page 28: [9] Deleted	Juliane Fry	5/26/18 10:23 PM

4.4 Two urban plume case studies

In addition to the nine power plant plumes analyzed above to determine the NO_3 + isoprene SOA molar yield, towards the end of the July 2 flight, the Birmingham urban plume was intercepted twice (around 5:36 am and 6:37 am UTC, Fig. 8). These downwind urban plumes are among the most aged plumes (estimated at 5.2 and 5.8 hours, respectively), but are also substantially more diffuse than the narrow power plant plume intercepts and have lower peak $P(\text{NO}_3)$. Nevertheless, we note that these two plumes contain periods of apparent anti-correlation of isoprene and organic nitrate aerosol time series and high apparent SOA molar yields (23%, 19%) and mass yields (62%, 51%), if calculated by the same method as above and omitting the period of vertical profiling in the second plume. Potentially complicating these urban SOA yield determinations is the fact that the inorganic fraction of nitrate was much larger than in the power plant plumes (see Fig. 8). The background isoprene is also somewhat lower in these urban plumes, potentially shifting the $\text{NO}_3/\text{N}_2\text{O}_5$ fate to reactions other than NO_3 + isoprene (see Fig. S4 in Edwards et al. (Edwards et al., 2017)). The aerosol surface area is not noticeably higher in these urban plumes, which one might expect to lead to a larger contribution of N_2O_5 uptake and hydrolysis. In the more complex mix of gases characteristic of an urban plume, we hesitate to attribute these apparent yields exclusively to the NO_3 + isoprene reaction.

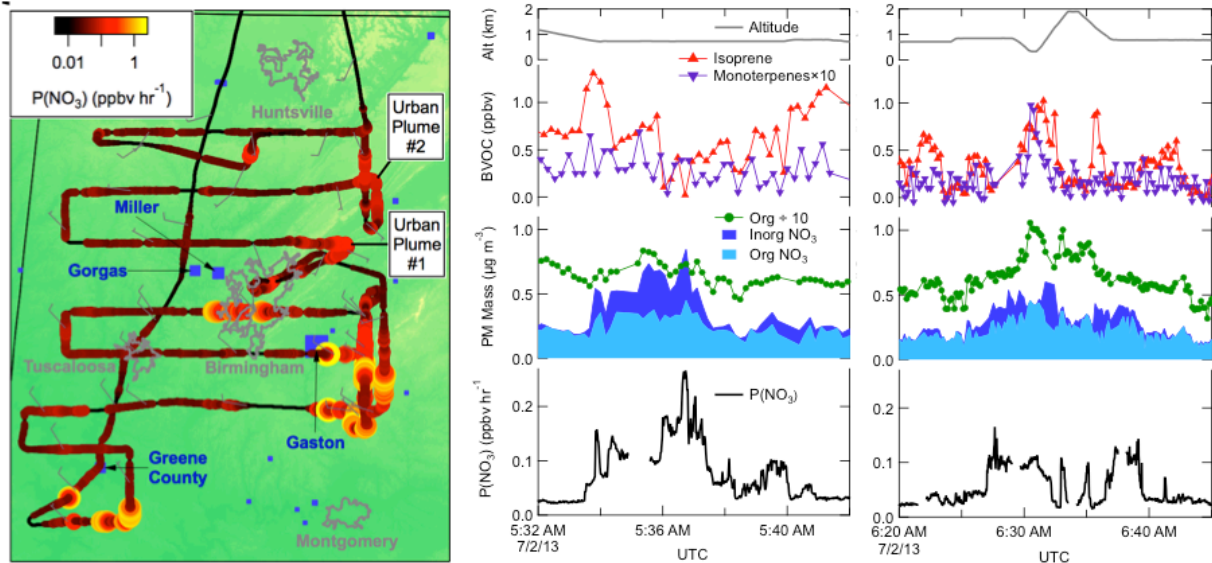


Figure 8. Flight map and time series of two urban plume intercepts, showing anticorrelation of organic nitrate and isoprene. These more diffuse plumes, with lower $P(\text{NO}_3)$ and larger inorganic nitrate contribution, make yield determination more uncertain, so we do not include them in the overall yield determination. However, using the same methodology as for the power plant plumes would give similarly high yields for these very aged plumes.

Page 45: [10] Formatted	Juliane Fry	6/1/18 8:26 AM
Normal		
Page 45: [11] Formatted	Juliane Fry	5/26/18 8:10 PM
Font:11 pt, Not Bold		
Page 45: [12] Formatted	Juliane Fry	5/26/18 8:10 PM
Font:11 pt, Not Bold		
Page 45: [13] Formatted	Juliane Fry	5/26/18 8:10 PM
Font:11 pt, Not Bold		
Page 45: [14] Formatted	Juliane Fry	6/1/18 8:25 AM
Font color: Auto		
Page 45: [15] Formatted	Juliane Fry	6/1/18 8:25 AM
Font:Not Bold, Font color: Auto		
Page 45: [16] Formatted	Juliane Fry	6/1/18 8:26 AM
Font:(Default) Times, 10 pt, Not Bold, Font color: Auto		

Page 45: [17] Formatted Table	Juliane Fry	5/26/18 6:54 PM
Formatted Table		
Page 45: [18] Formatted	Juliane Fry	5/26/18 7:59 PM
Right		
Page 45: [19] Formatted	Juliane Fry	5/26/18 8:07 PM
Font:(Default) Arial, 10 pt		
Page 45: [20] Formatted	Juliane Fry	5/26/18 7:59 PM
Right		
Page 45: [21] Formatted	Juliane Fry	5/26/18 8:07 PM
Font:(Default) Arial, 10 pt		
Page 45: [22] Formatted	Juliane Fry	5/26/18 7:59 PM
Right		
Page 45: [23] Formatted	Juliane Fry	5/26/18 8:07 PM
Font:(Default) Arial, 10 pt		
Page 45: [24] Formatted	Juliane Fry	5/26/18 7:59 PM
Right		
Page 45: [25] Formatted	Juliane Fry	5/26/18 8:07 PM
Font:(Default) Arial, 10 pt		
Page 45: [26] Formatted	Juliane Fry	5/26/18 7:59 PM
Right		
Page 45: [27] Formatted	Juliane Fry	5/26/18 8:07 PM
Font:(Default) Arial, 10 pt		
Page 45: [28] Formatted	Juliane Fry	5/26/18 7:59 PM
Right		
Page 45: [29] Formatted	Juliane Fry	5/26/18 8:07 PM
Font:(Default) Arial, 10 pt		
Page 45: [30] Formatted	Juliane Fry	5/26/18 7:59 PM
Right		
Page 45: [31] Formatted	Juliane Fry	5/26/18 8:07 PM
Font:(Default) Arial, 10 pt		
Page 45: [32] Formatted	Juliane Fry	5/26/18 7:59 PM
Right		
Page 45: [33] Formatted	Juliane Fry	5/26/18 8:07 PM
Font:(Default) Arial, 10 pt		
Page 45: [34] Formatted	Juliane Fry	5/26/18 7:59 PM
Right		

Font:(Default) Arial, 10 pt